CRREL
REPORT 82-40

US Army Corps of Engineers
Cold Regions Research & Engineering Laboratory

Breaking ice with explosives

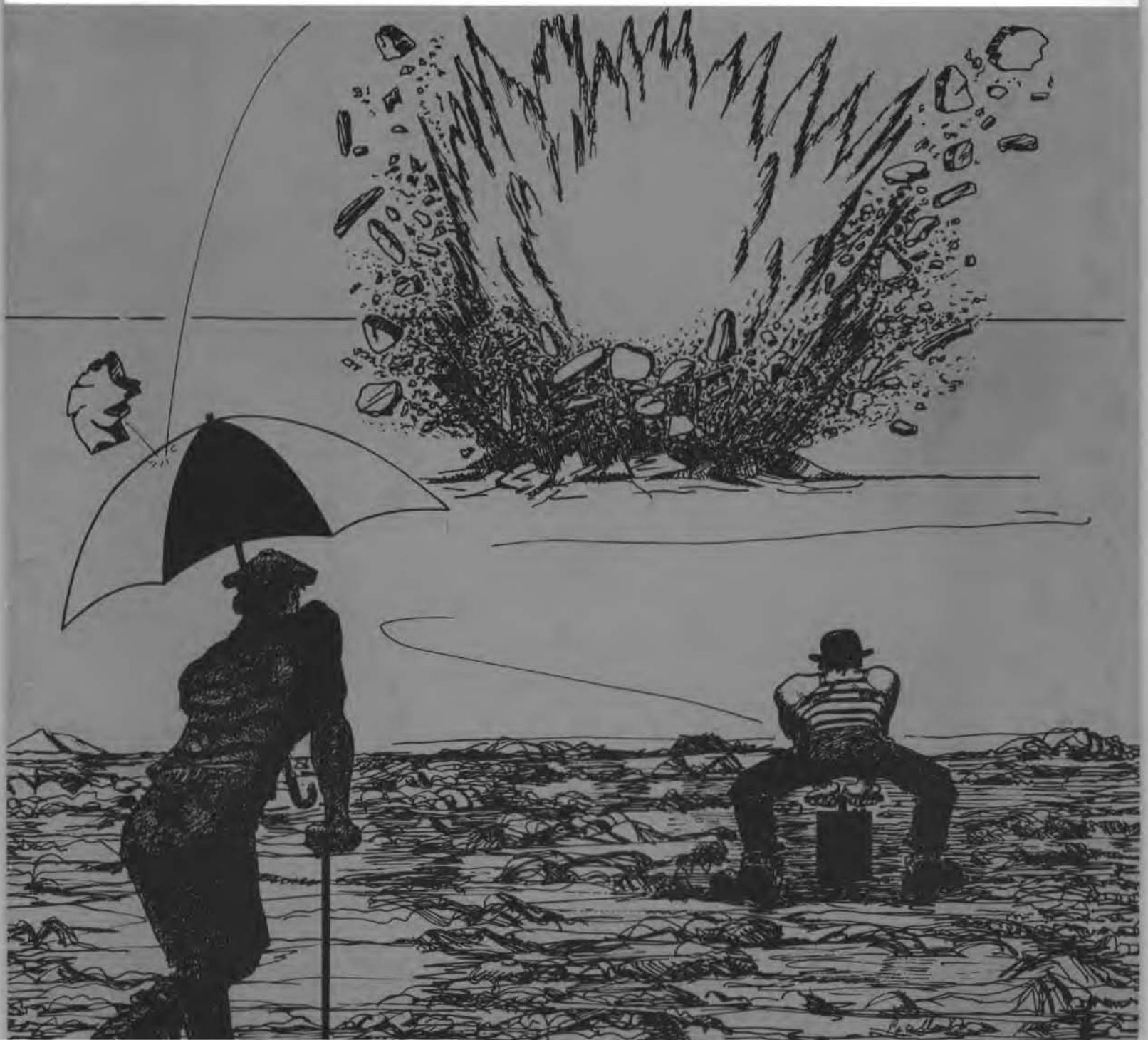

CRREL Report 82-40

December 1982

Breaking ice with explosives

Malcolm Mellor

Prepared for
OFFICE OF THE CHIEF OF ENGINEERS

REPORT DOCUMENTATION PAGE

READ INSTRUCTIONS BEFORE COMPLETING FORM

1. REPORT NUMBER: CRREL Report 82-40	2. GOVT ACCESSION NO.
3. RECIPIENT'S CATALOG NUMBER	
4. TITLE (and Subtitle): BREAKING ICE WITH EXPLOSIVES	5. TYPE OF REPORT & PERIOD COVERED
	6. PERFORMING ORG. REPORT NUMBER
7. AUTHOR(s): Malcolm Mellor	8. CONTRACT OR GRANT NUMBER(s)
9. PERFORMING ORGANIZATION NAME AND ADDRESS: U.S. Army Cold Regions Research and Engineering Laboratory, Hanover, New Hampshire 03755	10. PROGRAM ELEMENT, PROJECT, TASK AREA & WORK UNIT NUMBERS: DA Project 4A762730AT42, Task A, Work Unit 010
11. CONTROLLING OFFICE NAME AND ADDRESS: Office of the Chief of Engineers, Washington, D.C. 20314	12. REPORT DATE: December 1982
	13. NUMBER OF PAGES: 68
14. MONITORING AGENCY NAME & ADDRESS(if different from Controlling Office)	15. SECURITY CLASS. (of this report): Unclassified
	15a. DECLASSIFICATION/DOWNGRADING SCHEDULE

16. DISTRIBUTION STATEMENT (of this Report)

Approved for public release; distribution unlimited.

17. DISTRIBUTION STATEMENT (of the abstract entered in Block 20, if different from Report)

18. SUPPLEMENTARY NOTES

19. KEY WORDS (Continue on reverse side if necessary and identify by block number)

Ice
Explosion bubbles
Explosion effects
Explosions
Underwater explosions

20. ABSTRACT (Continue on reverse side if necessary and identify by block number)

The use of explosives to break floating ice sheets is described, and test data are used to develop design curves that predict explosives effects as ice thickness, charge size, and charge depth vary. Application of the curves to practical problems is illustrated by numerical examples. The general features of underwater explosions are reviewed and related to ice blasting. Quasi-static plate theory is considered, and is judged to be inapplicable to explosive cratering of ice plates. The specific energy for optimized ice blasting is found to compare quite favorably with the specific energy of icebreaking ships. All available field data for ice blasting are tabulated in appendices, together with details of the regression analyses from which the design curves are generated.

PREFACE

This report was prepared by Dr. Malcolm Mellor, Research Physical Scientist, Experimental Engineering Division, U.S. Army Cold Regions Research and Engineering Laboratory. The work was performed under DA Project 4A762730AT42, *Design, Construction and Operations Technology for Cold Regions,* Task A, *Cold Regions Combat Operations Support: Tactics, Doctrine, Logistics,* Work Unit 010, *Countermobility in Cold Regions.*

CONTENTS

	Page
Abstract	i
Preface	ii
Introduction	1
General behavior of underwater explosions	1
Regression analysis for ice-blasting data	9
General features of the regression curves	13
Use of the regression curves as design curves for ice blasting	15
Row charges and pattern charges	18
Response of floating ice sheets to underwater explosions	21
Specific energy and "powder factor"	26
Summary and conclusions	27
Literature cited	28
Appendix A: Basic data on ice blasting	29
Appendix B: Scaled input data	41
Appendix C: Initial regression analysis using complete polynomial	45
Appendix D: Regression analysis with two coefficients of the original polynomial deleted	57

ILLUSTRATIONS

Figure

1. Variation of peak pressure with scaled distance for a point charge of TNT in deep water 2
2. Conversion of scaled distance 3
3. Spalling of the water surface by an underwater explosion 3
4. Surface eruptions from underwater explosions 4
5. Surface effects from underwater explosion 4
6. Effect of charge depth on the maximum diameter at the base of the water column, the "effective" column diameter, and the water jet diameter 6
7. Depth d_* which is equal to the theoretical maximum bubble radius for the first pulse, R_{bm} 7
8. Theoretical maximum bubble radius R_{bm} scaled with respect to the cube root of charge weight and plotted against absolute charge depth 7
9. Initial velocity of the emerging water jet plotted against charge depth for underwater explosions 8
10. Force exerted on a horizontal plate by the waterspout from a 1-lb charge of TNT fired at various depths in the water 8
11. Re-plot of Figure 5 to show variation of waterspout characteristics with scaled charge depth 9
12. Values of scaled crater radius predicted by the regression relation plotted against the corresponding observed values 11

Figure Page
13. Predicted value of scaled crater radius as a function of scaled charge depth, with scaled ice thickness as parameter 14
14. Predicted value of scaled crater radius as a function of scaled ice thickness, with scaled charge depth as parameter 14
15. Geometry of row charges 19
16. Geometry of pattern charges 20
17. Shock wave paths for an underwater explosion with overlying ice 22
18. Variation of crater radius with charge depth according to a simple model 23
19. Scaled dimensions of waterspouts compared with crater diameter for zero ice thickness and with maximum bubble diameter 24
20. Waterspout characteristics from ordinary underwater explosions compared with ice crater predictions 24
21. Variation of crater radius with charge depth for explosions in a semi-infinite ice mass 25
22. Predicted specific energy for ice blasting when charges are at optimum depth 26

TABLES

Table
1. Analysis of departures from regression plane 12

BREAKING ICE WITH EXPLOSIVES

Malcolm Mellor

INTRODUCTION

Although explosives have been used to break floating ice sheets for at least 200 years, systematic design procedures for ice blasting are still evolving. In many cases, simple field tests can soon establish optimum procedures for the prevailing conditions but, taken in isolation, the results of such tests are of limited value for predicting blast effects under different conditions.

About 10 years ago, an attempt was made to develop design curves which could be used for studying the potential of ice blasting as an aid to ship navigation in ice-covered waters (Mellor 1972). All available data from field tests were compiled, and the dependence of "crater radius" on charge size, charge depth, ice thickness, ice type, and explosive type was considered. There were insufficient data for complete consideration of all variables, and some simplifications had to be made. Variations of ice type and explosive type were ignored, and cube root scaling was used to account for the variation of charge size when using point charges. Scaled crater radius was related to scaled charge depth and to scaled ice thickness by means of multiple regression analysis, and design curves were drawn. These curves ("MM 72 curves") proved instructive, and they gave good predictions for near-optimum blasting conditions. However, the curves could not be relied upon to predict behavior at large values of scaled charge depth, or large values of scaled ice thickness, since most of the test data used for the analysis referred to blasting conditions close to optimum.

In 1981, the MM72 curves were tested against the results of major field work by the Canadian Armed Forces (Fonstad et al. 1981). According to comparisons with the original data, the curves tended to underpredict scaled crater radius for large values, and to overpredict for small values; they did, however, give good prediction for the Canadian tests. In 1982 some further U.S. Army tests were made on very thin ice, and for the first time a few tests were deliberately made under conditions far from optimum.

In this report the general problem is reexamined, and the design curves are revised on the basis of currently available data.

GENERAL BEHAVIOR OF UNDERWATER EXPLOSIONS

When explosives are used to break a semi-infinite solid medium, detonation of charges on the surface is very inefficient. Experience suggests that the same is true of charges fired in air on top of a floating ice sheet. We are therefore concerned largely with the detonation of charges in water beneath the ice cover.

When a concentrated charge of high explosive is detonated well below the surface of deep water, it propagates a spherical shock wave and creates a gas bubble.

The shock propagates at high velocity and its pressure decays with distance, largely because of spherical spreading. From similitude considerations, radial distances from charges of different

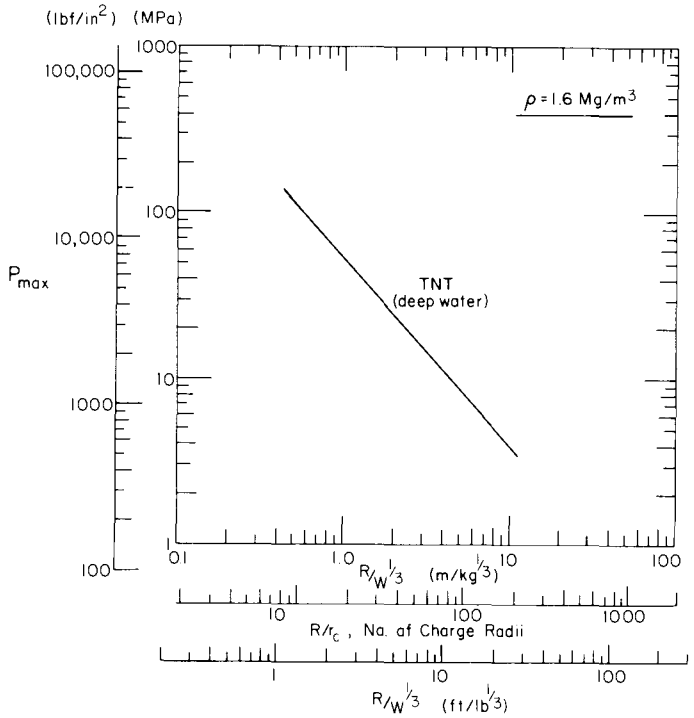

Figure 1. Variation of peak pressure with scaled distance for a point charge of TNT in deep water. (From a relation given by Swisdak [1978].)

size can be scaled with respect to charge radius, or with respect to the cube root of charge weight (assuming approximate constancy of charge density and specific energy and, if necessary, taking into account differences of detonation pressure and bubble characteristics for explosives of different type). Spherical spreading causes the shock wave energy to decay with the square of the radius of the source and, since wave energy is proportional to the square of wave amplitude, this leads to expectation that amplitude might be inversely proportional to radius. There is, in addition, some dissipation and dispersion, and this increases the rate of pressure decay with distance, probably by an exponential factor. In explosions technology, the variation of peak shock pressure with scaled distance is usually expressed by an empirical equation derived from log-log plots of test data, for example (Swisdak 1978):

$$P_{max} = P_*\left(\frac{W^{1/3}}{R}\right)^{\alpha} \qquad (1)$$

where P_{max} = peak shock pressure
P_* = reference "pressure"
R = radial distance from the source
W = charge weight
α = an exponent of order unity.

Since $W^{1/3}$ is proportional to charge radius R, $(W^{1/3}/R)$ can be treated as a dimensionless quantity for a given explosive type. For TNT, $P_* = 52.4$ and $\alpha = 1.13$ when P_{max} is in MPa, W is in kg, and R is in metres (see Fig. 1). The range of applicability of eq 1 is $3.4 < P_{max} < 138$ MPa. The numbers are not much different for other high-density solid explosives. Figure 2 gives a conversion of $(R/W^{1/3})$ to a true dimensionless radius, taking account of variations in charge density.

The detonation produces gas at high temperature and pressure, and this creates a bubble in the water. The gas bubble expands against hydrostatic pressure, but because of inertial effects the expansion does not cease until the bubble pressure has dropped well below the external water pressure. Eventually it collapses, again with inertial overrun, until the bubble pressure is well in excess of water pressure. This process gives rise to successive bubble pulsations. While these pulsations are occurring, a bubble in deep water rises by virtue of its buoyancy. However, proximity to surfaces complicates the translational motion; the bubble

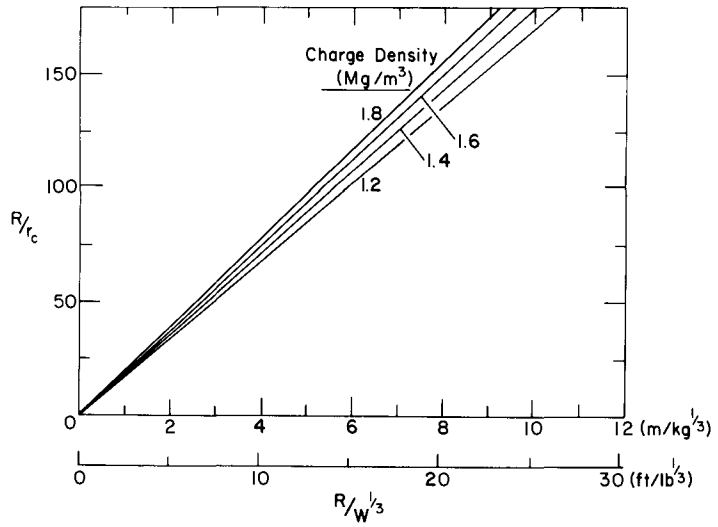

Figure 2. Conversion of scaled distance. The vertical axis gives distances normalized with respect to charge radius; the horizontal scale gives distances scaled with respect to the cube root of charge weight. The conversion is given for four values of charge density.

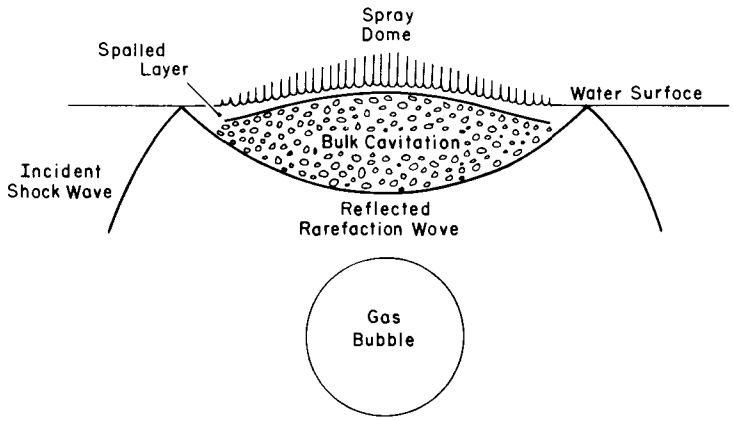

Figure 3. Spalling of the water surface by an underwater explosion. (After Young 1973.)

has a tendency to move towards solid boundaries and away from free boundaries. For present purposes, translational motion can be ignored. The maximum bubble radius R_{bm} for the first pulse in deep water* can be expressed as

$$\frac{R_{bm}}{W^{1/3}} = \frac{K}{(H+H_a)^{1/3}} \qquad (2)$$

where K is a constant for a given explosive type, H is charge depth (head of water) and H_a is the atmospheric pressure head ($\approx$ 10 m water). With R and H in metres and W in kg, the value of K for TNT is 3.50 and thus

$$\frac{R_{bm}}{W^{1/3}} = \frac{3.5}{(H+10)^{1/3}}. \qquad (3)$$

When an underwater charge is detonated at moderate depth, the water surface first receives an impulse from the shock wave. The incident (compressive) shock is reflected from the water/air interface as a rarefaction (tensile) wave, and the surface of the water "spalls off," creating a zone of cavitation behind the reflected wave (Fig. 3). However, the main surface disturbance is caused by the ejection of water displaced by the expand-

* An underwater explosion is usually considered to be "deep" when the charge depth is greater than R_{bm}. For present purposes, water can be regarded as "deep" when the depth is greater than $4R_{bm}$.

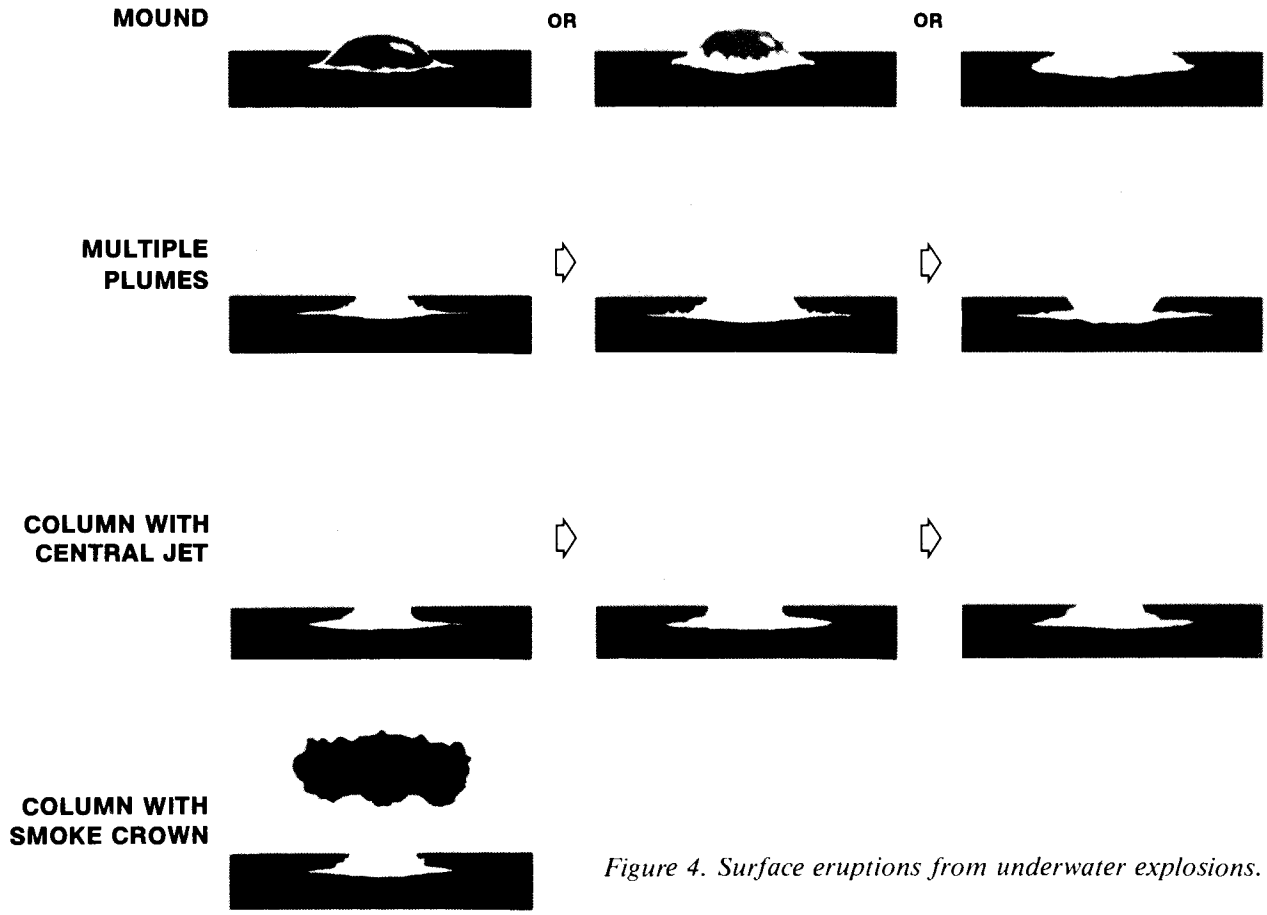

Figure 4. Surface eruptions from underwater explosions.

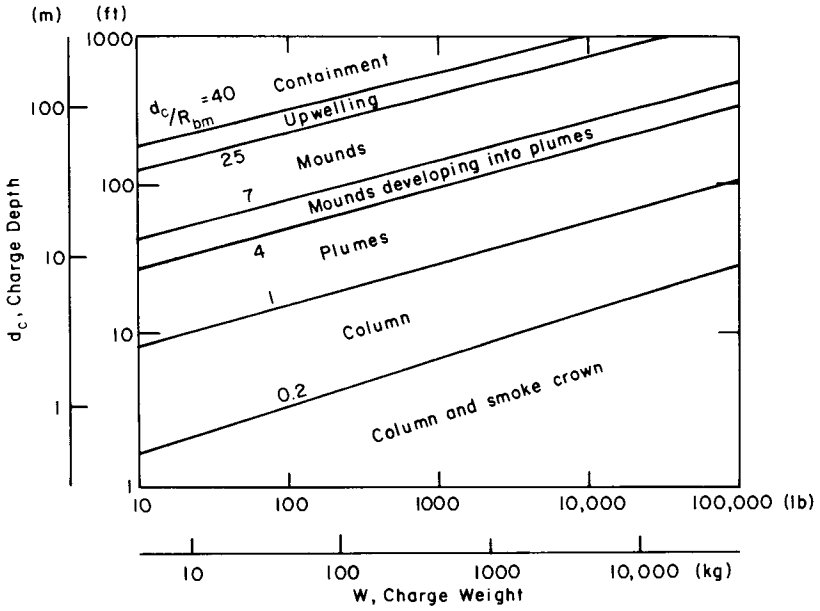

Figure 5. Surface effects from underwater explosions. (After Young 1971.)

ing gas bubble. If the scaled charge depth is not too great, the gas bubble causes an eruption of water, spray and gases (Fig. 4).

The general appearance of the overall waterspout changes with time, and its character varies with the scaled depth of the charge. Some limits for different types of surface behavior have been deduced by Young (1971), as shown in Figure 5. A charge which is sufficiently far below the surface does not produce any surface eruption or any emergence of explosion products. The limit for this kind of total containment has been deduced (Fig. 5) to be a charge depth d_c of at least 40 R_{bm}, where R_{bm} is the maximum bubble radius of the first pulse, as given by eq 3. For slightly shallower charges, with depths perhaps in the range $40 > d_c/R_{bm} > 25$, there is no surface eruption, but localized upwelling of explosion products occurs. As charge depth decreases into the range $25 > d_c/R_{bm} > 7$, the explosion forms a mound on the water surface. As d_c decreases through this range, the mound tends to change from a hump of turbulent water to a squat dome of foamy water and spray. Further decrease of d_c changes the surface mound to a low, rounded cloud of spray and eventually, say about $d_c/R_{bm} \approx 4$, this cloud starts to develop plumes shooting up around its perimeter. Within the range $4 > d_c/R_{bm} > 1$, plumes are well developed, looking like violently ejected projectiles of water which break up to form individual trails of spray. When the charge is at very shallow depth, with $d_c < R_{bm}$, the bubble bursts directly through the surface and forms a coherent vertical column of spray. At the heart of the column there may be a dense central plume, known as the jet. Smoke may emerge from the column, and if the charge is at very small depth ($d_c < 0.2\ R_{bm}$) there may be a visible "smoke crown" (black smoke in the case of an oxygen-deficient reaction).

The terminology for water thrown into the air by an underwater explosion is not always clear or consistent. This writer's understanding of U.S. terminology is as follows.

Upwelling. Water and explosion products rising to the surface at a point and flowing radially outward. There is no perceptible disturbance of the surface level.

Mound. A compact hump on the water surface consisting of turbulent water, foamy water, or foamy water plus spray. There is no ejection of discrete globs or jets of water.

Plume. The term "plume" should probably be reserved for the visible trail created by the high-speed ejection of a jet or glob of water. This plume is made up of a dense central core of water and a diffused boundary layer of spray. Plumes tend to shoot out in a ring near the perimeter of the waterspout, either vertically upward or inclined radially outward like the jets of a fountain. There may also be one or more plumes in the center of the cluster. Some people use the term "plume" to describe the entire outburst created by an underwater explosion, irrespective of its form. This latter usage undercuts the usefulness of the term, and seems to ignore the basic meaning of the word "plume."

Jet. The jet, or water jet, is the core of the central plume. It can sometimes be seen emerging from the top of the general spray cloud, reaching scaled heights of 30 m/kg$^{1/3}$ (75 ft/lb$^{1/3}$) or more when the charge depth is fairly small.

Column. The waterspout thrown up by a very shallow underwater explosion tends to have a more or less vertical columnar form. The term "column" is applied to either the entire waterspout, or to the outer sheath of the waterspout, recognizing that the column typically has a central *jet*. The column may have a slight flare at the base during the earlier stages of its development.

Base surge. When the waterspout collapses and falls back into the water, it creates an annular, or toroidal, cloud of spray and drives this spray radiantly outward as a "base surge."

For charges lying on the bed of shallow water, the maximum diameter of the base of the water column D_{max} is given by the following empirical relation (Swisdak 1978):

$$\frac{D_{max}}{W^{1/3}} = 3.71 \left(\frac{d}{W^{1/3}}\right)^{0.166} \approx 3.71 \left(\frac{d}{W^{1/3}}\right)^{1/6} \quad (4)$$

where d is charge depth (m) and D_{max} and W are in m and kg respectively. The limits of applicability for this empirical relation are $0.08 < (d/W^{1/3}) < 0.88$. Empirical relations are also available for the overall height and diameter of the waterspout from underwater TNT explosions (Swisdak 1978), but these are probably derived from large explosions going to large water depths (charge depth is scaled as m/kg$^{1/4}$).

Studies of waterspouts from underwater explosions (McAnally and Rand 1972, Outlaw and Strange 1974) have given empirical relations for the diameter of an "effective column" and for the internal jet of a waterspout. The effective column is a denser water column inside the masking spray cloud, while the jet is the high velocity vertical

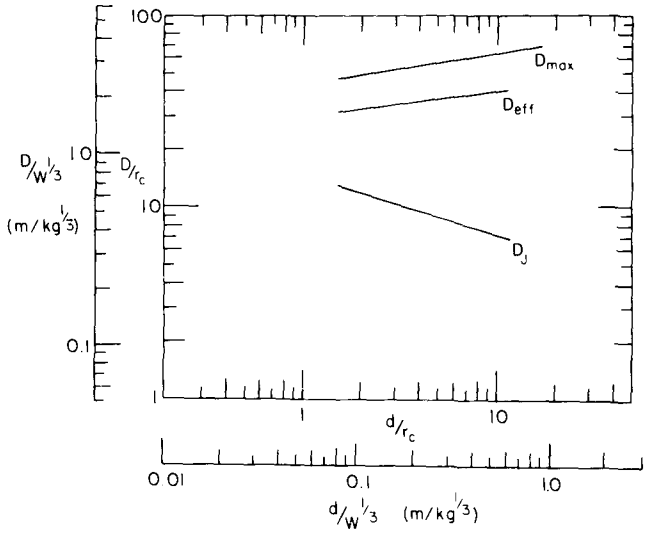

Figure 6. Effect of charge depth on: 1) the maximum diameter at the base of the water column, D_{max}, 2) the "effective" column diameter, D_{eff}, 3) the water jet diameter, D_j. (Data for D_{max} from Swisdak [1978]; data for D_{eff} and D_j from McAnally and Rand [1972] and Outlaw and Strange [1974].)

core of the waterspout. For deep water (and as a lower limit for shallow water) the effective column diameter D_{eff} and the jet diameter D_J are

$$\frac{D_{eff}}{r_c} = 29.6 \left(\frac{d}{r_c}\right)^{0.131} \quad (5)$$

and

$$\frac{D_J}{r_c} = 14.4 \left(\frac{r_c}{d}\right)^{0.3}. \quad (6)$$

There obviously ought to be limits set on these relations. The original data plots cover the range $2 < d/r_c < 11$.

Figure 6 displays the various empirical relations for column and jet diameters.

In considering charge depth, it is of some interest to define a depth d_*, where charge depth d is equal to the theoretical maximum bubble radius for the first pulse, R_{bm}. From eq 3:

$$d_* = R_{bm} = \frac{3.5\, W^{1/3}}{(H+10)^{1/3}} \quad (7)$$

where d_*, R_{bm} and H are in metres and W is in kg. In Figure 7 this relation (with slightly different constants) is plotted on logarithmic scales, and it is compared with a simple cube root relation between depth and charge weight. For the range of depths and charge sizes normally employed in ice blasting, the simple cube root relation is a good approximation. For very big charges (over 1 ton) at appropriate depths, scaling with respect to the one-fourth root of charge weight gives a better approximation. The approximation involved in cube root scaling of water depth effects is emphasized further in Figure 8, where $R_{bm}/W^{1/3}$ is plotted against absolute depth. Also marked on the graph are charge weights for which $d = R_{bm}$.

The vertical velocity of the water jet can be obtained from sequential photographs. The velocity of the jet tip decreases with time, down to zero at the maximum jet height. The initial jet velocity $(V_J)_0$ can be estimated by tracking back to time zero; values obtained in this way by McAnally and Rand (1972) and by Outlaw and Strange (1974)* are shown in Figure 9.

If a horizontal plate lies above the ejected waterspout, energy and force are transmitted to the plate. McAnally and Rand (1972) and Outlaw and Strange (1974) made observations on a target plate, and by suitable analysis derived values for the force transmitted by the water jets of 1-lb TNT charges (Fig. 10). The numbers are quite consistent, indicating that force is a maximum at a charge depth of $d/r_c \approx 5$, i.e. $d/W^{1/3} \approx 0.7$ fb/lb$^{1/3}$ $\approx$ 0.27 m/kg$^{1/3}$. Scaling factors for the water jet force were also considered.

* Equation 4.3 in Outlaw and Strange (1974) seems incorrect, and Figure 4.3 gives a "shallow water" curve that is not fully supported by experimental data.

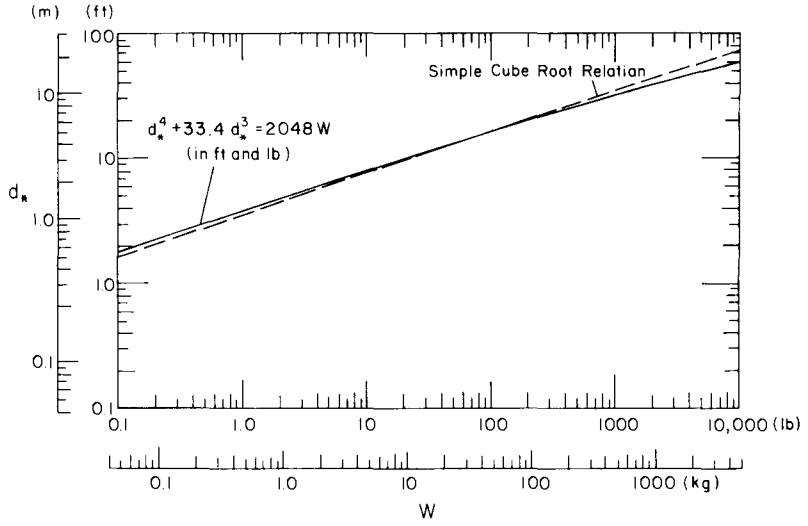

Figure 7. Depth d_* *which is equal to the theoretical maximum bubble radius for the first pulse,* R_{bm}. *The relation which takes account of hydrostatic pressure is compared with a simple cube root approximation.*

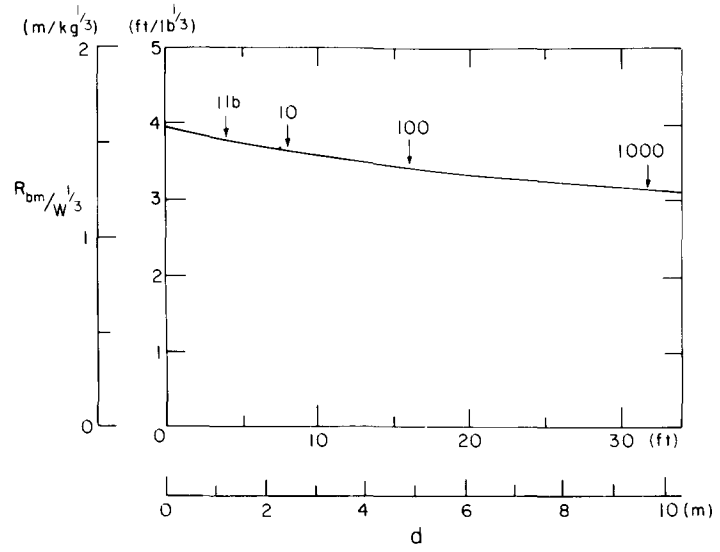

Figure 8. Theoretical maximum bubble radius R_{bm} *scaled with respect to the cube root of charge weight and plotted against absolute charge depth. The arrows indicate the values of* $R_{bm}/W^{1/3}$ *at which* $d = R_{bm}$ *for various charge weights.*

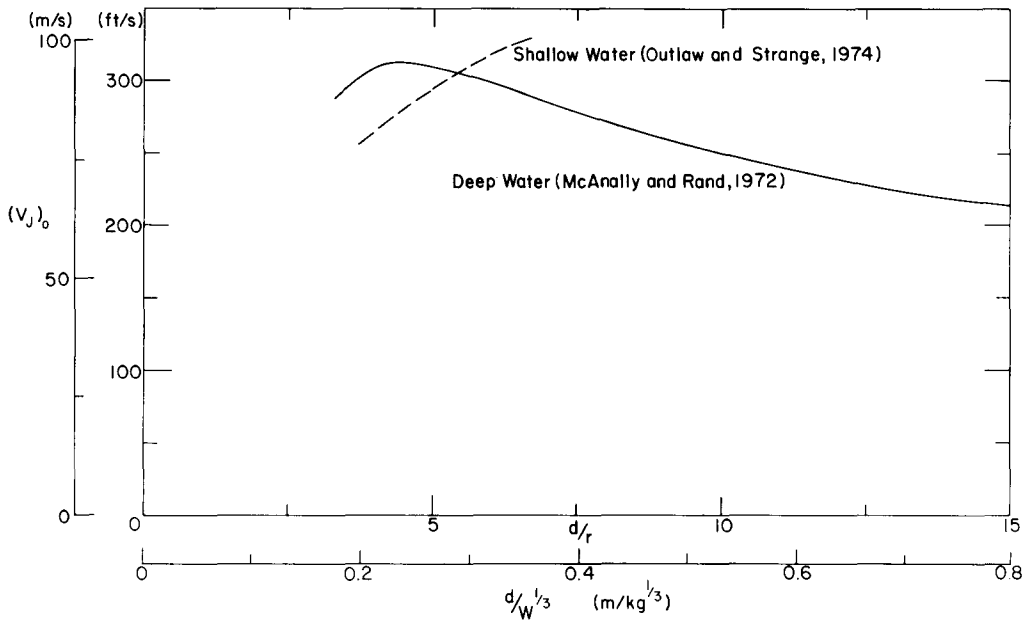

Figure 9. Initial velocity of the emerging water jet plotted against charge depth for underwater explosions. (Data from McAnally and Rand [1972] and Outlaw and Strange [1974].)

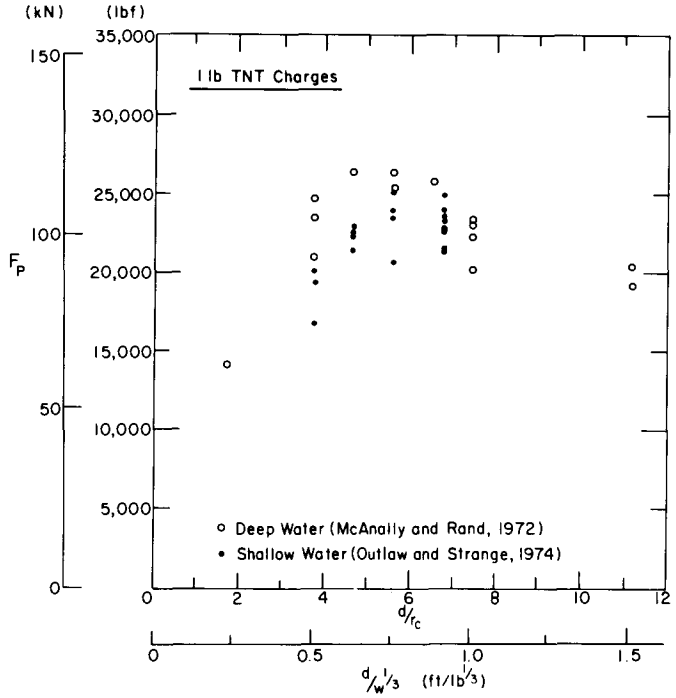

Figure 10. Force exerted on a horizontal plate by the waterspout from a 1-lb charge of TNT fired at various depths in the water.

REGRESSION ANALYSIS FOR ICE-BLASTING DATA

A basic requirement in ice blasting is to predict the size of the "crater" produced by a single charge. The dependent variable, which is what we want to predict, is crater radius. The independent variables, representing the input data for the prediction, are charge size, explosive type, charge depth, and ice thickness.

Because the number of data sets available for regression analysis is rather small, it is necessary to somehow reduce the number of variables.

Explosive type is the first candidate for deletion, since experience suggests that crater size does not vary greatly for different types of common explosives. Even extreme variations of explosive type may have relatively little effect, since tests with low-pressure gas-blasting devices (Mellor and Kovacs 1972) indicated that these devices broke just about the same area of ice as did high explosive charges of comparable energy content. There are equivalence factors for adjusting the charge weight of a given explosive so that it performs in some respect equal to a reference explosive. However, these factors differ depending on whether the adjustment is for peak shock pressure, bubble energy, total energy, impulse, time constant, energy flux density, or whatever. For production of the MM72 curves and for the present exercise, variation of explosive type was ignored. If a simple overall model for ice blasting should eventually emerge, the data can be reanalyzed with charge weights adjusted by an appropriate factor. If cube root scaling is used, the adjustment may not have a large effect, since the final factor is the cube root of a number which is usually not far from unity.

Another way to reduce the number of variables is to invoke some physics, so as to express one variable in terms of another. In the present context, an obvious expedient is cube root scaling, which derives from similitude considerations. One possible objection to this is that gravity effects are not covered by cube root scaling, as can be seen by referring back to the discussion of bubble size as a function of charge depth. However, for the ranges of charge size (mostly < 70 kg) and charge depth (mostly < 10 m) which are represented in the field data, cube root scaling of charge depth seems to be a perfectly acceptable approximation. The point is emphasized by Figure 11, which is a replotted version of Young's (1971) scheme for characterizing waterspouts. Figure 11 gives the proposed dividing lines between different forms of surface eruption in terms of scaled charge depth for a range of absolute charge sizes. Over the typical range of charge sizes used in icebreaking, say 1–100 lb (0.5–50 kg), the value of $d_c/W^{1/3}$ for transition from one type of waterspout to another does not vary much.

Perhaps to some people a more troubling factor is that the horizontal dimensions for *flexural* breakage of ice sheets might not necessarily depend on the magnitude of applied force or normal

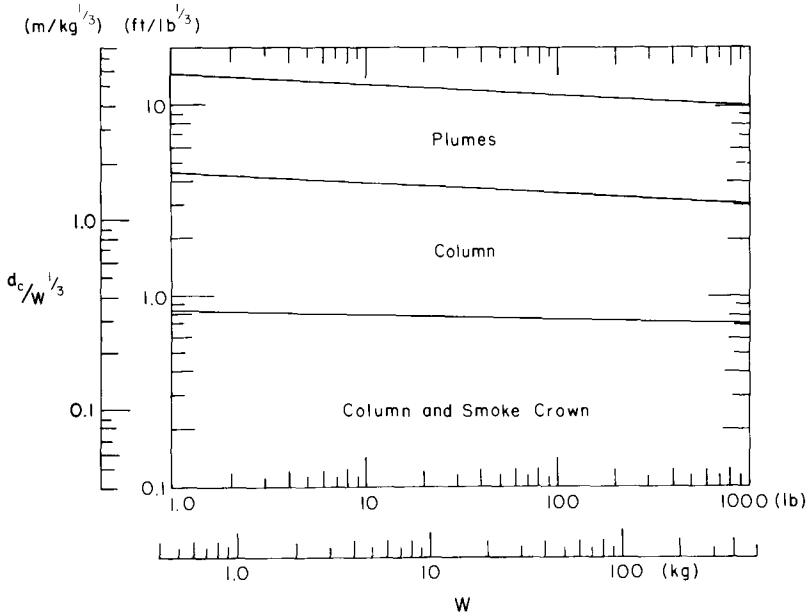

Figure 11. Re-plot of Figure 5 to show variation of waterspout characteristics with scaled charge depth.

displacement. In static cases, flexural dimensions are controlled largely by ice thickness, by the elastic properties of the ice, and by the reaction of the supporting water. Thus, if the underwater explosion had an effect similar to that of a concentrated static uplift force, the fracture radius might be independent of the magnitude of that force. For the purpose of regression analysis, cube root scaling of linear dimensions was adopted, but it was recognized that in some cases the crater radius might conceivably include an increment attributable to flexure, and controlled by ice thickness and ice properties. In particular, flexural breaks by charges of minimum effective weight or at maximum effective depth were of concern.

By ignoring variations of explosive type and by scaling the crater radius, the charge depth, and the ice thickness with respect to charge weight, we are left with only two independent variables:

$$\text{Scaled crater radius, } Y = R_c/W^{1/3}$$
$$\text{Scaled charge depth, } X_1 = d_c/W^{1/3}$$
$$\text{Scaled ice thickness, } X_2 = t/W^{1/3}.$$

The chosen regression equation is a polynomial with cross-products and terms up to the third power:

$$Y = b_0 + b_1X_1 + b_2X_2 + b_3X_1^2 + b_4X_1X_2 + b_5X_2^2 + b_6X_1^3 + b_7X_1^2X_2 + b_8X_1X_2^2 + b_9X_2^3. \quad (8)$$

The basic data used for the analysis are given in Appendix A, together with source references. The scaled input data, i.e. Y, X_1, X_2, are tabulated in Appendix B, and the weighting for replicate sets is explained. Appendix C gives the computer output for the initial regression analysis.

The analysis assumes that X_1 and X_2 are exact values and that all error is in determinations of Y. The effective number of data sets is 291, and the initial number of regression variables (the "b" coefficients) is 10. With the variables in English units (see Appendix B), the best values of the coefficients are as follows:

b_0	4.8722	b_5	-0.019293
b_1	0.14566	b_6	0.0079326
b_2	0.32645	b_7	0.0021915
b_3	-0.15269	b_8	-0.00052360
b_4	-0.0015176	b_9	0.00026389

With these coefficients, the standard error of Y about the regression plane is 1.268 ft/lb$^{1/3}$. The multiple correlation coefficient $r = 0.7066$ ($r^2 = 0.4993$), and the F-test value is 31.136 for 281 degrees of freedom with nine parameters.

To examine the relative significance of each term in the polynomial, stepwise regression was carried out, with coefficients being deleted successively on the basis of T-test values (Appendix C). Coefficients dropped out in the following order (least significant first):

$$b_4, b_1, b_8, b_7, b_6, b_9, b_2, b_5.$$

Dropping b_4 and b_1 resulted in a very slight improvement in the standard error of estimate (to 1.265 ft/lb$^{1/3}$) without significant change in the correlation coefficient. For final calculation of the design curves, b_4 and b_1 were deleted (Appendix D). In the 1972 work, the same two coefficients were dropped.

When the original work was done in 1972, it was obvious that the available data were ill-conditioned for regression analysis, since most tests had been made with conditions close to optimum. In subsequent field testing, the tendency to optimize was maintained. Experimenters avoided the use of charges that are too small for good breakage, charges that are unnecessarily large, and charge depths that are too great for good breakage. This means that the regression is likely to be unreliable for large-scaled charge depth, and for extremes of scaled ice thickness. Another source of uncertainty is inconsistency in defining and measuring crater radius. Some craters have a clear demarcation between the highly fragmented ice of the central crater and the surrounding intact ice. Other craters have a central zone with heavy fragmentation, surrounded by ice which has been flexed and cracked, but which is still in place. The transition from obvious flexural damage to the zone of insignificant radial and circumferential cracks may be hard to define, especially when the ice has a thick snow cover. We might add to this list a suspicion that observers occasionally suffer from the "fisherman syndrome," wanting to get the best possible values without actually cheating.

Figure 12 shows how well, or badly, the regression equation represents the data. For each reported value of scaled crater radius Y_a, the regression equation calculates a value Y_p, using the values of X_1 and X_2 which correspond to Y_a. In Figure 12 the predicted value Y_p is plotted against Y_a. The earlier tendency for the 1972 regression equation to underpredict for the largest craters (Fonstad et

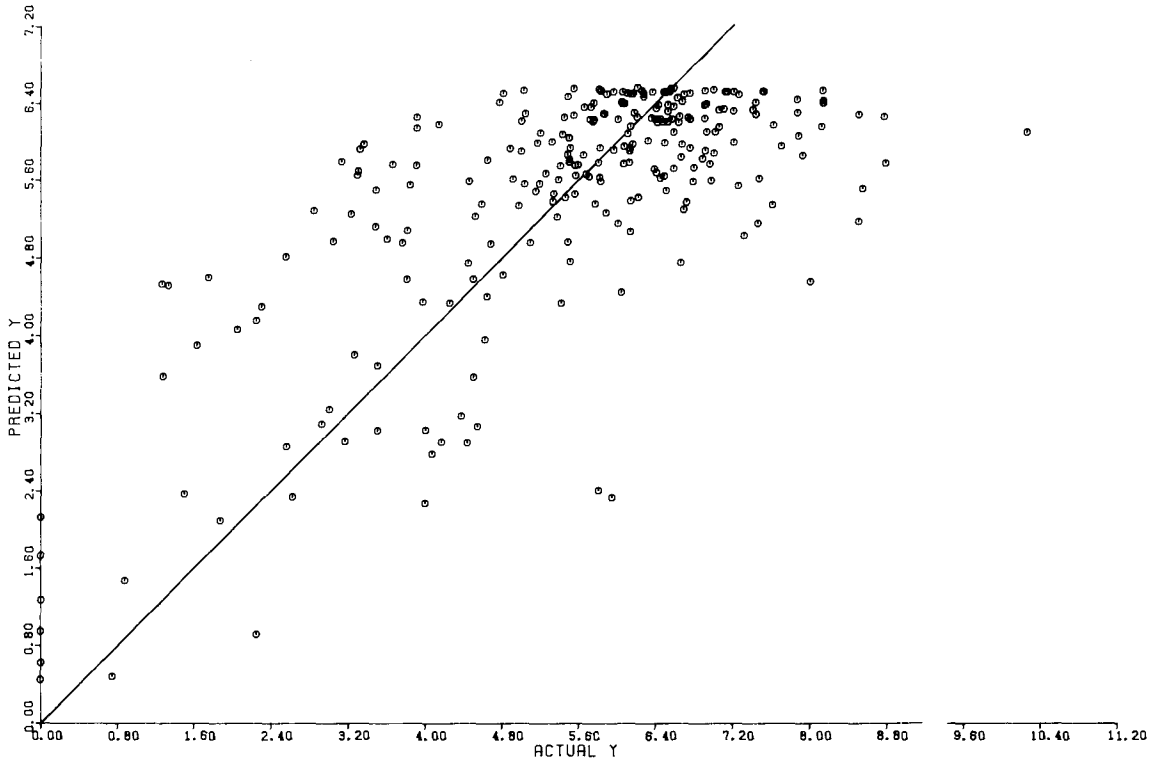

Figure 12. Values of scaled crater radius predicted by the regression relation plotted against the corresponding observed values.

al. 1981) is no longer apparent, but for very small craters the new regression equation still appears to overpredict. The scatter about the 1:1 line in Figure 12 is large, and it is worth looking at the data points more closely to see what might cause the greatest departures from the regression plane.

In Appendixes C and D, values of Y_a and Y_p are tabulated for each data set. Alongside each pair of Y values, the residual representing $Y_a - Y_p$ is given. Another value, in the last column, gives the residual divided by the standard error of Y about the regression plane. In Table 1, these residuals are used to compare the data from various sources and for various types of explosive. For each distinct group of data sets, the table gives the relative proportions of positive and negative residuals, i.e. the percentage of data sets for $Y_a > Y_p$ and for $Y_a < Y_p$ respectively. The table also gives the percentages where Y_a is above or below the standard error of Y_p. Finally, the table shows what proportion of the data has values of Y_a above or below a value that is outside a range more than twice the standard error of Y_p.

Because some of the residuals are very small, the overall ratio of positive to negative residuals is not very illuminating. A better test is provided by the relative proportions of Y_a values which fall outside the positive and negative limits set by the standard error. Looking down the appropriate columns of Table 1, it can be seen that for some of the data sources the Y_a values agree well with Y_p, having most results inside the limits of the standard error, and a balance between positive and negative values of the most extreme residuals. In this category are the results of Van der Kley for guncotton (nitrocellulose), American TNT, and dynamite; the Frankenstein and Smith results for ANFO; the results of Fonstad et al. for DM-12; and Nikolayev's results for trotyl (Russian TNT). Balanced results with somewhat greater scatter include those of Van der Kley for Dutch TNT, and of Mellor for TNT. A strong imbalance with $Y_a < Y_p$ appears in the entries of Van der Kley for gunpowder, of Fonstad et al. for the blasting agents Amex II (ANFO) and Hydromex (AN/TNT slurry), and of Wade for ANFO. Since all of these entries represent low velocity blasting agents rather than true high explosives, they suggest that such substances might systematically produce smaller craters than high explosives. The only contradiction is the single test result (or estimate) for ANFO by Frohle, which can probably be discounted in this context. Looking for strong imbalances with $Y_a > Y_p$, and ignoring the single shot described by

Table 1. Analysis of departures from regression plane.

Data source	*Explosive type*	*Effective no. of data sets*	*% of results above std error*	*% of results below std error*	*% pos. residuals*	*% neg. residuals*	*% std residuals above +2.0*	*% std residuals below −2.0*	*Ident. in App. D*
Van der Kley	Dutch TNT	22	14	18	41	59	0	5	A
Van der Kley	Guncotton	15	0	0	67	33	0	0	B
Van der Kley	American TNT	5	0	0	0	100	0	0	C
Van der Kley	Gunpowder	24	0	58	17	83	0	8	D
Van der Kley	Dynamite	29	7	0	72	28	0	0	E
Wade	ANFO	6	17	67	33	67	17	0	F
Froehle	ANFO	1	100	0	100	0	0	0	G
Kurtz et al.	C-4	18	11	17	72	28	6	0	H
Frankenstein & Smith	ANFO	3	0	0	67	33	0	0	I
Purple	C-4	4	25	0	50	50	25	0	J
Barash	TNT	33	36	6	67	33	3	3	K
Barash	HBX-3	5	40	0	60	40	40	0	K
Mellor & Kovacs	Dynamite	7	29	43	29	71	14	0	L
2nd Engr Battalion	TNT	4	50	0	100	0	0	0	M
Mellor	TNT	25	16	20	36	64	0	4	N
Fonstad et al.	DM-12 & dynamite	74	4	7	55	45	0	0	O
Fonstad et al.	Blasting agents	3	0	67	33	67	0	67	O
Nikolayev	Trotyl (TNT)	13	0	0	31	69	0	0	P

Frohle, the candidates are the results by Purple (C-4), Barash (TNT and HBX-3), and the 2nd Engineer Battalion (TNT). They all represent high velocity high explosives, but there are other data sets for TNT, C-4, and DM-12 which show good balance and good agreement with the regression relations.

Another characteristic which can be examined is the distribution of "wild points" which have departures of twice the standard error or more. "Wild points" for gunpowder (Van der Kley) and for AN blasting agents (Fonstad et al.) are negative, and consistent with the general distributions for the data group. In the opposite sense (positive residuals), the trend for "wild points" remains consistent with the overall distribution for the HBX-3 data of Barash, and for the C-4 data of Purple. In all the other groups there is no obvious relation of "wild points" to explosive type or to overall distributions.

To push the exploration a bit further, all data sets with a residual greater than 1.8 times the standard error were identified, and the basic test records were examined. To check for a possible breakdown of cube root scaling, these "wild points" were arranged in three groups according to absolute charge weight. For charges $\leq$ 1 kg, there were only two data sets with positive residuals, but six sets with negative residuals. However, two of the latter were for low velocity blasting agents. For charges between 1 and 10 kg, there were three positive and four negative residuals. Two of the positive residuals were for HBX-3 and the other was for C-4. Two of the negative residuals were for gunpowder, and two were for dynamite when the ice carried a very thick snow cover. For charges heavier than 10 kg, there were five positive and five negative residuals. Four of the negative residuals were for gunpowder, and one was for C-4. Two of the positive residuals were for ANFO, two for TNT and one for C-4. In short, there is no clear relation between the charge weight and the distribution of "wild points."

The same data sets were examined for possible dependence on absolute ice thickness, scaled ice thickness, and scaled charge depth, but there were no obvious relationships.

One thing which is fairly obvious, both from Figures 13 and 14, is the inability of the regression equations to predict reliably the limiting charge depth at which crater radius goes to zero. There is no mystery about why this should be so, since only six data sets give zero values for Y_a (two from Barash, four from Mellor, all for TNT). The scarcity of data sets giving small values of Y_a allows the regression equation to be controlled by more heavily populated parts of the data domain.

Not much can be said about the possibility of errors in the input data. The most likely sources of error are inconsistencies in defining crater radius, and imprecise measurement of ice thickness. There are indications that some data sets might have been affected in this way, but for present purposes they have to be accepted at face value. Inspection of the data in Appendix A gives some idea of the possibilities for input error. Crater dimensions given by Wade were measured to the nearest 10 ft, giving an uncertainty of $\pm 8\%$ to $\pm 17\%$. The 1977 data from the 2nd Engineer Battalion suggest an uncertainty of $\pm 8\%$ in crater diameter.

No consideration has been given yet to ice type. The effective mechanical properties of the ice vary with absolute thickness of the ice cover, and with the temperature of the upper layers. With thick ice and low air temperatures, the ice tends to be elastic and brittle. With thin ice and/or high air temperatures, the ice may be relatively soft, or even mushy. Another oversight is failure to account for snow cover on the ice. Even though the strength of snow may be negligible, its mass could be significant where small charges are involved. For example, 16 in. of snow at a mean density of 0.25 Mg/m^3 (specific gravity 0.25) is equivalent to 4 in. of water, and for a 1-lb charge this might have a similar effect to increase of the charge depth by an increment of 0.33 ft (i.e. 0.33 $ft/lb^{1/3}$).

GENERAL FEATURES OF THE REGRESSION CURVES

The curves shown in Figures 13 and 14, referred to as the MM82 curves, are broadly similar to the MM72 curves, but there are some significant differences.

Looking first at the effect of charge depth (Fig. 13), it can be seen that for all ice thicknesses the crater radius is greatest where charge depth is close to zero; the crater size decreases as charge depth increases. The curves are considered unreliable for $(d_c/W^{1/3}) > 7$ $ft/lb^{1/3}$, since there are very few data sets for large charge depth. The curve shown for $(t/w^{1/3}) = 0$ is, of course, unsupported by actual data. The curves for $(t/W^{1/3}) = 35$ and 40 $in./lb^{1/3}$ have only weak support from actual data. The distinctive optimum depth pattern of the MM72 curves has virtually disappeared, and for most practical purposes, zero charge depth is optimum.

Turning to the effect of ice thickness (Fig. 14),

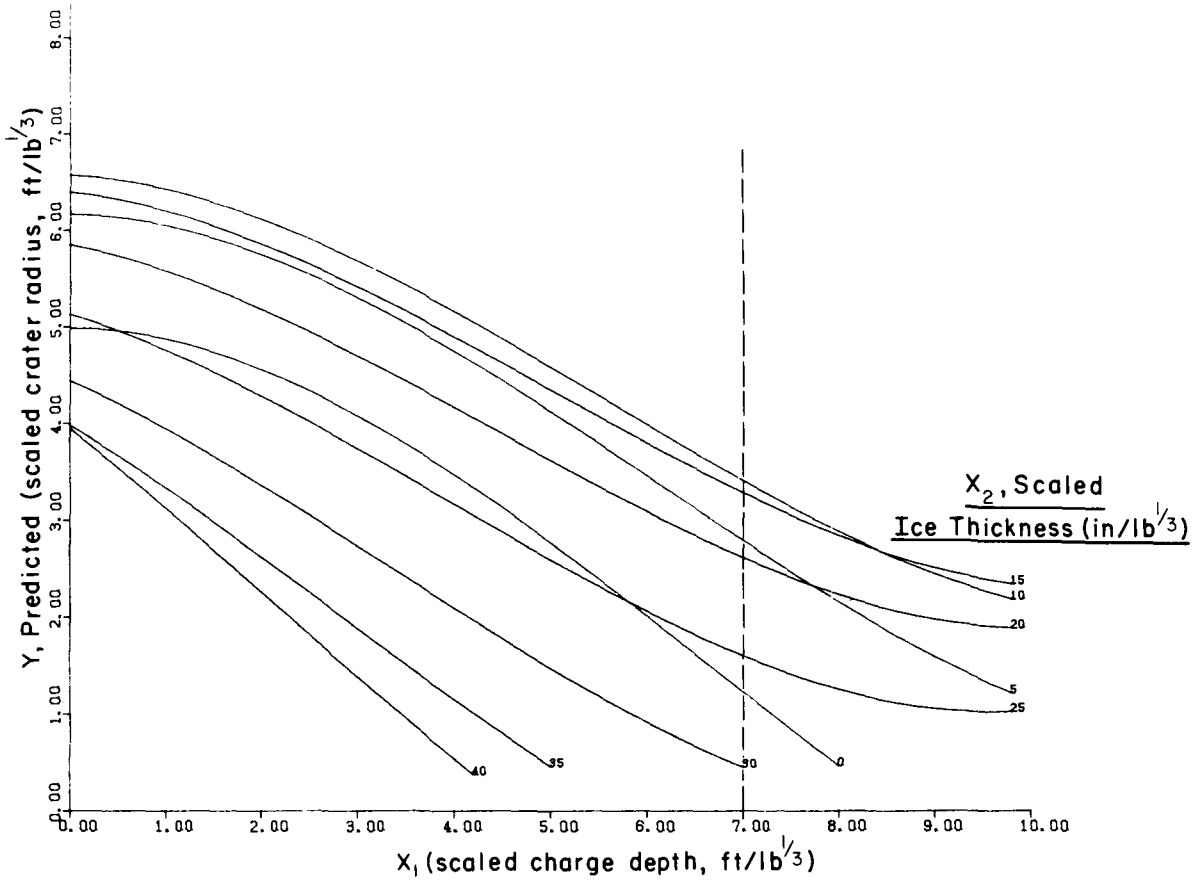

Figure 13. Predicted value of scaled crater radius as a function of scaled charge depth, with scaled ice thickness as parameter.

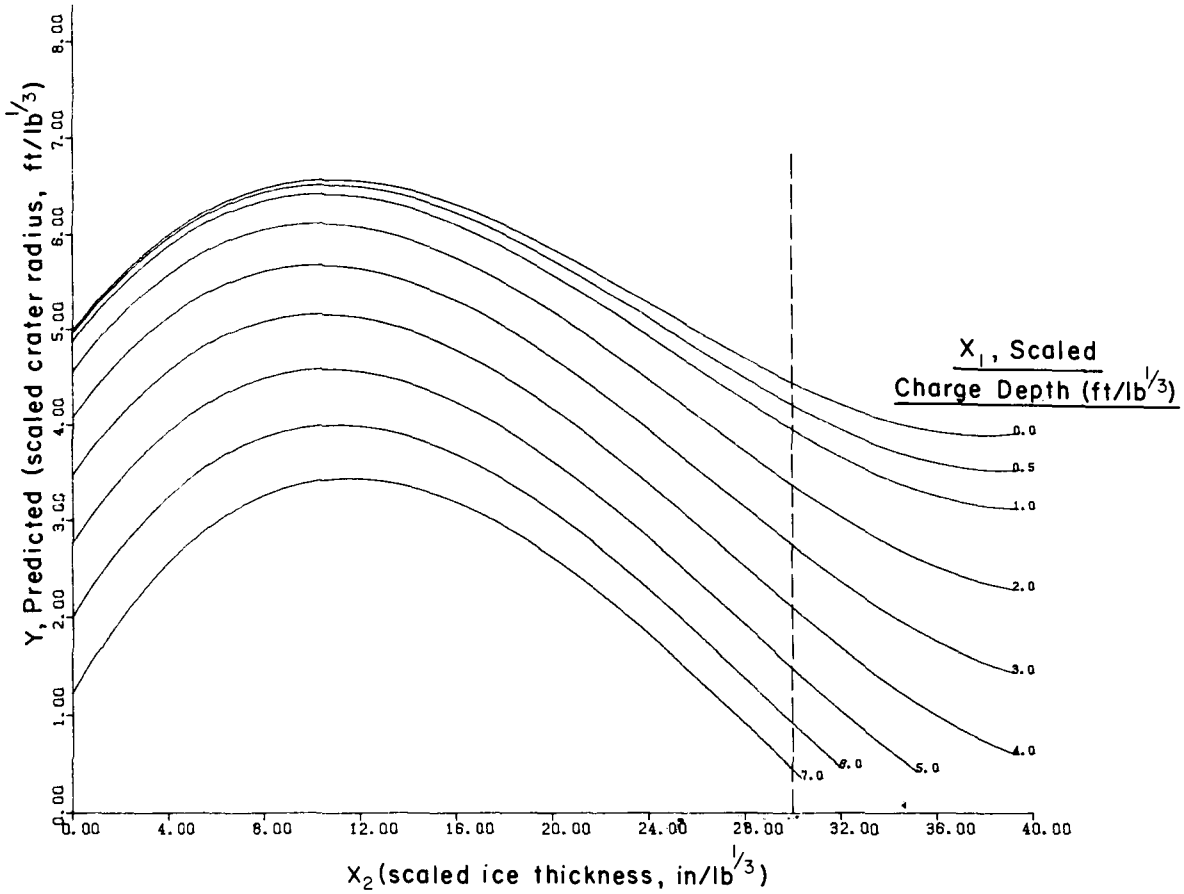

Figure 14. Predicted value of scaled crater radius as a function of scaled ice thickness, with scaled charge depth as parameter.

there is a very clear indication of optimum ice thickness at all charge depths. There is a slight shift of optimum ice thickness as charge depth varies, but for most practical purposes it seems sufficient to accept a constant value of $(t/w^{1/3})$ = 10.5 in./lb$^{1/3}$ as the optimum thickness when charge depth is in the range 0 to 5 ft/lb$^{1/3}$. The MM72 curves gave optimum thickness of $(t/w^{1/3})$ = 10 in./lb$^{1/3}$ for small charge depths. For scaled thicknesses greater than 11 in./lb$^{1/3}$, crater radius decreases for all charge depths. The curves are considered unreliable for thicknesses greater than 30 in./lb$^{1/3}$ because of the shortage of data at large values of scaled thickness.

For a charge of optimum weight placed at optimum depth, the MM82 curves predict a maximum crater radius of almost 6.6 ft/lb$^{1/3}$. The MM72 curves were a little bit more optimistic, predicting about 6.9 ft/lb$^{1/3}$.

USE OF THE REGRESSION CURVES AS DESIGN CURVES FOR ICE BLASTING

The regression curves, Figures 13 and 14, can be used to predict the effects of under-ice explosions, or to select charge sizes and charge spacings for ice demolition. For a start, we consider only single charges.

In typical circumstances, the user can measure or estimate the ice thickness t. If the aim is to maximize the damage from a blast, the user can plan on firing the charge at essentially zero depth, i.e. directly beneath the ice cover. In order to calculate the optimum charge weight W, it can be assumed that greatest efficiency will be achieved when $(t/W^{1/3})$ = 10.5 in./lb$^{1/3}$, so that

$$W_{opt} = (t/10.5)^3 \qquad (9)$$

where W_{opt} is in lb and t is in inches. If the user prefers to work with SI units, the optimum condition is given by

$$t/W^{1/3} = 0.347 \text{ m/kg}^{1/3}$$

or,

$$W_{opt} = (t/0.347)^3 \text{ kg}$$

when t is in metres and W is in kg. The procedure can be illustrated by a numerical example.

Example. The measured ice thickness on Lake Jokich is 17½ in. What size of explosive charge will be most efficient for breaking the ice? What will be the diameter of the crater made by a charge of optimum weight?

Ice thickness t = 17.5 in.

Optimum condition is:

$$\frac{t}{W^{1/3}} = 10.5 \text{ in./lb}^{1/3}$$

$$W^{1/3} = \frac{t}{10.5}$$

$$= \frac{17.5}{10.5} \text{ lb}^{1/3}$$

$$W = \left(\frac{17.5}{10.5}\right)^3 = 4.63 \text{ lb.}$$

If the explosive is packaged in pound quantities, the probable practical choice would be a 5-lb charge. If the explosive is packaged in kilogram quantities, a 2-kg charge would be close enough.

For prediction of the crater radius, the actual charge weight is used. The best result is likely to be obtained with the charge in the water immediately below the ice cover. Reading from the curves in Figures 13 and 14 for scaled charge depths close to zero and $t/W^{1/3}$ close to optimum, the highest value of the predicted crater radius R is about 6.57 ft/lb$^{1/3}$, i.e.

$$\frac{R}{W^{1/3}} = 6.57 \text{ ft/lb}^{1/3}.$$

Taking W = 5 lb,

$$R = 6.57 \times 5^{1/3} \times = 11.23 \text{ ft}$$

and the predicted crater diameter is 22.5 ft for typical high explosives.

In some circumstances the use of optimum size charges may be a false economy. For example, if the ice is very thin the optimum charge weight will be small and the size of a single crater will be small. This means that in order to blast a broad area of ice, many shotholes have to be drilled and many individual charges have to be placed and connected to firing lines. Provided that plenty of explosive is available, it may be quicker and cheaper to use a few big charges instead of many small charges. The general idea can be illustrated by a numerical sample.

Example. The ice on the Slim Jim River is 6 in. thick. Calculate the optimum charge weight for best explosive energy efficiency, and estimate the crater size for a single charge of

optimum weight. Consider some alternative charge sizes, and estimate the corresponding effects.

Taking $(t/W^{1/3}) = 10.5$ in./lb$^{1/3}$ as the optimum condition, and noting that $t = 6$ in.,

$$W_{opt} = \left(\frac{t}{10.5}\right)^3$$

$$= \left(\frac{6}{10.5}\right)^3$$

$$= 0.19 \text{ lb.}$$

This weight is about one-fifth of the weight of a standard 1-lb block of military TNT. If the cardboard sheath of a 1-lb TNT charge is removed, five small slabs of cast TNT are revealed. The optimum charge weight just calculated is equal to only one of these small slabs.

If one of these optimum charges is placed immediately beneath the 6-in. ice cover, the predicted value of scaled crater radius is 6.57 ft/lb$^{1/3}$, and so the actual crater radius is:

$$R = 6.57\,W^{1/3}$$

$$= 6.57 \times 0.57$$

$$= 3.75 \text{ ft.}$$

This means that the crater diameter is 7.5 ft.

A crater 7.5 ft in diameter is a good return for a few ounces of explosive, but it is an unimpressive hole in the ice cover of a wide river. As alternatives to the optimum charge, consider the effects of a 5-lb charge and a 20-lb charge, each fired immediately below the ice.

Taking $R = 6.57\,W^{1/3}$ ft/lb$^{1/3}$, the predicted crater radii for a 5-lb charge and a 20-lb charge are:

5 lb $\quad R = 6.57 \times 1.71 = 11.23$ ft

20 lb $\quad R = 6.57 \times 2.71 = 17.83$ ft.

The respective diameters are 22 ft and 36 ft.

The approximate areas of ice broken by charges of 0.19, 5, and 20 lb are 44, 400 and 1000 ft^2 respectively. The returns in terms of demolished area per unit charge weight are: 233 ft^2/lb for an optimum (0.19-lb) charge, 79 ft^2/lb for a 5-lb charge, and 50 ft^2/lb for a 20-lb charge. However, the work involved in drilling and loading one shothole is about the same for any of these charges, and it may be more efficient operationally to use a relatively small number of big charges rather than a very large number of little charges.

There may be situations in which the charge will not be at optimum depth for some operational reason. In such cases, the design curves might be entered for finite values of scaled charge depth. The procedure can be illustrated by a numerical example.

Example. An ice bridge is to be built across Maird Inlet, where the mean water depth is 4 m. The ice bridge will not have continuous reinforcement, and its design thickness is 0.8 m. Demolition charges will be laid on the sea bed beneath the bridge. Estimate the size of a single charge which will be capable of cratering the ice bridge efficiently.

Looking at the curves in Figure 14, the optimum value of scaled ice thickness (peak of the curve) will probably be slightly greater than the value 10.5 in./lb$^{1/3}$ used in previous examples, but not much. We can take the value 11 in./lb$^{1/3}$, but the small difference from 10.5 in./lb$^{1/3}$ is hardly worth fussing over. Using the design ice thickness of 0.8 m (31.5 in.) to estimate the best charge weight from the relation $(t/W^{1/3}) = 11$ in./lb$^{1/3}$,

$$W = \left(\frac{t}{11}\right)^3$$

$$= \left(\frac{31.5}{11}\right)^3$$

$$= 23.5 \text{ lb.}$$

For practical reasons we round this value up to 25 lb, and then check the probable effects of a 25-lb charge.*

The charge will be set approximately 4 m below the water surface, and the ice will extend almost 0.8 m below the water surface. Thus the depth of the charge below the base of the ice (d_c) will be about 3.2 m (10.5 ft). The scaled charge depth ($d_c/W^{1/3}$) will thus be

$$\frac{d_c}{W^{1/3}} = \frac{10.5}{25^{1/3}}$$

$$= 3.56 \text{ ft/lb}^{1/3}$$

and the scaled ice thickness for a 25-lb charge will be

$$\frac{t}{W^{1/3}} = \frac{31.5}{25^{1/3}}$$

$$= 10.8 \text{ in./lb}^{1/3}.$$

*We could equally well round this off to a 10-kg charge and continue the calculation with that value.

In Figure 13, a vertical line drawn through the value 3.56 on the horizontal axis cuts the curve for 10 in./lb$^{1/3}$ at a Y-value of about 5.4 ft/lb$^{1/3}$. It cuts the curve for 15 in./lb$^{1/3}$ at a Y-value of about 5.1 ft/lb$^{1/3}$. The Y-value for $t/W^{1/3}$ = 10.8 in./lb$^{1/3}$ is, by interpolation, about 5.35 ft/lb$^{1/3}$. Finally the predicted radius of the crater R_c is given by

$$\frac{R_c}{W^{1/3}} = 5.35 \text{ ft/lb}^{1/3}$$

i.e.

$$R_c = 5.35\, W^{1/3}$$

$$= 5.35 \times 25^{1/3}$$

$$= 15.64 \text{ ft},$$

which means a predicted crater diameter of 31 ft (9.5 m) for a single 25-lb (11.3-kg) charge lying on bottom.

A similar, but less closely defined, problem is given in the following example.

Example. Mines are to be laid on a river bed to permit demolition of the winter ice cover while hostile forces are crossing. Each mine contains 150 lb of explosives, and the maximum recorded winter ice thickness is 21 inches. Calculate the maximum water depth for effective operation of the mines.

For this problem, assume that there will be no enhancement of the explosion effect by having the charge lying on the river bed, and make the arbitrary assumption that the mine has to produce a crater that is within 25% of the maximum possible size. The scaled ice thickness is very small:

$$\frac{t}{W^{1/3}} = \frac{21}{150^{1/3}}$$

$$= 3.95 \text{ in./lb}^{1/3}.$$

A scaled crater radius 25% smaller than the maximum value of 6.57 ft/lb$^{1/3}$ has the value 4.93 ft/lb$^{1/3}$. Referring to Figure 14 and drawing lines through X_2 = 3.95 and Y = 4.93, the intersection point lies just below the curve for X_1 = 3 ft/lb$^{1/3}$. Making an arbitrary (and slightly conservative) choice of X_1 = 3 ft/lb$^{1/3}$ for the maximum operational water depth, the absolute depth value d is

$$d = 3 \times (150)^{1/3}$$

$$= 15.94$$

$$\approx 16 \text{ ft}.$$

The mines should therefore be laid in places where the winter river depth is not more than 16 ft.

Another use for the design curves is prediction of the cratering effects from an underwater charge when all input data are given, as in the example below.

Example. What size of crater can be expected if a 40-lb charge is fired 7 ft below the base of a 19-in.-thick ice cover?

Scaling the charge depth and the ice thickness:

$$\frac{d_c}{W^{1/3}} = \frac{7}{40^{1/3}}$$

$$= 2.05 \text{ ft/lb}^{1/3}$$

$$\frac{t}{W^{1/3}} = \frac{19}{40^{1/3}}$$

$$= 5.56 \text{ in./ft}^{1/3}.$$

It is convenient to use the curves in Figure 14, drawing a vertical line through the X_2 value of 5.56 in./lb$^{1/3}$. This cuts the curve for X_1 = 2 ft/lb$^{1/3}$ at a Y-value of about 5.8 ft/lb$^{1/3}$. The small difference between $(d_c/W^{1/3})$ = 2.05 and $(d_c/W^{1/3})$ = 2.0 is not worth bothering about. Thus,

$$\frac{R_c}{W^{1/3}} = 5.8 \text{ ft/lb}^{1/3}$$

and

$$R_c = 5.8 \times 40^{1/3}$$

$$= 19.84 \text{ ft}.$$

The expected crater diameter is approximately 40 ft.

The design curves are based on test data for ice that is mostly no more than 1 m thick, but in the absence of data for thick ice some cautious extrapolations might be in order, as in the following example.

Example. A submarine has to surface through ice which is 2.3 m thick, and it is considered necessary to pre-break the ice by releasing a buoyant charge and firing it in contact with the underside of the ice. What size of charge would be appropriate? What area of ice would be broken by a single charge?

Ice thickness is 90.6 in., and the optimum condition for a charge fired at zero depth below the ice is $(t/W^{1/3})$ = 10.5 in./lb$^{1/3}$. Thus the optimum charge weight is

$$W = \left(\frac{90.6}{10.5}\right)^3$$

$$= 641 \text{ lb}$$

$$= 291 \text{ kg.}$$

The predicted crater radius R for an optimum charge at zero depth is given by $(R/W^{1/3}) = 6.57$ ft/lb$^{1/3}$:

$$R = 6.57 \times 641^{1/3}$$

$$= 56.6 \text{ ft.}$$

The charge would therefore break ice over a roughly circular area 113 ft (34.5 m) in diameter, and some cracking of the ice could be expected over a wider area.

A safe standoff distance for the submarine could be determined from a graph of the type shown in Figure 1. Taking an accepted value for safe overpressure on the hull, a corresponding value of scaled range $R/W^{1/3}$ can be read off, and this scaled value can be converted to absolute distance by multiplying by the cube root of the charge weight (641 lb, or 291 kg).

In the regression analysis, variation of explosive type was ignored, although it is fairly clear that different explosives produce different results. The design curves apply to some undefined "average" explosive. They are likely to overpredict for propellants and blasting agents of low velocity and low specific energy. They are likely to underpredict for explosives with very high specific energy. For common explosives such as TNT, C-4, good ANFO, sensitized or aluminized slurries, nitromethane, PETN, RDX, and nitrocellulose, the specific energy of explosion ("heat of explosion") is likely to be in the range 0.9 to 1.4 kcal/g (3.8 to 5.9 kJ/g), and we can perhaps accept this as the range of specific energy* to which the curves apply. Within this range, there is a possible variation of energy about the mean by ±22%, but because linear dimensions such as crater radius, charge depth and ice thickness scale with the cube root of charge weight, they also scale with respect to the cube root of specific energy. The variation of a linear dimension with variation of specific energy might, to a first approximation, be given by the cube root of the energy ratio. In other words, if the reference value of specific energy is 1.15 kcal/g (4.8 kJ/g) and one extreme value is 1.4 kcal/g (5.9 kJ/g), linear dimensions would differ by a factor of $(1.4/1.15)^{1/3}$, or 1.07. Since the curves cannot predict to an accuracy of 7%, there is little point in making adjustments within the range outlined above.

If a propellant or explosive with very low specific energy is being used, it might be worth making an adjustment. For example, the heat of explosion of black powder is 0.6–0.7 kcal/g (2.5–2.9 kJ/g), and ANFO with a very small oil content might be about 0.6 kcal/g (2.5 kJ/g) or less. Taking the energy of explosion as 0.6 kcal/g (2.5 kJ/g) against a reference value of 1.15 kcal/g (4.8 kJ/g), the adjustment factor is $(0.6/1.15)^{1/3}$, or 0.81. In other words, the crater radius would perhaps be about 20% less than the radius predicted by the design curves.

Going to the other extreme, some special highly aluminized formulations might have values for the energy of explosion up to 2 kcal/g. At this extreme, the adjustment factor for crater radius might be about $(2/1.15)^{1/3} = 1.2$, which means a crater radius 20% bigger than that predicted by the curves.

ROW CHARGES AND PATTERN CHARGES

So far, the discussion has been limited to the effects of single charges, but in dealing with real problems it may be necessary to use a row of charges, multiple rows of charges, or some other kind of pattern. Since there have been few systematic tests with row charges and patterns, it is necessary to work largely from the data for single charges in preliminary design.

If a number of charges, each of weight W, are set in a row with spacing s, the results are predictable from Figures 13 and 14 if s is big enough for the charges to act independently (Fig. 15). If, by contrast, s is relatively small and adjacent charges interact, it is possible for the width of the channel formed by the connected craters to be greater than the diameter of a crater formed by an independent single charge. This is sometimes called "row charge enhancement," although in some cases the row charge may be less efficient than a single charge. In the limit, where s becomes very small, the row of charges acts like a linear charge, so that the blast effects spread cylindrically rather than spherically, and linear dimensions scale with the square root of unit charge weight instead of with the cube root of total charge weight.

*See section on specific energy (p. 26) for further discussion.

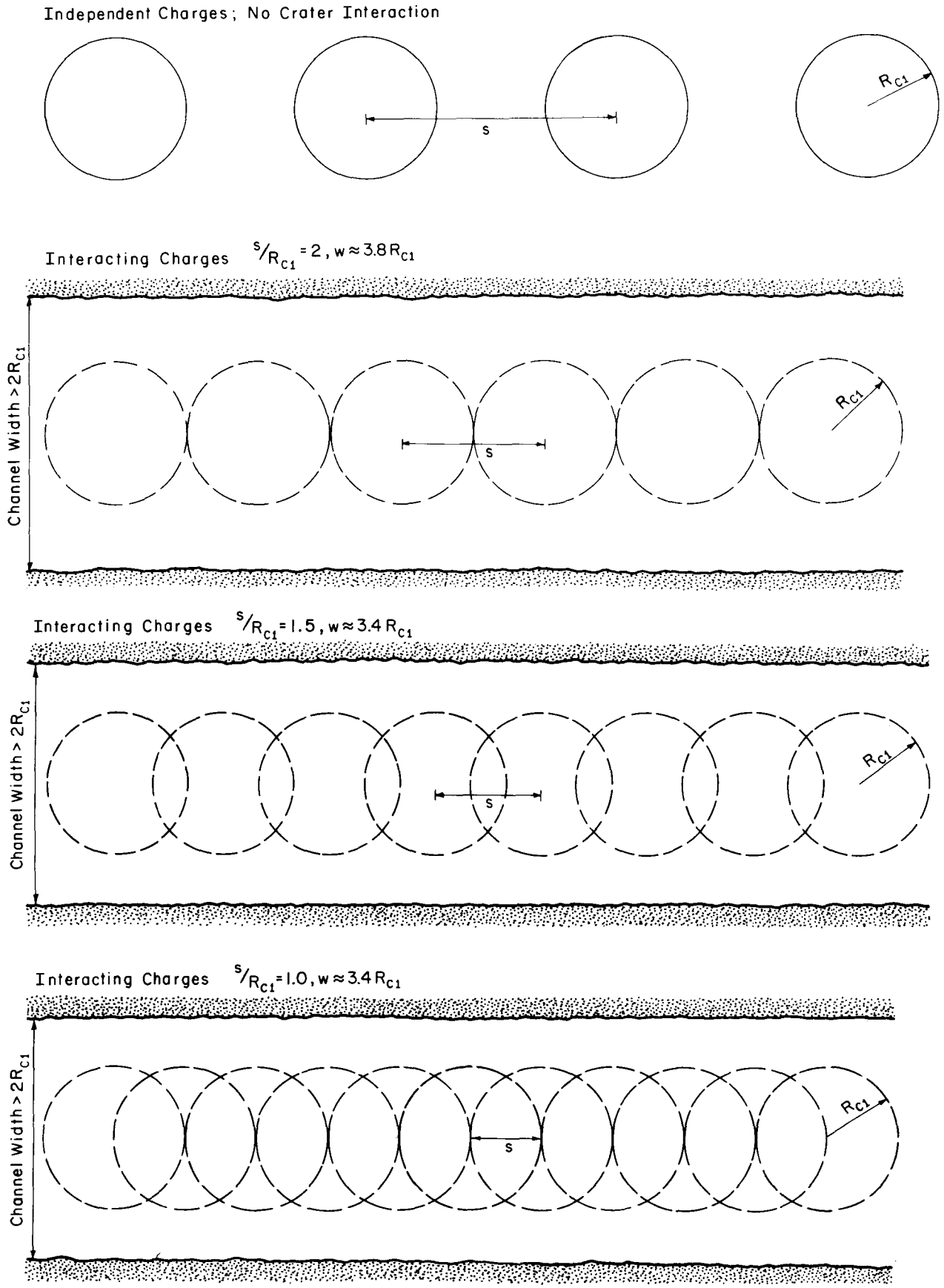

Figure 15. Geometry of row charges.

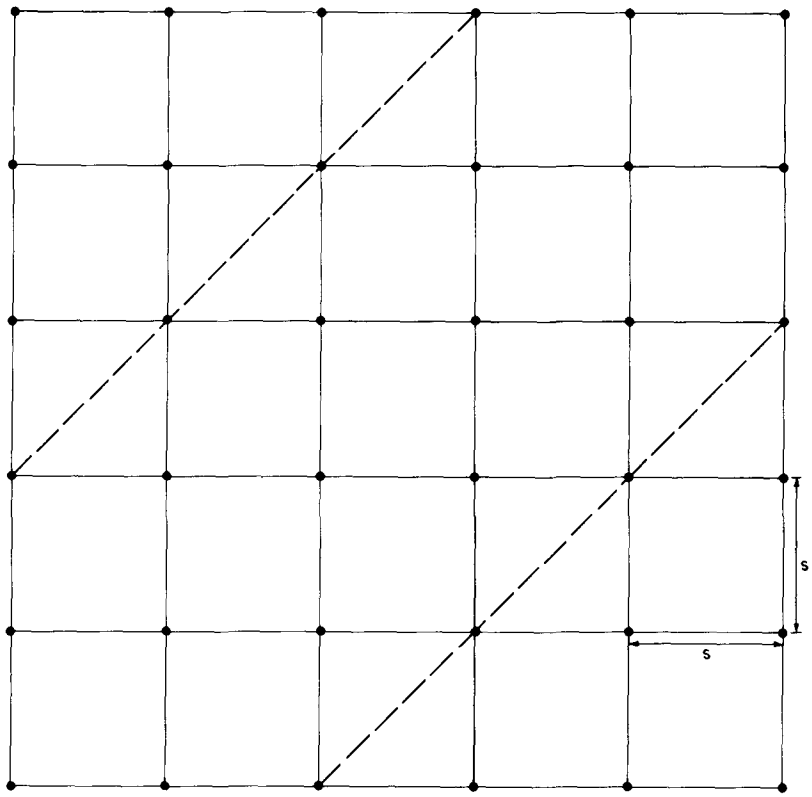

Figure 16. Geometry of pattern charges.

The value of s for charge interaction has not been firmly established, but a reasonable condition for the upper limit of interaction is $(s/R_{cl}) = 2$, where R_{cl} is the radius of the crater formed by a single independent charge of weight W. With greater spacing the row charge is likely to form a chain of craters rather than a continuous channel. Limited testing by Kurtz et al. (1966) suggested that the maximum channel width w was achieved with $(s/R_{cl}) = 2$, but the broken ice was not well fragmented at this spacing. With $(s/R_{cl}) = 2$ the channel width w was about $1.9\,D_{cl}$, where $D_{cl} = 2R_{cl}$. With $(s/R_{cl}) = 1.5$ and $(s/R_{cl}) = 1$, the channel width w was about $1.7D_{cl}$. For planning purposes it is probably best to allow for some overlap of the craters that would be formed by single charges, i.e. take (s/R_{cl}) as less than 2 but not less than 1.5. The resulting channel width might then be about $1.7D_{cl} = 3.4R_{cl}$.

When a pattern of charges is laid out to break a wide area of ice, the logical arrangement is to have the charges at the node points of a square net, in which the spacing s between charges in a row is equal to the spacing between adjacent rows (Fig. 16). If the aim is to break a wide strip of ice, the charges may be laid out in a "5-spot" pattern, but this is just a square grid rotated through 45° relative to the axis of the strip (Fig. 16).

If the mesh size s is very small, then the pattern acts like a sheet of explosive, producing essentially plane wave propagation in one dimension only. The trick is to find the value of s which gives the most efficient fragmentation of the complete area.

From what has already been said about the row charges, a first guess might be that $(s/R_{cl}) = 2$ represents a reasonable condition. However, for a multi-row pattern this is probably too conservative, because a single row with $(s/R_{cl}) = 2$ will break over a half-width of about $1.9R_{cl}$, albeit with poor fragmentation. The writer has blasted a pattern with $(s/R_{cl}) = 2.3$ and judged the result to be an overkill. This suggests that the mesh size should be bigger than $2.3R_{cl}$, but probably no more than $3.8R_{cl}$. In the absence of firm test data, it is suggested that a mesh size of $s = 3R_{cl}$ can be adopted for planning purposes. This should do the job without being unduly wasteful.

Example. Design a pattern charge capable of breaking river ice up to 0.5 m thick, with good fragmentation. The approximate width of the river is 120 m, and the required width of the broken channel is 45 m.

The first job is to determine the required size for a single charge, and to estimate the cratering effect of this charge when it acts alone. If we were concerned solely with ice 0.5 m (19.7

in.) thick, the optimum charge, placed at zero depth below the ice, would be as given by:

$$t/W^{1/3} = 10.5 \text{ in./lb}^{1/3}$$

$$W = (t/10.5)^3$$

$$= (19.7/10.5)^3$$

$$= 6.6 \text{ lb}$$

$$= 3 \text{ kg.}$$

Assuming metric packaging and taking $W = 3$ kg (6.62 lb), the predicted crater radius in ice 0.5 m thick would be, from Figure 14:

$$\frac{R_{cl}}{W^{1/3}} = 6.57 \text{ ft/lb}^{1/3}$$

or,

$$R_{cl} = 6.57 \times 6.62^{1/3}$$

$$= 12.3 \text{ ft}$$

$$= 3.76 \text{ m.}$$

In this problem, the charge design has to cope with any ice thickness up to 0.5 m, and it can be seen from Figure 14 that the 3-kg charge will create a smaller radius in thin ice than it will in ice 0.5 m thick, which is optimum for this charge size. The thinnest ice which is of concern is 4 in., since thinner ice will not safely support men to place the charges, and also 4 in. of ice or less can be broken up by bridge boats. With a charge weight of 6.62 lb, the scaled thickness of 4 in. of ice is 2.13 in./lb$^{1/3}$. Checking the design curves, Figures 13 and 14, for a charge depth of zero and a scaled ice thickness of 2.1 in./lb$^{1/3}$, the predicted scaled crater radius is 5.6 ft/lb$^{1/3}$. Thus the actual crater radius R_{cl} in thin ice should be:

$$R_{cl} = 5.6 \times 6.62^{1/3}$$

$$= 10.5 \text{ ft}$$

$$= 3.2 \text{ m.}$$

The charge weight has to be sufficient to break the thickest ice efficiently, and 3 kg is a suitable choice. However, the value of R_{cl} which will decide the spacing of the charges has to be the lowest value expected for the possible range of ice conditions, and for a 3-kg charge this is 3.2 m, rather than the 3.76 m expected in the thickest ice.

To obtain uniform spacing, the charges are laid out in a square grid with a mesh size s. Whether or not the lines of the grid are parallel and perpendicular to the center line of the river is immaterial in principle, but in practice the grid lines should either be aligned with the river direction, or else set at 45°. For the charge spacing (grid size) s, we take

$$s = 3R_{cl}$$

$$= 3 \times 3.2$$

$$= 9.6 \text{ m.}$$

If the grid lines run directly across the river, the space between cross-stream rows is 9.6 m. To break a channel of width 45 m, five rows will be needed. In each row there will be about 12 or 13 charges, giving a total requirement for 60–65 charges, or 180–195 kg of explosive.

If the grid lines run at 45° to the cross-stream direction, then in each of the cross-stream rows the space between charges increases to $9.6 \times \sqrt{2} = 13.58$ m. The transverse spacing between adjacent rows decreases to $9.6/\sqrt{2} = 6.79$ m. The direct distance between charges remains exactly the same. To cover the required width of 45 m, seven cross-stream rows are required, each of them having about nine charges. The total requirement is about 63 charges, or about 189 kg of explosive, which is essentially the same as with the net laid out the other way. In cases where the required channel width is not very much bigger than the spacing between cross-stream rows, one grid orientation might be slightly more economical than the other because the row spacing divides more neatly into the channel width.

RESPONSE OF FLOATING ICE SHEETS TO UNDERWATER EXPLOSIONS

The mechanical effects of explosives on floating ice have not been studied in detail, and these notes are in the nature of exploratory speculations. Three things are considered: 1) direct damage to the ice by the shock wave, 2) gross displacement of the ice by water erupting in response to the gas bubble, 3) planar flexure of the ice by a concentrated uplift force.

The initial shock wave from a concentrated charge can be assumed to propagate through the water spherically, attenuating as discussed earlier. When this wave reaches the ice it will be reflected from the lower surface of the ice, and it will be refracted and reflected within the ice layer. Shock measurements were made in water just below an ice cover in a U.S. Navy study (Barash 1966b).

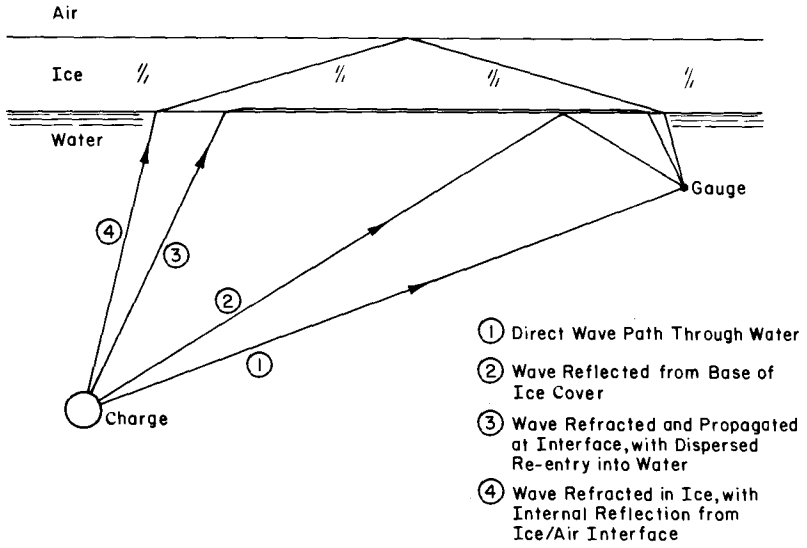

Figure 17. Shock wave paths for an underwater explosion with overlying ice. (After Barash 1966b.)

The pressure-time records could be interpreted in accordance with the scheme of ray paths shown in Figure 17, subject to the usual limitations of critical angles.

Two potential modes of failure for the ice are: 1) internal cracking under impact from a compression wave, and 2) spalling of the upper surface in tension when the wave is reflected from the ice/air interface. The amplitude of a plane wave which is needed to crack a wide sheet of ice is not known. The quasi-static strength of ice under uniaxial compression reaches about 10 MPa at the highest loading rates used in testing laboratories, but with effective lateral confinement this value could easily be doubled. From Figure 1 it can be seen that, for TNT in water, shock pressures in excess of 10 MPa can be expected at ranges up to 4.3 m/kg$^{1/3}$ ($\approx$ 11 ft/lb$^{1/3}$, or about 80 charge radii). Pressures in excess of 20 MPa can be expected at ranges up to 2.3 m/kg$^{1/3}$ ($\approx$ 6 ft/lb$^{1/3}$, or about 44 charge radii). The quasi-static strength of ice under uniaxial tension is about 2 MPa at the highest loading rates which have been studied, so that incident shock waves which are too weak to cause crushing could conceivably cause surface spalling. Another possibility is that the ice might be shattered by some kind of interaction between compression and tension, i.e. by failure in a stress field which has both tensile and compressive principal stresses. Studies of failure criteria for ice under multiaxial stress suggest that failure in a mixed tension-compression state can occur with the tensile and compressive principal stresses both below the uniaxial failure values.

If it is postulated that craters are formed solely by direct shock-wave shattering of the ice, a simplistic model for charge depth effects can be obtained. Assuming that shock waves propagate in the surface water layers as they do through deep water, the crater radius R_c can be expressed in terms of the maximum range for damaging shock waves ℓ_*:

$$R_c = (\ell_*^2 - d_c^2) \tag{11}$$

where d_c is charge depth, and ℓ_* varies with the ice thickness. R_c, d_c and ℓ_* can all be scaled with respect to $W^{1/3}$, but this is unnecessary if eq 11 is written as:

$$R_c/\ell_* = [1 - (d_c/\ell_*)^2]^{1/2}. \tag{12}$$

This relation is shown in Figure 18. It predicts that crater radius will be a maximum at zero charge depth, which is not unrealistic, and that R_c will decrease with increasing charge depth. The limiting value of d_c, where R_c drops to zero, is itself equal to the maximum value of R_c (for d_c = 0). The maximum scaled crater radius $R_c/W^{1/3}$ is

$$\frac{R_c}{W^{1/3}} = \frac{\ell_*}{W^{1/3}}.$$

If $R_c/W^{1/3}$ = 6.5 ft/lb$^{1/3}$, then $\ell_*/W^{1/3}$ = 6.5 ft/lb$^{1/3}$, and this implies that the limiting shock wave pressure is about 18 MPa (see Fig. 1). If $R_c/W^{1/3} = \ell_*/W^{1/3}$ = 4 ft/lb$^{1/3}$, the limiting shock pressure is about 31 MPa. These stress levels are

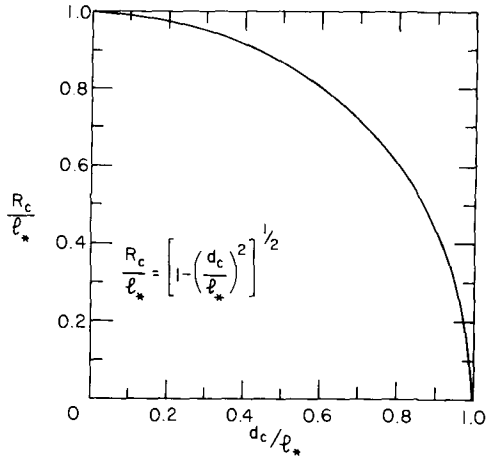

Figure 18. Variation of crater radius with charge depth according to the simple model described by eq 12.

rather high in comparison with accepted values for the uniaxial compressive strength of ice.

While the preceding considerations do not lead to any very definite conclusions, they do suggest that internal fracture of the ice by the shock wave could be a factor for virtually the entire crater zone when a high velocity explosive like TNT is used. On the other hand, low velocity explosives or propellants with low detonation or deflagration pressures are not likely to produce much internal shattering of the ice. Because the latter materials can certainly break ice by heaving and flexing the sheet, it is obviously necessary to consider processes other than shock wave shattering.

Going to the other extreme of rates and time durations, we can consider how the ice might behave if the explosive were to push it slowly and gently upward, forming a crater by flexure. For static loads pushing up or down on a floating ice sheet, the scale of the flexural deformation can be given in terms of a "characteristic length" λ, defined as

$$\lambda = \left(\frac{4EI}{k}\right)^{1/4} = \left(\frac{4Et^3}{12k(1-\nu^2)}\right)^{1/4}$$

$$= \left(\frac{1}{3k}\right)^{1/4}\left(\frac{E}{1-\nu^2}\right)^{1/4} t^{3/4} \qquad (13)$$

where E = Young's modulus
I = moment of inertia of the plate's cross section
k = foundation modulus (unit weight of water)
ν = Poisson's ratio
t = ice thickness.

For a load applied to a circular area of radius a, the radius to the extreme circumferential crack R_{ec} is (Assur 1961)

$$R_{ec} = 2.06\lambda + a/3. \qquad (14)$$

Gold (1971) summarized field data and deduced a representative relation for λ in the form of eq 13 above, with substitution of $E/(1+\nu^2) = 7.65$ GPa. Using this value, together with the substitution $k = 10$ kN/m^3,

$$\lambda = 22.47\, t^{3/4} \quad \text{m} \qquad (15)$$

when t is in metres. Assuming a compact loading area, and thus ignoring $a/3$ in eq 14,

$$R_{ec} \approx 46.3\, t^{3/4} \quad \text{m}. \qquad (16)$$

If R_{ec} is identified with the crater radius R_c for explosive events, a quasi-static flexural mechanism would give the same size of crater for any size of effective charge, with R_c being determined solely by the ice thickness. For ice 1 m thick, R_c would be 46.3 m. For thicknesses of 0.5 m and 0.1 m, the values of R_c would be 27.5 m and 8.2 m respectively. These values are much larger than typical values for real craters made by explosive charges of reasonable size. In short, there is neither qualitative nor quantitative similarity between quasi-static flexural breakage and explosive cratering.

Actually, common sense should tell us that static theory is unlikely to be applicable to very rapid loadings. A cantilever given a swift karate chop will not necessarily break at the beam root. A heavy rock tossed from a bridge will punch a small hole through ice instead of flexing and cracking a wide area. Thus we should probably go back to a consideration of how the ice might be affected by the eruption of a waterspout.

An easy case to think about is the situation where the scaled thickness of the ice is very small, so that the surface skim of ice has little effect on the venting of the waterspout. In this case, we would expect the crater diameter to be at least equal to the diameter of the water column. In Figure 19, waterspout dimensions and bubble diameter are compared with crater diameters for zero scaled ice thickness (according to the regression equation). For small scaled charge depths, crater diameter is 20% greater than the bubble diameter. For very small charge depths, crater diameter is 50% bigger than the diameter of the water column, but the crater and the water column have the same diameter at $d/r_c \approx 14.5$ (i.e. $d/W^{1/3} \approx 0.77$

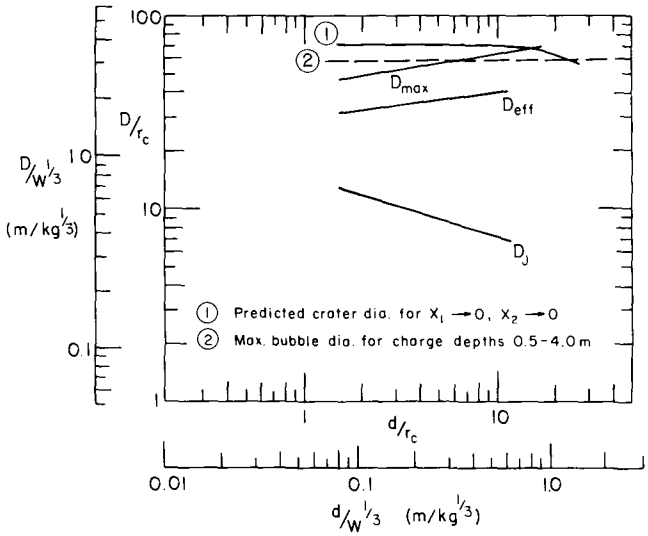

Figure 19. Scaled dimensions of the waterspouts from underwater explosions compared with: 1) predicted crater diameter as scaled ice thickness tends to zero, and 2) theoretical maximum bubble diameter.

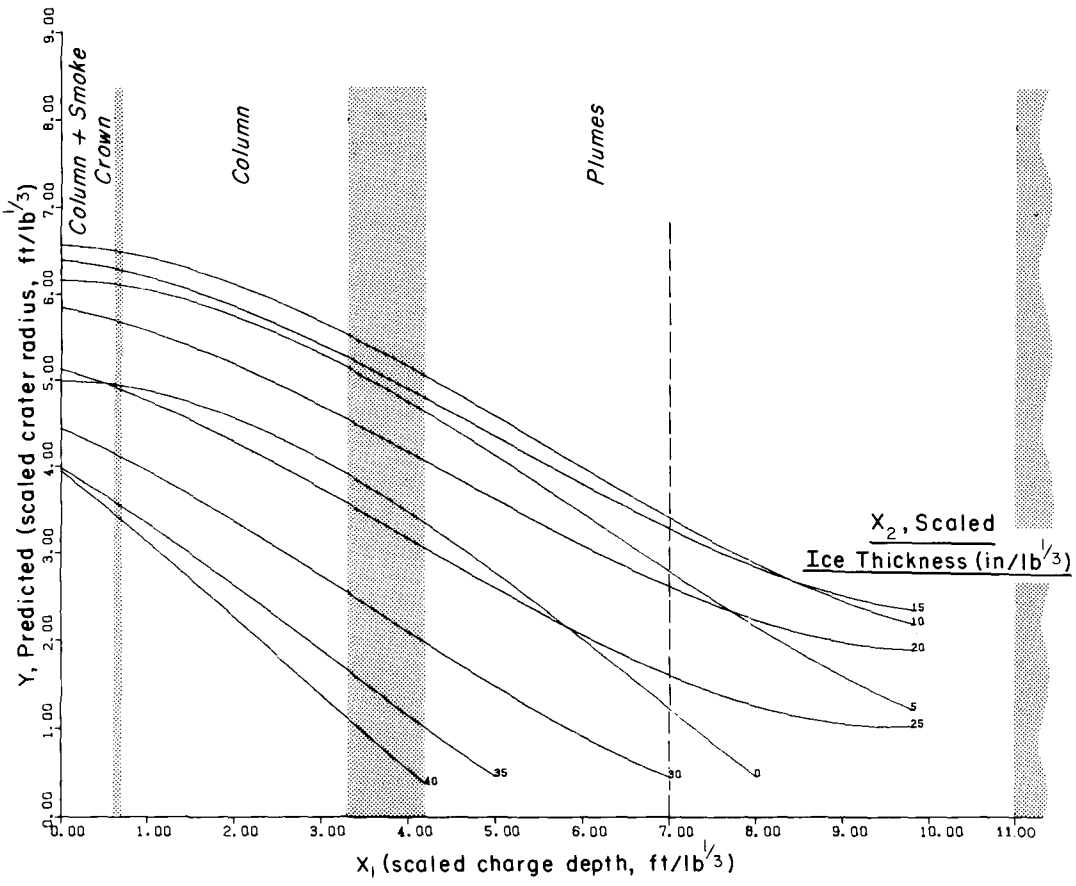

Figure 20. Waterspout characteristics from ordinary underwater explosions (see Figures 5 and 11) compared with ice crater predictions.

m/kg$^{1/3}$ ≈ 1.94 ft/lb$^{1/3}$). This is actually quite close agreement, since the relation for water column diameter refers to a finite distance above water level, where it may have narrowed somewhat.

As a matter of interest, Figure 20 shows the boundaries delineated by Young (1971) for different types of waterspouts from underwater explosions, and it compares these boundaries with the curves relating crater radius and charge depth. The range of charge depths over which ice can be broken is the range corresponding to columns and plumes for ordinary underwater explosions. Charges which would create mounds on an open water surface are too deep to blow craters in ice.

If the scaled ice thickness is small but finite, ejection of the waterspout will not be significantly impeded by the ice, but there will be a tendency for ice to "peel back" at the rim of the crater. Thus it is reasonable to expect the diameter of the crater to be somewhat bigger than that of the water column for this condition.

When there is an outer annulus of ice broken by flexure, we must consider whether or not the width of that annulus is likely to scale with respect to the charge weight. By analogy with static flexure, the width of the flexed rim might depend largely on the ice thickness, and not on the charge yield. It has already been shown that flexure by "point loads" gives a large radius to the extreme circumferential crack. For the flexure of a long floating beam or for a semi-infinite ice sheet, the distance from the loaded free edge to the critical crack is quite similar to R_{ec} for the radially symmetrical case. For a semi-infinite sheet or a wide beam, the critical length λ is as given by eq 13, and the distance to the critical crack is $(\pi/2)\lambda = 1.57\lambda$ instead of 2.06λ (Mellor, in press). There is no need to repeat the arithmetic that was given for the radially symmetric flexure; the width of annulus predicted by static theory is far bigger than the observed cracked rims of explosion craters. It seems more reasonable to expect that peripheral flexure will be caused by "heave" or "fallback" at the base and rim of the waterspout, and the dimensions of this water disturbance are likely to scale with the charge weight.

Looking at the opposite extreme of ice thickness, there must obviously be some ice thickness limit for crater formation. With a charge at zero depth, i.e. in contact with the base of the ice, a very thick ice cover might behave in a similar way to a semi-infinite ice mass when a charge is embedded inside it. Test data exist for explosive cratering of a semi-infinite ice mass (Fig. 21), and they indicate that crater radius drops to zero when the

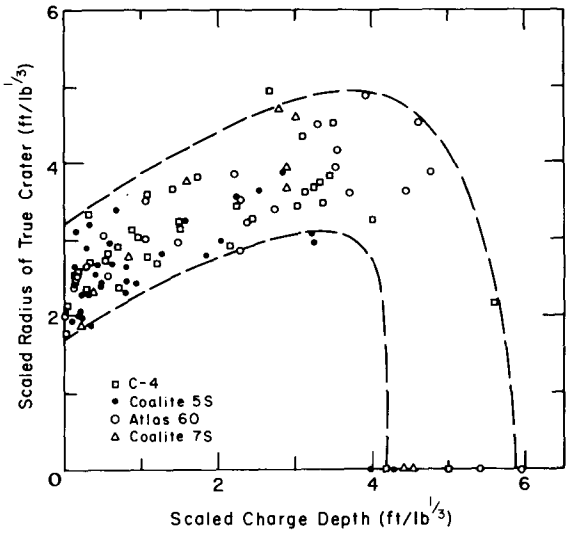

Figure 21. Variation of crater radius with charge depth for explosions in a semi-infinite ice mass. (Data from Livingston [1960].)

charge depth reaches about 5 ft/lb$^{1/3}$. By analogy, it might therefore be expected that crater radius in floating ice would drop to zero when the scaled ice thickness is around 5 ft/lb$^{1/3}$ (60 in./lb$^{1/3}$), and when charge depth is zero. The regression curve for $(R_c/W^{1/3})$ versus $(t/W^{1/3})$ with $(d_c/W^{1/3}) = 0$ does not give this result, but extrapolation of the curve from its range of validity would certainly not conflict with the idea that the limiting value of $(T/w^{1/3})$ is around 60 in./lb$^{1/3}$.

If the direct explosive attack (shock wave plus gas expansion) reaches a limit at scaled ice thicknesses somewhere near 60 in./lb$^{1/3}$, the remaining question is whether some kind of flexural breakage occurs at such ice thicknesses. One way of looking at this question is to pose it specifically for a 1-lb charge with ice 60 in. thick, since there are data for the water jet force imparted to overlying plates by 1-lb underwater charges of TNT (Fig. 10). With ideal conditions, the force imparted to a plate by a 1-lb charge is about 25,000 lbf. For short-term static failure of an ice plate by flexure, the failure force P is in the range (Gold 1971)

$$P/t^2 = 50 \text{ to } 1000 \text{ lbf/in.}^2 \qquad (17)$$

with the largest values probably most appropriate for very rapid failure. With ice of 60 in. thickness, P might therefore be in the range 180,000 to 3,600,000 lbf for flexural failure. This is vastly in excess of the water jet force for 1 lb of TNT.

The only remaining question for thick ice is whether the explosive might crack ice by creating a

wave. However, small amplitude flexure is only likely to crack the ice—it is not likely to form a recognizable crater.

SPECIFIC ENERGY AND "POWDER FACTOR"

The concept of specific energy is very useful for assessing the efficiency of cutting and breaking processes. The specific energy E_s is the energy utilized to cut or break unit volume of material. For an explosive charge, the energy can be expressed as kW, where W is the charge weight and k is a characteristic specific energy content for the explosive. For breakage of floating ice, the volume of material fragmented by an explosive charge can be taken as the crater area multiplied by the ice thickness. Thus,

$$E_s = \frac{kW}{\pi R_c^2 t} \tag{18}$$

where R_c is crater radius and t is ice thickness.

In mining and rock blasting, a traditional term is "powder factor," which means the volume of rock broken by unit weight of explosive, i.e.

$$\text{Powder factor} = \frac{V}{W} \tag{19}$$

where V is the volume broken by charge weight W. In effect, the powder factor is the inverse of specific energy. When applied to breakage of floating ice,

$$\text{Powder factor} = \frac{\pi R_c^2 t}{W} . \tag{20}$$

If appropriate and consistent units are used for R_c, t and W, specific energy and powder factor can be written in terms of the scaled variables as

$$E_s = \frac{k/\pi}{(R_c/W^{1/3})^2 (t/W^{1/3})} \tag{21}$$

$$\text{Powder factor} = \pi (R_c/W^{1/3})^2 (t/W^{1/3}). \tag{22}$$

When applied to explosives, the term *specific energy* is open to some degree of interpretation. U.S. and Canadian commercial handbooks do not mention the term, and neither do most of the (few) textbooks in the field. Specific energy can be taken as the theoretical work done by expansion of the gases produced by the explosion (see Meyer 1981). Alternatively, it can be taken as the *heat of explosion*, which is the total energy liberated in the reaction. The latter interpretation is used in this report, partly because values for heat of explosion are relatively easy to obtain from reference books, and partly because it more truly represents the

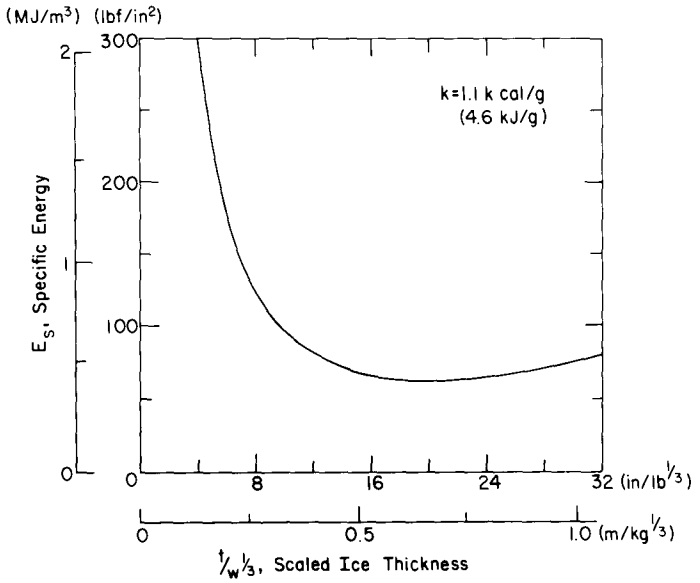

Figure 22. Predicted specific energy for ice blasting when charges are at optimum depth. For this plot, specific energy is based on the heat of explosions.

energy actually consumed. The work of gas expansion is roughly 20% of the heat of explosion.

Taking k as the heat of explosion, values for typical explosives range from about 0.6 kcal/g (2.5 kJ/g) for ANFO with low oil content and for propellant powder, to almost 2 kcal/g (8.3 kJ/g) for heavily aluminized high explosive formulations. For cast TNT and nitromethane, the heat of explosion is about 1.1 kcal/g (4.6 kJ/g). For RDX (Cyclonite) and HMX (Octogen), $k \approx 1.3$ kcal/g (5.4 kJ/g); for PETN, C-3/C-4 (plasticized RDX) and MS 80-20 slurry, $k \approx 1.4$ kcal/g (5.9 kJ/g).

By taking values of $(R_c/W^{1/3})$ and $(t/W^{1/3})$ from the regression curves, and assuming a value of k, then E_s can be plotted against $(t/W^{1/3})$ for optimum charge depth. This plot (Fig. 22) gives the best possible value of E_s according to the regression. It brings out the point that, whereas maximum crater radius is achieved with $t/W^{1/3} \approx 11$ in./lb$^{1/3}$, specific energy is minimized when $t/W^{1/3} \approx 20$ in./lb$^{1/3}$.

For crater blasting in a semi-infinite ice mass, the best values of E_s are in the range 90–270 lbf/in.^{2} (0.6–1.8 MJ/m^3). A representative best value for optimum charge depth might be 150 lbf/in.^{2} (1 MJ/m^3).

To put the absolute values of specific energy in context, we might note first of all that, with optimum conditions, blasting is about as efficient as the best possible mechanical cutting by drag-bit machines (e.g. large and well-designed saws, milling drums, or rotary drills). E_s for blasting is also comparable to the specific energy for icebreaking ships (Mellor 1980). What this means is that, in terms of energy, blasting is a very efficient way to break ice. If specific energy for explosives is based on the work of gas expansion instead of the heat of explosion, specific energy for ice breaking looks even more favorable.

Just to complete the picture, it is worth making an estimate for the specific energy of ice breakage by slow flexure. For a static load P acting on a small circular area, Assur (1961) gives the vertical deflection at failure, w_f, as

$$w_f = \frac{P}{8k\lambda^2} \tag{23}$$

where k is the foundation reaction and λ is the characteristic length (see eq 13). Thus the work done in flexing the ice to failure is

$$\text{Work} = Pw_f = \frac{P^2}{8k\lambda^2}. \tag{24}$$

Assur (1961) also gives the radius to the extreme circumferential crack (see eq 14). Ignoring the small effect of the loading area, the radius to the extreme crack, R_{ec}, is:

$$R_{ec} = 2.06\lambda. \tag{25}$$

If the volume of ice broken V_b is taken as the volume bounded by the extreme circumferential crack, then

$$V_b = \pi(2.06\lambda)^2 t. \tag{26}$$

Finally, the specific energy for the slow flexural breakage is

$$\begin{aligned} E_s &= \frac{P^2}{8k\lambda^2 \pi(2.06\lambda)^2 t} \\ &= \frac{P^2}{106.7kt} \cdot \frac{1}{\lambda^4} \\ &= \frac{P^2}{106.7kt} \cdot \frac{12k(1-\nu^2)}{Et^3} \\ &= \frac{0.1125}{E/(1-\nu^2)} \cdot \left(\frac{P}{t^2}\right)^2. \end{aligned} \tag{27}$$

Gold (1971) summarized field data which indicated that P/t^2 was in the range 50 to 1000 lbf/in.^{2} (0.35 to 6.9 MN/m^2), with the effective value of $E/(1-\nu^2)$ equal to 1.11×10^6 lbf/in.^{2} (7.65 GN/m^2). Substitution of these values puts E_s for slow flexure in the range 2.5×10^{-4} to 0.1 lbf/in.^{2} (1.7 J/m^3 to 0.7 kJ/m^3). Such values for E_s are completely outside the range for any practical methods which have been applied to the cutting and breaking of ice. It is interesting to note that these values are orders of magnitude lower than the specific energy for icebreaking ships, prompting one to question whether conventional plate flexure analyses are of direct relevance to ship action.

SUMMARY AND CONCLUSIONS

For the range of conditions and variables that apply to typical ice blasting operations, test data can be scaled in a simple but rational manner in order to produce manageable design curves for ice blasting.

All available test data have been compiled and analyzed to provide design curves which predict crater size as a function of charge weight, ice

thickness, and charge depth. The curves are believed to provide a reliable guide for optimum performance blasting with typical explosives. Their application to engineering problems is illustrated by means of worked sample problems.

The design curves could be improved by additional data and more refined analysis. There is a need for test data derived from blasts at large scaled depths, and from blasts under very thick ice. Systematic investigation of explosives with widely differing characteristics would be useful.

Interaction of charges to create channels or to break broad areas of ice has not received much study, but some interim working guidelines have been deduced. These need to be checked by field testing.

The optimum specific energy for ice breaking by explosives is surprisingly favorable, being compared to the best attainable values for ice-cutting machines, and not much different from good values for ice-breaking ships. Since explosives represent energy which requires little capital equipment for utilization, they may be of interest for the protection of offshore structures against ice forces.

The basic mechanics of ice blasting is still not well understood. With typical high explosives the ice is likely to be damaged over most of the crater area by the incident shock wave and its reflections. However, the breakout and displacement of ice appears to be controlled largely by the eruption of water impelled by the first phase of gas bubble expansion. The characteristics of ice breakage and displacement can probably be related to the characteristics of waterspouts created by ordinary underwater explosions. The mechanics of quasi-static flexure in floating ice sheets does not seem to have much relevance to the formation of explosive craters. In future studies it might be worth exploring the use of theoretical maximum bubble radius as a scaling parameter, taking water level as the datum for charge depth.

The basic data used in the study have been appended to the report, since some of the original sources are not easily accessible. Scaled data and details of the computer analysis are also given.

LITERATURE CITED

Assur, A. (1961) Traffic over frozen or crusted surfaces. First International Conference on Mechanics of Soil-Vehicle Systems, Torino.

Barash, R.M. (1966a) Ice-breaking by explosives. NOLTR 66-229, U.S. Naval Ordnance Laboratory, White Oak, Silver Spring, Maryland.

Barash, R.M. (1966b) Measurements of underwater explosion pulses reflected from an ice layer. In unpublished report, Office of Naval Research, Code 468, April.

Fonstad, G.D., R. Gerard and B. Stimpson (1981) Authors' reply to discussions by M. Mellor and G. Frankenstein. *Proceedings of POAC 80,* vol. III, p. 1615-1620.

Fonstad, G.D., R. Gerard and B. Stimpson (1982) The explosive demolition of floating ice sheets. *Proceedings of POAC 81,* vol. II, p. 1114-1123.

Froehle, H.A. (1966) ANFO in the Arctic. *The Military Engineer,* Jan-Feb.

Gold, L.W. (1971) Use of ice covers for transportation. *Canadian Geotechnical Journal,* vol. 8, no. 170, p. 170-181.

Kurtz, M.K., R.H. Benfer, W.G. Christopher, G.E. Frankenstein, G. Van Wyhe and E.A. Roguski (1966) Consolidated report, Operation Break-up, FY 66. Ice cratering experiments, Blair Lake, Alaska. NCG/TM 66-7, Nuclear Cratering Group, Lawrence Radiation Laboratory, Livermore, Calif.

Livingston, C.W. (1960) Explosions in ice. U.S. Army Snow, Ice and Permafrost Research Establishment, SIPRE Technical Report 75. AD-276605.

McAnally, W.H. and R.L. Rand (1972) Bridge response to explosion-produced water plumes, Report 1. U.S. Army Engineer Waterways Experiment Station, Technical Report N-72-4.

Mellor, M. (1972) Data for ice blasting. U.S. Army Cold Regions Research and Engineering Laboratory, CRREL Technical Note (unpublished).

Mellor, M. (1980) Icebreaking concepts. CRREL Special Report 80-2. ADA-082175.

Mellor, M. (1982) Ice blasting tests, Ferry Site 1, Imjin River. In CRREL field report dated 24 February 1982 (unpublished).

Mellor, M. (In press) Mechanical behaviour of sea ice. In *Air-Sea-Ice Interactions* (N. Untersteiner, Ed.). NATO Advanced Study Institutes, Series C: Mathematical and Physical Sciences. Boston: D. Reidel.

Mellor, M. and A. Kovacs (1972) Breakage of floating ice by compressed gas blasting. CRREL Special Report 184. AD755504.

Meyer, R. (1981) *Explosives.* Weinheim, Germany: Verlag Chemie GmbH, 440 p.

Nikolayev, S.Ye. (1970) Blasting fast ice in the Antarctic. Information Bulletin, Soviet Antarctic Expedition, English translation, vol. 8, no. 3, p. 164-166, Feb 1973. (Translated from *Informatsionyyi Bulleten'*, no. 81, 1970.)

Outlaw, D.G. and J.N. Strange (1974) Bridge response to explosion-produced water plumes, Report 2. U.S.A. Waterways Experiment Station, Technical Report N-72-4.

Purple, R.A. (1965) Crossing frozen rivers in Korea. *The Military Engineer,* Sept-Oct.

Swisdak, M.M. (1978) Explosion effects and properties: Part II—Explosion effects in water. Naval Surface Weapons Center, NWSC/W01 TR 76-116.

Van der Kley, J. (1965) The use of explosives for clearing ice. *Rijkswaterstaat Communications,* no. 7.

Wade, M.D. (1966) Operation Peggy, cratering experiments 1966. U.S. Army Engineer District, Alaska.

Willey, R.L. and D.E. Phillips (1968) Surface phenomena measurements and experimental procedures in 4000-lb HBX-1 shallow underwater explosive tests (Project "HEAT"). U.S. Naval Ordnance Laboratory, White Oak, Silver Spring, Md., NOLTR 68-74.

Young, G.A. (1971) The physical effects of conventional explosions on the ocean environment. U.S. Naval Ordnance Laboratory, White Oak, Silver Spring, Md., NOLTR 71-120.

Young, G.A. (1973) Plume and ejecta hazards from underwater explosions. U.S. Naval Ordnance Laboratory, White Oak, Silver Spring, Md., NOLTR 73-111.

APPENDIX A: BASIC DATA ON ICE BLASTING

A1.	Van der Kley	Gunpowder
A2.	Van der Kley	Dynamite
A3.	Van der Kley	Guncotton
A4.	Van der Kley	American TNT
A5.	Van der Kley	Dutch TNT
A6.	Wade	ANFO
A7.	Kurtz et al.	C-4
A8.	Frankenstein and Smith	ANFO
A9.	Purple	C-4
A10.	Barash	TNT and HBX-3
A11.	Mellor and Kovacs	Dynamite
A12.	2nd Engineer Battalion, USA CE	TNT
A13.	Mellor	TNT
A14.	Fonstad et al.	DM-12, dynamite, blasting agents
A15.	Nikolayev	TNT

Table A1. Data of Van der Kley, Gunpowder.

No. of tests	Charge weight (kg)	Ice thickness (m)	Charge depth (m)	Crater radius (m)
5	7.0	0.25	1.25	2.50
5	12.0	0.25	1.75	4.00
5	12.0	0.35	1.65	3.50
5	15.0	0.35	2.15	3.75
5	25.0	0.35	2.15	6.00
5	12.0	0.45	1.55	3.00
5	25.0	0.45	2.05	7.00
5	12.0	0.55	1.45	3.50
5	25.0	0.55	1.95	7.00
5	12.0	0.65	1.35	3.50
3	25.0	0.65	1.85	6.00
3	25.0	1.90	0.60	4.25

Table A2. Data of Van der Kley, Dynamite.

No. of tests	Charge weight (kg)	Ice thickness (m)	Charge depth (m)	Crater radius (m)
4	2.50	0.15	0.85	3.75
4	2.50	0.25	0.25	3.50
8	5.00	0.25	0.25	3.75
12	5.00	0.25	1.75	4.25
30	2.50	0.35	0.65	4.00
3	5.00	0.35	1.65	4.50
16	2.50	0.45	0.55	4.00
12	2.50	0.55	0.45	3.25
7	2.50	0.65	0.35	3.50
5	2.50	0.85	0.15	2.625

Table A3. Data of Van der Kley, Guncotton.

No. of tests	Charge weight (kg)	Ice thickness (m)	Charge depth (m)	Crater radius (m)
6	0.28	0.63	0.32	1.20
1	0.28	0.52	0.43	1.25
4	0.28	0.47	0.48	1.425
6	0.28	0.95	0.00	1.105
3	0.56	0.63	0.32	2.00
2	0.56	0.52	0.43	1.90
6	0.56	0.47	0.48	1.79
3	0.84	0.63	0.47	2.00
1	0.84	0.52	0.58	2.50
2	0.84	0.47	0.63	2.50

Table A4. Data of Van der Kley, American TNT.

No. of tests	Charge weight (kg)	Ice thickness (m)	Charge depth (m)	Crater radius (m)
1	0.454	0.09	0.00	1.525
1	0.454	0.11	0.50	1.70
1	0.908	0.10	0.00	2.11
1	0.908	0.14	0.50	2.10
1	0.908	0.13	2.00	1.25

Table A5. Data of Van der Kley, Dutch TNT.

No. of tests	Charge weight (kg)	Ice thickness (m)	Charge depth (m)	Crater radius (m)
1	0.25	0.40	1.00	0.575
1	0.25	0.35	0.00	1.25
1	0.50	0.36	0.00	1.725
1	1.00	0.39	0.00	2.30
1	2.00	0.35	0.00	3.075
1	0.25	0.30	0.00	1.20
1	0.50	0.30	0.00	1.95
1	1.00	0.30	0.00	2.65
1	8.50*	0.40	2.70	4.75
1	0.50	0.40	2.00	0.40
1	1.00	0.40	2.00	0.50
1	2.00	0.40	2.00	3.00
1	3.00	0.40	2.00	3.50
1	8.50*	0.30	1.50	5.25
1	0.50	0.40	1.00	2.10
1	1.00	0.40	1.00	3.15
1	2.00	0.40	1.00	3.50
1	3.00	0.40	1.00	4.625
1	0.50	0.30	0.50	1.95
1	1.00	0.30	0.50	2.45
1	2.00	0.30	0.50	3.00

* M-26 mine.

Table A6. Test results reported by Wade (1966), ANFO, all charges 80 lb.

Charge depth was measured from snow surface. Depths have been adjusted so that they are referred to the bottom of the ice cover.

Charge depth (ft)	Water depth below ice (ft)	Approx. ice thickness (in.)	Crater diam/ cracked diam (ft)
31	31	17	50/100
14	20	20	30/100
6	18	17	60/80
9	18	16	30/100
9	18	16	30/100
9	18	16	30/100

A 160-lb charge of ANFO was fired on top of the ice, producing a crater 30 ft in diam.

Table A7. Data for single charges by Kurtz et al. (1966).

Explosives: C-4 for shots 1-31
ANFO for shot FF1
TNT for shot FF2

Ice thickness is the average around the shot point as reported by CRREL.

Shot no.	Charge weight (lb)	Ice thickness (in.)	DOB[a] (ft)	DOW[a] (ft)	R_a[b] (ft)	R_{eb}[b] (ft)	R_{me}[c] (ft)
1	$136\frac{1}{2}$	34.4	0	38	33.9	60.0	580
2	135	33.5	5	$43\frac{3}{4}$	33.6	69.3	208
3	130	35.8	10	$33\frac{3}{4}$	36.4	60.5	350
4	$141\frac{1}{2}$	29.8	15	36	35.3	54.8	189
5	130	31.6	20	$46\frac{1}{2}$	19.0	54.8	269
6	142	30.9	25	$48\frac{3}{4}$	24.2	60.0	260
7	138	33.0	$7\frac{1}{2}$	$42\frac{1}{3}$	35.7	59.0	263
8	$127\frac{1}{2}$	31.9	35	$51\frac{2}{3}$	22.8	55.8	257
9	$130\frac{1}{2}$	31.6	10	10	30.2	40.3	150
20	140	32.8	10	21	35.0	60.0	150
21	$134\frac{1}{2}$	31.0	15	20	26.3	47.8	205
22	$130\frac{1}{2}$	32.2	20	$19\frac{1}{2}$	15.4	31.5	195
23	135	31.4	10	30	35.4	40.0	257
24	$142\frac{1}{2}$	31.3	20	29	18.8	39.8	215
25	$140\frac{1}{2}$	36.1	30	30	8.5	30.2	75
31	940	34.5	19	$46\frac{1}{2}$	83.6	139.5	336
FF1	160 (ANFO)	27.9	35	$51\frac{1}{2}$	23.7	55.9	163
FF2	150 (TNT)	29[d]	20	$51\frac{1}{2}$[d]	27.0	67.5	242

[a] Below bottom of ice layer

[b] Average

[c] Maximum

[d] Approximate

DOB - Depth of burst

DOW - Depth of water

R_a - Crater radius

R_{eb} - Radius to ejecta boundary

R_{me} - Maximum range for ejecta

Table A8. Results of tests on Mississippi River by Frankenstein and Smith (1966).

Explosive: ANFO

Note: No snow cover, melting ice, low strength

Charge weight (lb)	Water depth below top of ice (ft)	Charge depth (ft)	Ice thickness (in.)	Crater diam (ft)
50	14	11	19.5	42.4
50	13	10.5	19.5	40.1
33.3	11	1.0	18.0	32.0

Table A9. Data reported by R.A. Purple (1965).

Explosive: C-4, all charges 5 lb.

Ice thickness: 4-6 in

Charge depth (ft)	Crater diam. (ft)	Size of ice fragments (ft)
10	10	2
5	16	1.5
2	22	1
0	30	1
-0.5*	24	1.5

*On top of ice, capped by sandbags.

Table A10. Ice blasting tests reported by R.M. Barash (1966), lake ice.

Charge depth below top of ice (ft)	Expl.	Ice thickness (in.)	Water depth from top of ice (ft)	Average diam of open water area (ft)	Average diam of broken ice area (ft)	More or less than half of original ice returned	Average diameter of buckling or severe crack (ft)
42-lb CHARGES							
d+2.5*	TNT	24.5	48	40	49	less	--
d+3.75	TNT	28	50.4	27.5	51.5	less	--
d+5	TNT	24	36.5	49	49	less	--
d+5	TNT	29.5	30.9	0	61	less	--
d+6	TNT	30	25.8	0	53	less	--
d+8	TNT	29.5	46	0	53.5	more	--
d+10	TNT	25	50.5	0	52	more	--
d+17.22	TNT	25	57.9	0	42	more	--
8-lb CHARGES							
-2	TNT	23	24.7	0	0	--	--
-1	TNT	23	24.7	0	0	--	--
-1	TNT	27	16.7	0	0	--	--
0	TNT	27	18.3	0	4.5	less	--
d*	TNT	25	33.9	0	25	less	--
d+0.27	TNT	26	15.4	0	23.5	more	--
d+1.45	TNT	25	33.9	3	32.5	more	--
d+1.45	TNT	26	17.2	0	32.5	more	--
d+2.9	TNT	22.5	40	12	34	less	--
d+2.9	HBX-3	29	27.8	0	41	less	--
d+4	TNT	24.5	27.3	0	31.5	more	--
d+5	TNT	23	32.2	0	28	more	--
d+5	TNT	25.5	24.8	0	27.5	more	--
d+7.5	TNT	29	27.8	0	15.25	less	27.25
d+10	TNT	20	33	0	15.25	more	--
d+10	TNT	20	33	0	18	more	--
d+13	TNT	29	35.2	0	18	less	25
d+16	TNT	28	32.5	0	17.75	less	--
d+20	TNT	27	60	4.5	10.5	less	--
d+20	HBX-3	29	66.3	0	23.75	less	--
1-lb CHARGES							
0	TNT	24	23.8	0	0	--	--
d/2*	TNT	24	26	0	3	less	--
d/2	TNT	27	16	0	3	less	--
d	TNT	22.5	26.8	0	13	more	--
d+1.45	TNT	25	24.2	0	16	more	--
d+1.45	HBX-3	30	18	0	7	less	20
d+2.5	TNT	22	43.3	3.5	3.5	less	15
d+2.5	HBX-3	29	19.2	0	6	less	19.5
d+4	TNT	30	67.3	0	3.75	less	11
d+5	TNT	23	35	0	7	less	20
d+5	HBX-3	23	31	0	8	more	25
d+5	TNT	26	20.3	0	3	more	14
d+5	TNT	30	67.3	1.75	1.75	less	14
d+6	TNT	30	64.7	0	4.5	less	--
d+7.5	TNT	29	30.8	0	1.5	more	--
d+10	TNT	27	32.5	0	0	--	--
d+11	TNT	29	65.3	0	0	--	--

*d - ice thickness given in col. 3, and converted to feet.

Table A11. Tests by M. Mellor and A. Kovacs (1972).

Results of dynamite shots under lake ice in New Hampshire.
Date 24 February 1971, mean snow cover approx. 7 in. All charges 1 lb of 40% gelatin dynamite.

Shot no.	Charge depth* (ft)	Ice thickness (in.)	Mean diam of hole or cracked zone (ft)	Remarks
1	0	16	10.5/12.9	10.5-ft-diam open hole with depressed rim of 12.0 ft diam.
2	1.5	19	14.5	No open hole. Ice thoroughly broken, but fragments fell back.
3	3	17	17.0	No open hole. Fragments fell back.
4	4.5	19	4.1/33	4.0-ft-diam open hole with a 33-ft-diam circumferential crack. Flyrock travel 50 ft or more.

* Depth below bottom of ice.

Results of dynamite shots on lake ice in Alaska.

Date 24 March 1971, snow cover 16.5 in., ice thickness 2.71 ft, water depth 10-12 ft, charges: military dynamite.

Shot no.	Charge weight (ft)	Charge depth (ft)	Effect of shot
1	2	2	Circumferential cracks to 21 ft diam, slight depression inside this area. 10-ft-diam central area domed and fragmented.
2	4	2.5	Circumferential cracks to diameter of 34.5 ft. Slight depression 28 ft diam. Central hump to 9 ft diam. Open hole 5 ft diam.
3	3.5	0	Circumferential cracks and slight depression 25 ft diam. Hole completely choked with ice fragments 10 ft diam.

Table A12. Record of 1977 tests found in files of Echo Company, 2nd Engr. Bn., U.S. Army, Camp Pelham, Korea.

Ice thickness: 30-40 cm

Charge depth: 60 cm

Explosive: TNT

		Scaled mean values		
Charge weight (lb)	Crater diam (m)	$d/W^{1/3}$ ($ft/lb^{1/3}$)	$t/W^{1/3}$ ($in./lb^{1/3}$)	$\bar{R}/W^{1/3}$ ($ft/lb^{1/3}$)
0.5	3.0 - 3.5	2.48	17.35	6.71
1.0	3.5 - 4.0	1.97	13.78	6.15
2.5	6.0 - 7.0	1.45	10.16	7.86
5.0	7.0 - 8.0	1.15	8.06	7.20

Table A13. Data recorded in unpublished CRREL field report by M. Mellor dated 24 February 1982.

Test site: Ferry Site 1, Imjin River, Korea
Test date: 16-17 February 1982
Site air temperature: Approx. -5° to +5°C
Explosive: Military TNT initiated by det. cord
Personnel: E Co., 2nd Engr. Bn.. O.I.C. Lt. Mark Stevens, CRREL advisor M. Mellor

Charge weight		Charge depth		Ice thickness		Water depth		Crater diameter		
(lb)	(kg)	(ft)	(m)	(in.)	(m)	(ft)	(m)	(ft)	(m)	Comments
1	0.454	8	2.44	5.5	0.14	14.9	4.55	8.0	2.44	Open hole 52 in. diam
1	0.454	4	1.22	5.0	0.13	14.3	4.35	13.3	4.05	
1	0.454	2	0.61	5.1	0.13	13.9	4.25	11.1	3.38	
1	0.454	0	0	5.5	0.14	12.3	3.75	11.5	3.51	
10	4.536	13.1	4	5.25	0.13	13.1	4.0	17.55	5.35	
10	4.536	0	0	4.75	0.12	13.0	3.95	21.16	6.45	
10	4.536	4	1.22	4.5	0.11	11.6	3.55	23.12	7.05	
10	4.536	8	2.44	4.75	0.12	8.5	2.6	23.29	7.1	
20	9.072	15.7	4.8	5.75	0.15	15.7	4.8	22.63	6.9	
20	9.072	8	2.44	6.0	0.15	15.3	4.65	29.85	9.1	
20	9.072	4	1.22	6.0	0.15	13.9	4.25	28.86	8.8	
20	9.072	0	0	6.0	0.15	12.3	3.75	29.19	8.9	
0.6	0.272	8	2.44	5.5	0.14	13.1	4	0	0	Slight doming and internal cracks
0.6	0.272	4	1.22	5.5	0.14	13.1	4	2.25	0.69	Domed slightly with internal cracks
0.6	0.272	2	0.61	5.5	0.14	13.1	4	10.33	3.15	
0.6	0.272	0	0	6.0	0.15	13.1	4	8.04	2.45	
2	0.907	12	0	6.0	0.15	13.1	4	0	0	
1	0.454	12	0	5.75	0.15	13.1	4	0	0	
8	3.63	0	0	5.0	0.13	13.1	4	21	6.40	
4	1.81	0.33	0.1	5.0	0.13	13.1	4	14.75	4.50	
2	0.907	0	0	5.0	0.13	13.1	4	13	3.96	
40	18.14	6	1.83	5.75	0.15	13.1	4	51	15.55	
0.6	0.272	0.33	0.10	5.25	0.13	13.1	4	8.5	2.59	

Table A14. Data from tests at Drummond Lake, B.C. (Fonstad et al., 1981; data given on p. 1618-1620 of vol. III, Proceedings of POAC 81).

Shot no.	Placement hole diam (mm)	Charge weight (kg)	Ice thickness (m)	Placement depth (m)	Water depth (m)	Crater radius (m)
1	152.4	1.00	0.439	0.19	-	3.12
2	152.4	2.00	0.439	0.15	-	4.06
3	152.4	1.25	0.340	0.12	2.28	2.79
4	152.4	1.25	0.355	0.13	3.45	2.95
5	(1)	0.50	0.368	-0.29	-	0.55
6	(1)	1.00	0.387	-0.31	-	0.74
7	(1)	2.25	0.343	-0.27	-	1.26
8	(1)	4.50	0.381	-0.30	-	2.14
9	152.4	0.50	0.318	0.00	4.33	2.20
10	152.4	1.00	0.305	0.00	4.34	2.31
11	152.4	2.25	0.343	0.00	4.41	3.26
12	152.4	4.50	0.356	0.00	4.50	4.19
13	304.8	0.50	0.330	0.00	4.98	2.36
14	304.8	1.00	0.381	0.00	4.55	2.61
15	304.8	2.25	0.305	0.00	4.50	2.99
16	304.8	4.50	0.305	0.00	4.50	4.22
17	457.2	0.50	0.324	0.00	4.83	1.58
18	457.2	1.00	0.381	0.00	4.67	2.20
19	457.2	2.25	0.362	0.00	4.72	3.19
20	457.2	4.50	0.375	0.00	4.83	4.52
21	Refrozen	0.50	0.381	0.00	5.05	2.10
22	(152.4)	1.00	0.381	0.00	4.88	2.60
23	(152.4)	2.25	0.356	0.00	4.83	3.77
24	(152.4)	4.50	0.381	0.00	4.93	4.53
25	152.4	0.50	0.381	0.14	4.85	1.78
26	152.4	1.00	0.318	0.11	4.74	2.31
27	152.4	2.25	0.343	0.12	4.23	3.44
28	152.4	4.50	0.330	0.12	4.17	3.84
29	304.8	0.50	0.318	0.11	4.10	1.92
30	304.8	1.00	0.305	0.11	4.24	2.58
31	304.8	2.25	0.406	0.15	4.52	3.37
32	304.8	4.50	0.381	0.14	5.11	4.27
33	457.2	0.50	0.368	0.13	4.99	1.91
34	457.2	1.00	0.381	0.14	4.60	2.40
35	457.2	2.25	0.381	0.14	4.27	3.26
36	457.2	4.50	0.387	0.14	4.29	3.96
37	Refrozen	0.50	0.381	0.14	4.14	1.80
38	(152.4)	1.00	0.381	0.14	4.19	2.98

Table A14 (cont'd).

Shot no.	Placement hole diam (mm)	Charge weight (kg)	Ice thickness (m)	Placement depth (m)	Water depth (m)	Crater radius (m)
39	Refrozen	2.25	0.381	0.14	4.37	3.51
40	(152.4)	4.50	0.356	0.13	4.70	4.65
41	152.4	0.50	0.337	0.70	4.79	1.83
42	152.4	1.00	0.330	0.69	5.11	2.63
43	152.4	2.25	0.394	0.82	-	3.32
44	152.4	4.50	0.368	0.77	-	4.24
45	152.4	0.50	0.394	0.78	4.71	1.75
46	152.4	1.00	0.394	0.78	4.64	2.42
47	152.4	2.25	0.387	0.77	4.74	3.45
48	152.4	4.50	0.394	0.78	4.59	4.16
49	152.4	2.25	0.406	1.50	-	3.53
50	152.4	2.25	0.394	1.54	-	3.33
51	304.8	20.00	0.334	1.83	8.81	6.26
52	304.8	25.00	0.367	1.83	8.78	7.40
53	152.4	0.25	0.368	0.61	8.17	1.90
54	152.4	0.25	0.368	0.91	8.17	1.11
55	152.4	0.25	0.356	1.22	8.18	0.56
56	152.4	0.25	0.356	1.83	8.18	0.79 (2)
57	152.4	1.00	0.356	0.91	8.18	2.57
58	152.4	1.00	0.356	1.22	8.18	2.26
59	152.4	1.00	0.356	1.52	8.18	1.28
60	152.4	1.00	0.356	1.83	8.18	1.01
61	152.4	1.50	0.356	0.14	4.22	3.23
62	152.4	1.50	0.356	0.14	4.22	2.70
63	152.4	1.50	0.356	0.14	3.99	3.24
64	152.4	1.50	0.356	0.14	3.91	3.27
65	152.4	1.50	0.356	0.14	3.61	2.89
66	152.4	1.50	0.356	0.14	3.45	2.97
67	152.4	0.60 (3)	0.356	0.47	4.25	1.82
68	152.4	1.20	0.349	0.73	4.32	2.70
69	152.4	2.25	0.356	0.74	4.32	3.50
70	152.4	4.51	0.330	0.70	4.34	4.02
71	152.4	0.60 (3)	0.356	0.69	4.27	2.11
72	152.4	1.20	0.349	0.73	4.48	2.42
73	152.4	2.25	0.356	0.70	3.99	2.88
74	152.4	4.51	0.375	0.74	3.84	4.42
75	152.4	0.57 (4)	0.381	0.79	4.45	1.03
76	152.4	1.13	0.387	0.82	4.39	2.72
77	152.4	2.27	0.394	0.82	4.38	3.60

Table A14 (cont'd).

Shot no.	Placement hole diam (mm)	Charge weight (kg)	Ice thickness (m)	Placement depth (m)	Water depth (m)	Crater radius (m)
78	152.4	4.54	0.394	0.82	4.38	3.75
79	152.4	2.27 (4)	0.387	0.53	4.34	3.35
80	152.4	0.57 (5)	0.356	0.74	4.27	1.09
81	152.4	1.13	0.387	0.73	4.19	1.71
82	152.4	2.27	0.356	0.74	4.75	1.12 (6)
83	152.4	4.45	0.387	0.81	4.74	1.11 (6)
84	152.4	4.45 (5)	0.343	0.77	4.25	1.15 (6)
85	At Ice	9.00	0.395	-0.39	-	1.86
86	Surface	18.00	0.395	-0.39	-	2.99

Unless otherwise specified, the explosive used was DM-12, a German PETN - based explosive with oil and grease plasticizer.

All placement depths and depths of water are measured from the ice/water interface.

NOTES:

1. In shallow (3-in) hole at ice surface, tamped with snow.
2. Ice bordering crater bent up, crater radius large, suspect measurement error.
3. Explosive for this series was CIL 40% Forcite.
4. Explosive for this series was CIL Amex II.
5. Explosive for this series was CIL Hydromex.
6. Crater radius small, suspected partial detonation of explosive due to water seepage into the charges.

Data from tests 5-8 and 82-86 not used for MM82 regression analysis.

Table A15. Results of ice blasting tests reported by S. Ye. Nikolayev.

Explosive: Trotyl (Russian TNT)

Ice thickness, t		Charge weight, W		Charge depth, d		Crater radius, R*		Scaled dimensions $t/W^{1/3}$	$d/W^{1/3}$	$R/W^{1/3}$
(m)	(in.)	(kg)	(lb)	(m)	(ft)	(m)	(ft)	(in./lb)$^{1/3}$	(ft/lb)$^{1/3}$	(ft/lb)$^{1/3}$
1.07	42.13	25.2	55.57	2.4	7.87	6.3/11.97	20.67/39.27	11.04	2.06	5.42/10.29
1.07	42.13	25.2	55.57	2.8	9.19	6.4/11.65	21.0/38.22	11.04	2.41	5.50/10.02
1.07	42.13	25.2	55.57	3.2	10.5	6.75/12.83	22.15/42.1	11.04	2.75	5.80/11.04
1.07	42.13	25.2	55.57	3.5	11.48	6.6/13.53	21.65/44.39	11.04	3.01	5.67/11.63
1.07	42.13	25.2	55.57	4.0	13.12	6.45/13.8	21.16/45.28	11.04	3.44	5.55/11.87
1.07	42.13	25.2	55.57	4.5	14.76	5.25/13.49	17.23/44.26	11.04	3.87	4.52/11.60
1.1	43.31	30.0	66.15	2.8	9.19	6.55/11.92	21.49/39.11	10.71	2.27	5.31/9.67
1.1	43.31	30.0	66.15	3.2	10.5	6.95/13.21	22.8/43.34	10.71	2.60	5.64/10.72
1.1	43.31	30.0	66.15	3.5	11.48	6.65/13.63	21.82/44.72	10.71	2.84	5.40/11.06
1.1	43.31	30.0	66.15	4.0	13.12	6.2/14.14	20.34/46.39	10.71	3.24	5.03/11.47
1.1	43.31	30.0	66.15	4.5	14.76	5.65/13.73	18.54/45.05	10.71	3.65	4.58/11.14
1.1	43.31	25.0	55.13	2.85	9.35	7.1/15.19	23.3/49.84	11.38	2.46	6.12/13.1
1.1	43.31	30.0	66.15	3.0	9.84	7.55/15.48	24.77/50.79	10.71	2.43	6.12/12.56

* First figure is crater radius, second is radius to limits of cracks.

APPENDIX B: SCALED INPUT DATA

X_1: scaled charge depth (ft/lb$^{1/3}$) X_2: scaled ice thickness (in./lb$^{1/3}$) Y: scaled crater radius (ft/lb$^{1/3}$)

The data of Van der Kley in Appendix A give mean results for multiple tests in some cases. In this table each mean result from a multiple test is entered $\sqrt{n}$ times, where n is the number of replications of the multiple test.

X_1	X_2	Y	X_1	X_2	Y
4.0000	19.230	2.3000	1.7300	6.0200	3.3500
			1.7300	6.0200	3.3500
			1.7700	4.6600	6.0600
			1.7700	4.6600	6.0600
4.0000	19.230	2.3000	1.6200	7.3800	3.9100
0.00000	16.860	5.0000	1.6200	7.3800	3.9100
0.00000	13.750	5.4800	1.6800	5.7100	6.0600
0.00000	11.800	5.8000	1.6800	5.7100	6.0600
0.00000	8.4100	6.1600	1.5000	8.7100	3.9100
0.00000	13.180	4.8100	1.5000	8.7100	3.9100
0.00000	10.470	6.2000	1.6000	6.7300	5.1900
0.00000	10.470	6.2000	1.6000	6.7300	5.1900
0.00000	8.3000	6.6900	0.52000	19.700	3.6600
3.3300	5.9300	5.8800	0.52000	19.700	3.6600
6.3600	15.270	1.2700	1.5800	3.3500	6.9700
5.0500	12.120	1.2600	1.5800	3.3500	6.9700
4.0000	9.6000	6.0000	0.46400	5.5800	6.5200
3.5000	8.4000	6.1300	0.46400	5.5800	6.5200
1.8500	4.0700	6.4800	0.36600	4.4000	5.4900
3.1800	15.270	6.6800	0.36600	4.4000	5.4900
2.5200	12.120	7.9200	0.36600	4.4000	5.4900
2.0000	9.6000	7.0100	2.5600	4.4000	6.2100
1.7500	8.4000	8.1100	2.5600	4.4000	6.2100
1.5900	10.470	6.2000	2.5600	4.4000	6.2100
1.2600	8.3000	6.1700	1.2060	7.8200	7.4300
1.0000	6.5800	6.0000	1.2060	7.8200	7.4300
1.2300	29.100	4.6200	1.2060	7.8200	7.4300
1.2300	29.100	4.6200	1.2060	7.8200	7.4300
1.6550	24.050	4.8100	1.2060	7.8200	7.4300
1.8400	21.700	5.4800	2.4200	6.1600	6.5800
1.8400	21.700	5.4800	2.4200	6.1600	6.5800
0.00000	43.900	4.2500	1.0200	10.000	7.4300
0.00000	43.900	4.2500	1.0200	10.000	7.4300
0.98100	23.200	6.1300	1.0200	10.000	7.4300
0.98100	23.200	6.1300	1.0200	10.000	7.4300
1.3200	19.150	5.8200	0.83600	12.230	6.0400
1.4700	17.300	5.4900	0.83600	12.230	6.0400
1.4700	17.300	5.4900	0.83600	12.230	6.0400
1.2500	20.150	5.3300	0.65200	14.500	6.5200
1.5450	16.660	6.6600	0.65200	14.500	6.5200
1.6750	15.030	6.6600	0.65200	14.500	6.5200
0.00000	3.5400	5.0000	0.27800	18.900	4.8800
1.6400	4.3300	5.5800	0.27800	18.900	4.8800
0.00000	3.1250	5.4900	7.2000	3.9500	5.8000
1.3000	4.3700	5.4700	3.2500	4.6400	3.4800
5.2100	4.0700	3.2600	1.3900	3.9500	6.9600
1.6500	3.9550	3.3000	2.0900	3.7100	3.4800
1.6500	3.9550	3.3000	2.0900	3.7100	3.4800
1.9500	3.9550	4.4600	2.0900	3.7100	3.4800

X_1	X_2	Y	X_1	X_2	Y
1.9500	3.9550	4.4600	3.5100	4.9700	7.3100
1.8400	4.6900	3.9100	0.00000	6.6800	6.5800
1.8400	4.6900	3.9100	0.97300	6.5400	6.5600
2.2000	4.3100	3.8400	1.9800	7.0800	7.2000
2.2000	4.3100	3.8400	2.8800	6.7800	6.7800
1.8600	3.6300	5.1800	3.9500	6.2500	3.7600
1.8600	3.6300	5.1800	4.7900	5.9200	4.6400
1.4500	6.4000	6.9200	11.000	29.000	0.00000
6.9600	6.3400	4.5400	0.00000	16.000	5.8500
1.9700	6.2300	5.9600	1.5000	19.000	7.2500
1.9300	6.3200	6.7500	3.0000	17.000	8.5000
2.9300	6.0500	5.1400	4.5000	19.000	2.0500
3.9400	6.3500	3.0400	1.5900	25.800	3.9700
1.9500	6.1300	6.9100	1.5800	20.500	2.8400
3.8300	6.0000	3.6000	0.00000	21.400	3.2900
5.7700	6.9400	1.6300	2.4800	17.350	6.7100
1.9400	3.5200	8.5400	1.9700	13.780	6.1500
6.4600	5.1500	4.3700	1.4500	10.160	7.8600
3.7700	5.4600	5.0900	1.1500	8.0600	7.2000
2.9900	5.3000	5.7600	8.0000	5.5000	4.0000
2.8500	5.3000	5.4500	4.0000	5.0000	6.6500
3.1000	5.5900	4.9700	2.0000	5.1000	5.5500
5.8500	2.9200	2.9200	0.00000	5.5000	5.7500
2.9200	2.9200	4.6800	6.0800	2.4400	4.0700
1.1700	2.9200	6.4400	0.00000	2.2100	4.9100
0.00000	2.9200	8.7800	1.8600	2.0900	5.3700
0.71900	7.0500	7.0500	3.7100	2.2100	5.4100
1.0700	8.0600	7.4000	5.7800	2.1200	4.1700
1.4370	6.9100	7.0500	2.9500	2.2100	5.5000
1.4370	8.4900	8.7600	1.4700	2.2100	5.3200
1.7250	8.6300	7.6100	0.00000	2.2100	5.3800
2.3000	8.4900	7.6900	9.4900	6.5200	0.00000
2.8750	7.2000	7.4700	4.7400	6.5200	1.3300
4.9600	7.2000	6.0400	2.3700	6.5200	6.1200
0.00000	12.500	6.2500	0.00000	7.1100	4.7700
0.13500	13.000	5.8800	6.0000	2.5000	2.5600
0.72500	12.500	8.1300	7.5600	3.7800	0.00000
0.72500	13.000	8.1300	9.5200	4.7600	0.00000
1.4500	11.250	8.5000	12.000	5.7500	0.00000
1.4500	14.500	10.250	0.00000	2.5000	5.2500
2.0000	12.250	7.8700	0.21000	3.1500	4.6500
2.5000	11.500	7.0000	0.00000	3.9700	5.1600
2.5000	12.750	6.8800	1.7500	1.6800	7.4600
3.7500	14.500	3.8100	0.39000	6.2200	5.0400
5.0000	10.000	3.8100	0.48000	13.270	7.8600
5.0000	10.000	4.5000	0.30000	10.540	8.1200
6.5000	14.500	4.5000	0.28000	9.5500	6.5300
8.0000	14.000	4.4400	0.30000	9.9700	6.9000
10.000	13.500	2.6200	0.00000	12.120	6.9900
10.000	14.500	5.9400	0.00000	9.2200	5.8200
0.00000	22.500	6.5000	0.00000	7.9200	6.2700
1.4500	25.000	8.0000	0.00000	6.5200	6.4000
1.4500	30.000	3.5000	0.00000	12.580	7.5000
2.5000	22.000	1.7500	0.00000	11.520	6.5800
2.5000	29.000	3.0000	0.00000	7.0400	5.7500

X_1	X_2	Y	X_1	X_2	Y
4.0000	30.000	1.8750	0.00000	5.5900	6.4400
5.0000	23.000	3.5000	0.00000	12.350	5.0200
5.0000	23.000	4.0000	0.00000	11.520	5.5400
5.0000	26.000	1.5000	0.00000	8.3500	6.1400
5.0000	30.000	0.87500	0.00000	6.8700	6.9000
6.0000	30.000	2.2500	0.00000	14.520	6.6700
7.5000	29.000	0.75000	0.00000	11.520	6.5500
10.000	27.000	0.00000	0.00000	8.2200	7.2500
0.00000	6.9800	6.9200	4.6100	10.760	2.5500
0.44000	14.520	5.6500	0.31000	9.4100	7.1100
0.28000	9.6200	5.8200	0.31000	9.4100	5.9500
0.23000	7.9200	6.6200	0.31000	9.4100	7.1300
0.18000	6.0500	5.8600	0.31000	9.4100	7.2000
0.35000	12.120	6.1000	0.31000	9.4100	6.3600
0.28000	9.2200	6.5000	0.31000	9.4100	6.5400
0.29000	9.3700	6.4800	1.4000	12.410	5.4400
0.21000	6.9800	6.5200	1.7300	9.9400	6.4100
0.41000	14.030	6.0700	1.4200	8.2200	6.7300
0.35000	11.520	6.0500	1.0700	6.0400	6.1300
0.27000	8.7900	6.2700	2.0600	12.760	6.3100
0.21000	7.0900	6.0500	1.7300	9.9400	5.7400
0.44000	14.520	5.7200	1.3500	8.2200	5.5400
0.35000	11.520	7.5100	1.1300	6.8700	6.7500
0.27000	8.7900	6.7500	2.4000	13.900	3.1300
0.20000	6.5200	7.1000	1.9800	11.240	6.5800
2.2200	12.840	5.8100	1.5700	9.0700	6.9000
1.7400	9.9800	6.6300	1.2500	7.2000	5.7100
1.5800	9.0900	6.3900	1.0200	8.9000	6.4200
1.1800	6.7400	6.4700	2.2500	12.990	3.3100
2.4800	15.020	5.5600	1.7700	11.240	4.1400
1.9700	11.910	6.1000	2.0600	11.040	5.4200
1.4800	8.9300	6.6400	2.4100	11.040	5.5000
1.1900	7.2200	6.3500	2.7500	11.040	5.8000
2.8800	9.3700	6.7900	3.0100	11.040	5.6700
2.9600	9.0900	6.4000	3.4400	11.040	5.5500
1.7000	3.7200	5.8100	3.8700	11.040	4.5200
1.4700	3.8000	6.3800	2.2700	10.710	5.3100
2.4400	17.670	7.6000	2.6000	10.710	5.6400
3.6400	17.670	4.4400	2.8400	10.710	5.4000
4.8800	17.090	2.2400	3.2400	10.710	5.0300
7.3200	17.090	3.1600	3.6500	10.710	4.5800
2.2900	10.760	6.4800	2.4600	11.380	6.1200
3.0700	10.760	5.7000	2.4300	10.710	6.1200
3.8300	10.760	3.2300			

APPENDIX C: INITIAL REGRESSION ANALYSIS USING COMPLETE POLYNOMIAL

```
# OF OBSERVATIONS = 291
# OF VARIABLES    =  10
DATA FORMAT       = (10G13.5)


 THE MATRIX OF CORRECTED SUMS OF SQUARES AND CROSS PRODUCTS
          VAR  1       VAR  2       VAR  3       VAR  4       VAR  5
          VAR  6       VAR  7       VAR  8       VAR  9       VAR 10

 VAR   1  1356.984
 VAR   2  316.4450      13506.07
 VAR   3  11122.82      3847.509      107506.8
 VAR   4  17423.44      37928.35      151712.9      409046.1
 VAR   5  12729.39      44C245.8      150691.2      1193606.     0.1626475E 08

 VAR   6  96397.88      37844.24      1022243.      1362633.      1454390.
        0.1031309E 08
 VAR   7  146475.1      233512.9      1462337.      3336613.      7753955.
        0.1416536E 08 0.3122043E 08
 VAR   8  336311.0      1109542.      3080069.     0.1018639E 08 0.3667886E 08
        0.2841263E 08 0.8400481E 08 0.2795254E 09
 VAR   9  313493.7     0.1375857E 08  4340306.     0.3238093E 08 0.5622751E 09
        0.4307228E 08 0.2202168E 09 0.1042440E 10 0.2109822E 11
 VAR  10 -677.0793      -821.6802     -5830.070     -10561.18     -35335.82
        -50474.70      -85460.37     -243978.2     -1176479.      902.6241



 THE INVERSE OF THE ABOVE MATRIX
 THE GAUSSIAN MULTIPLIERS - CIJ
          VAR  1       VAR  2       VAR  3       VAR  4       VAR  5
          VAR  6       VAR  7       VAR  8       VAR  9       VAR 10

 VAR   1 0.3164392E-01
 VAR   2 0.4200333E-02 0.6523490E-02
 VAR   3-0.5190748E-02-0.1691900E-03 0.1396311E-02
 VAR   4-0.1791126E-02-0.6130154E-03 0.7529107E-04 0.2436045E-03
 VAR   5-0.1291725E-03-0.3769453E-03 0.3231437E-05 0.2262274E-04 0.2406608E-04

 VAR   6 0.2597093E-03 0.1108469E-04-0.8586747E-04 0.1145565E-05-0.8871812E-06
        0.6220975E-05
 VAR   7 0.8171819E-04-0.1018447E-04-0.9329943E-05-0.7026746E-05 0.1565851E-05
       -0.2629901E-06 0.1174514E-05
 VAR   8 0.2887713E-04 0.2311406E-04 0.2784674E-06-0.5202772E-05-0.1304508E-05
        0.3723608E-07-0.1253193E-06 0.2003564E-06
 VAR   9 0.1222075E-05 0.5606212E-05-0.2369765E-07-0.2376414E-06-0.3767201E-06
        0.1568884E-07-0.2940027E-07 0.1858839E-07 0.6106491E-08
 VAR  10-0.3223029E-03-0.7223418E-03 0.3378536E-03 0.3357886E-05 0.4268880E-04
       -0.1755235E-04-0.4849075E-05 0.1158573E-05-0.5838990E-06 0.2212690E-02
```

THE SAMPLE PARTIAL CORRELATION COEFFICENTS:RIJ
RIJ = CIJ / (CII * CJJ)**.5
THESE REPRESENT CORRELATIONS BETWEEN THE VARIABLES
THE CLOSER TO +- 1, THE MORE DEPENDENCE
THE CLOSER TO 0 THE MORE INDEPENDENCE

	VAR 1	VAR 2	VAR 3	VAR 4	VAR 5
	VAR 6	VAR 7	VAR 8	VAR 9	VAR 10
VAR 1	1.000000				
VAR 2	0.2923469	1.000000			
VAR 3	-0.7808969	-0.5605878E-01	1.000000		
VAR 4	-0.6451168	-0.4862826	0.1290951	1.000000	
VAR 5	-0.1480206	-0.9513397	0.1762796E-01	0.2954609	1.000000
VAR 6	0.5853466	0.5502427E-01	-0.9213155	0.2942713E-01	-0.7250709E-01
	1.000000				
VAR 7	0.4238814	-0.1163507	-0.2303874	-0.4154153	0.2945227
	-0.9729284E-01	1.000000			
VAR 8	0.3626664	0.6393440	0.1664875E-01	-0.7447158	-0.5940766
	0.3335286E-01	-0.2583374	1.000000		
VAR 9	0.8791379E-01	0.8882467	-0.8115557E-02	-0.1948425	-0.9826984
	0.8049443E-01	-0.3471573	0.5314280	1.000000	
VAR 10	-0.3851756E-01	-0.1901264	0.1922106	0.4573651E-02	0.1849912
	-0.1496048	-0.9511947E-01	0.5502519E-01	-0.1588479	1.000000

THE STANDARD ERRORS OF THE ABOVE RIJ : SIJ
SIJ = ((1 - RIJ*RIJ) / DOF RESIDUAL)**.5

	VAR 1	VAR 2	VAR 3	VAR 4	VAR 5
	VAR 6	VAR 7	VAR 8	VAR 9	VAR 10
VAR 1	0.0000000				
VAR 2	0.5704881E-01	0.0000000			
VAR 3	0.3726409E-01	0.5956119E-01	0.0000000		
VAR 4	0.4558143E-01	0.5212663E-01	0.5915582E-01	0.0000000	
VAR 5	0.5899786E-01	0.1838234E-01	0.5964573E-01	0.5699169E-01	0.0000000
VAR 6	0.4836727E-01	0.5956462E-01	0.2319481E-01	0.5962916E-01	0.5949798E-01
	0.0000000				
VAR 7	0.5403059E-01	0.5924983E-01	0.5805022E-01	0.5426409E-01	0.5700897E-01
	0.5937198E-01	0.0000000			
VAR 8	0.5559363E-01	0.4586997E-01	0.5964673E-01	0.3981266E-01	0.4798699E-01
	0.5962181E-01	0.5763000E-01	0.0000000		
VAR 9	0.5942402E-01	0.2740352E-01	0.5965303E-01	0.5851168E-01	0.1104887E-01
	0.5946142E-01	0.5594487E-01	0.5053396E-01	0.0000000	
VAR 10	0.5961073E-01	0.5856687E-01	0.5854265E-01	0.5965437E-01	0.5862536E-01
	0.5898363E-01	0.5938451E-01	0.5956462E-01	0.5889756E-01	0.0000000

1 ACTUAL	PREDICTED	RESIDUAL	ST. RESIDUAL
2.300000	4.322512	-2.022512	-1.594794
5.000000	6.156770	-1.156770	-0.9121377
5.480000	6.399461	-0.9194613	-0.7250149
5.799999	6.471604	-0.6716051	-0.5295751
6.160000	6.410108	-0.2501078	-0.1972153
4.809999	6.427693	-1.617694	-1.275586
6.200000	6.478167	-0.2781668	-0.2193405
6.200000	6.478167	-0.2781668	-0.2193405
6.690000	6.403580	0.2864199	0.2258482
5.879999	5.322294	0.5577049	0.4397622
1.270000	3.518832	-2.248832	-1.773252
1.260000	4.524147	-3.264147	-2.573850
6.000000	5.194230	0.8057699	0.6353668
6.129999	5.440581	0.6894178	0.5436207
6.480000	5.699246	0.7807531	0.6156405
6.679999	5.349003	1.330997	1.049519
7.919999	5.917610	2.002389	1.578926
7.009999	6.164141	0.8458586	0.6669775
8.109999	6.208746	1.901253	1.499178
6.200000	6.297118	-0.9711838E-01	-0.7657993E-01
6.169999	6.328126	-0.1581268	-0.1246864
6.000000	6.242813	-0.2428131	-0.1914634
4.620000	3.997135	0.6228652	0.4911425
4.620000	3.997135	0.6228652	0.4911425
4.809999	4.676984	0.1330156	0.1048857
5.480000	5.015120	0.4648800	0.3665678
5.480000	5.015120	0.4648800	0.3665678
4.250000	4.348463	-0.9846306E-01	-0.7764024E-01
4.250000	4.348463	-0.9846306E-01	-0.7764024E-01
6.129999	5.098335	1.031664	0.8134890
6.129999	5.098335	1.031664	0.8134890
5.820000	5.627734	0.1922655	0.1516055
5.490000	5.834403	-0.3444033	-0.2715694
5.490000	5.834403	-0.3444033	-0.2715694
5.330000	5.499974	-0.1699743	-0.1340284
6.660000	5.889662	0.7703381	0.6074280
6.660000	6.025513	0.6344872	0.5003066
5.000000	5.797777	-0.7977772	-0.6290644
5.580000	5.807294	-0.2272940	-0.1792262
5.490000	5.712016	-0.2220163	-0.1750647
5.469999	5.895696	-0.4256964	-0.3356707
3.260000	3.799948	-0.5399480	-0.4257606
3.300000	5.738327	-2.438327	-1.922673
3.300000	5.738327	-2.438327	-1.922673
4.459999	5.645411	-1.185412	-0.9347231
4.459999	5.645411	-1.185412	-0.9347231
3.910000	5.807120	-1.897120	-1.495920
3.910000	5.807120	-1.897120	-1.495920
3.840000	5.617790	-1.777791	-1.401826
3.840000	5.617790	-1.777791	-1.401826
5.179999	5.613799	-0.4337997	-0.3420604
5.179999	5.613799	-0.4337997	-0.3420604
3.350000	6.022786	-2.672786	-2.107549
3.350000	6.022786	-2.672786	-2.107549
6.059999	5.824012	0.2359877	0.1860813
6.059999	5.824012	0.2359877	0.1860813

3.910000	6.183818	-2.273818	-1.792954
3.910000	6.183818	-2.273818	-1.792954
6.059999	5.999811	0.6018829E-01	0.4745975E-01
6.059999	5.999811	0.6018829E-01	0.4745975E-01
3.910000	6.291606	-2.381606	-1.877948
3.910000	6.291606	-2.381606	-1.877948
5.190000	6.133983	-0.9439831	-0.7443509
5.190000	6.133983	-0.9439831	-0.7443509
3.660000	5.759581	-2.099581	-1.655565
3.660000	5.759581	-2.099581	-1.655565
6.969999	5.640507	1.329493	1.048333
6.969999	5.640507	1.329493	1.048333
6.520000	6.165604	0.3543959	0.2794487
6.520000	6.165604	0.3543959	0.2794487
5.490000	5.985950	-0.4959497	-0.3910670
5.490000	5.985950	-0.4959497	-0.3910670
5.490000	5.985950	-0.4959497	-0.3910670
6.209999	5.483028	0.7269707	0.5732318
6.209999	5.483028	0.7269707	0.5732318
6.209999	5.483028	0.7269707	0.5732318
7.429999	6.310980	1.119020	0.8823707
7.429999	6.310980	1.119020	0.8823707
7.429999	6.310980	1.119020	0.8823707
7.429999	6.310980	1.119020	0.8823707
7.429999	6.310980	1.119020	0.8823707
6.580000	5.791819	0.7881813	0.6214978
6.580000	5.791819	0.7881813	0.6214978
7.429999	6.423399	1.006600	0.7937258
7.429999	6.423399	1.006600	0.7937258
7.429999	6.423399	1.006600	0.7937258
7.429999	6.423399	1.006600	0.7937258
6.040000	6.419282	-0.3792820	-0.2990720
6.040000	6.419282	-0.3792820	-0.2990720
6.040000	6.419282	-0.3792820	-0.2990720
6.520000	6.313617	0.2063828	0.1627372
6.520000	6.313617	0.2063828	0.1627372
6.520000	6.313617	0.2063828	0.1627372
4.879999	5.904298	-1.024299	-0.8076814
4.879999	5.904298	-1.024299	-0.8076814
5.799999	2.317914	3.482085	2.745698
3.480000	5.178669	-1.698669	-1.339437
6.959999	5.802749	1.157250	0.9125166
3.480000	5.549845	-2.069845	-1.632117
3.480000	5.549845	-2.069845	-1.632117
3.480000	5.549845	-2.069845	-1.632117
7.309999	5.086012	2.223988	1.753662
6.580000	6.270692	0.3093081	0.2438960
6.559999	6.242435	0.3175640	0.2504060
7.200000	6.049043	1.150957	0.9075543
6.780000	5.647773	1.132227	0.8927851
3.760000	5.000769	-1.240769	-0.9783729
4.639999	4.416367	0.2236328	0.1763392
6.919999	6.139118	0.7808809	0.6157413
4.540000	2.984984	1.555016	1.226163
5.959999	5.970359	-0.1035976E-01	-0.8168897E-02
6.750000	5.993528	0.7564716	0.5964940
5.139999	5.545798	-0.4057989	-0.3199812

3.040000	5.018438	-1.978438	-1.560041
6.910000	5.966016	0.9439840	0.7443515
3.600000	5.042948	-1.442948	-1.137795
1.630000	3.877679	-2.247679	-1.772343
8.539999	5.565712	2.974287	2.345289
4.370000	3.116086	1.253913	0.9887375
5.089999	5.006434	0.8356476E-01	0.6589259E-01
5.759999	5.418088	0.3419113	0.2696044
5.450000	5.487806	-0.3780651E-01	-0.2981124E-01
4.969999	5.401546	-0.4315462	-0.3402835
2.920000	3.049366	-0.1293664	-0.1020082
4.679999	5.017040	-0.3370409	-0.2657640
6.440000	5.639977	0.8000231	0.6308353
8.779999	5.667517	3.112482	2.454258
7.049999	6.317603	0.7323961	0.5775100
7.400000	6.349758	1.050241	0.8281378
7.049999	6.191698	0.8583012	0.6767888
8.759998	6.297883	2.462115	1.941431
7.610000	6.226301	1.383698	1.091076
7.690000	6.020459	1.669540	1.316468
7.469999	5.687214	1.782785	1.405764
6.040000	4.454331	1.585669	1.250334
6.250000	6.453784	-0.2037840	-0.1606880
5.879999	6.438199	-0.5581999	-0.4401526
8.129999	6.423483	1.706516	1.345624
8.129999	6.400278	1.729721	1.363922
8.500000	6.324190	2.175810	1.715672
10.25000	6.143608	4.106392	3.237978
7.870000	6.118374	1.751626	1.381194
7.000000	5.950857	1.049143	0.8272715
6.879999	5.892477	0.9875221	0.7786822
3.810000	5.122766	-1.312767	-1.035145
3.810000	4.584194	-0.7741942	-0.6104687
4.500000	4.584194	-0.8419418E-01	-0.6638892E-01
4.500000	3.512161	0.9878387	0.7789320
4.440000	2.812549	1.627451	1.283280
2.620000	2.332145	0.2878547	0.2269796
5.940000	2.330984	3.609015	2.845786
6.500000	5.456409	1.043591	0.8228934
8.000000	4.598853	3.401147	2.681877
3.500000	3.730584	-0.2305841	-0.1818205
1.750000	4.644468	-2.894468	-2.282351
3.000000	3.270216	-0.2702165	-0.2130715
1.875000	2.059444	-0.1844444	-0.1454384
3.500000	2.988802	0.5111976	0.4030902
4.000000	2.988802	1.011198	0.7973509
1.500000	2.316247	-0.8162470	-0.6436282
0.8750000	1.389722	-0.5147221	-0.4058694
2.250000	0.7840884	1.465912	1.155903
0.7500000	0.3426785	0.4073215	0.3211817
0.0000000	0.6266217	-0.6266217	-0.4941047
0.0000000	0.5972332	-0.5972332	-0.4709312
5.849999	6.237408	-0.3874083	-0.3054797
7.250000	5.588769	1.661231	1.309916
8.500000	5.223693	3.276307	2.583438
2.050000	4.069355	-2.019355	-1.592305
3.970000	4.388676	-0.4186759	-0.3301349

2.840000	5.325740	-2.485740	-1.960059
3.290000	5.609191	-2.319191	-1.828732
6.709999	5.427681	1.282318	1.011135
6.150000	6.032910	0.1170893	0.9232739E-01
7.860000	6.334590	1.525410	1.202818
7.200000	6.336077	0.8639231	0.6812217
4.000000	2.160582	1.839418	1.450420
6.650000	4.795046	1.854954	1.462671
5.549999	5.816327	-0.2663279	-0.2100052
5.750000	6.127997	-0.3779974	-0.2980590
4.070000	2.738162	1.331838	1.050183
4.910000	5.502283	-0.5922832	-0.4670280
5.370000	5.272045	0.9795475E-01	0.7723941E-01
5.410000	4.390880	1.019120	0.8035980
4.169999	2.875768	1.294231	1.020529
5.500000	4.831560	0.6684399	0.5270791
5.320000	5.413430	-0.9343052E-01	-0.7367197E-01
5.379999	5.502283	-0.1222839	-0.9642351E-01
0.0000000	1.646255	-1.646255	-1.298107
1.330000	4.526943	-3.196943	-2.520858
6.120000	5.850915	0.2690849	0.2121792
4.770000	6.312851	-1.542851	-1.216572
2.560000	2.817309	-0.2573090	-0.2028936
0.0000000	2.020229	-2.020229	-1.592994
0.0000000	1.173855	-1.173855	-0.9256097
0.0000000	1.131901	-1.131901	-0.8925278
5.250000	5.571877	-0.3218775	-0.2538073
4.650000	5.739481	-1.089481	-0.8590794
5.160000	5.880660	-0.7206602	-0.5682560
7.459999	5.201477	2.258522	1.780893
5.040000	6.244391	-1.204391	-0.9496886
7.860000	6.412027	1.447972	1.141757
8.119999	6.488779	1.631220	1.286252
6.530000	6.473336	0.5666351E-01	0.4468039E-01
6.900000	6.482731	0.4172688	0.3290253
6.990000	6.464739	0.5252609	0.4141794
5.820000	6.448898	-0.6288986	-0.4959000
6.270000	6.378656	-0.1086569	-0.8567828E-01
6.400000	6.253687	0.1463127	0.1153707
7.500000	6.451098	1.048902	0.8270812
6.580000	6.476042	0.1039581	0.8197320E-01
5.750000	6.306323	-0.5563231	-0.4386727
6.440000	6.140313	0.2996864	0.2363091
5.020000	6.458466	-1.438466	-1.134261
5.540000	6.476042	-0.9360418	-0.7380891
6.139999	6.406593	-0.2665939	-0.2102150
6.900000	6.289943	0.6100569	0.4810429
6.669999	6.352664	0.3173351	0.2502255
6.549999	6.476042	0.7395744E-01	0.5831702E-01
7.250000	6.398646	0.8513536	0.6713105
6.919999	6.300648	0.6193514	0.4883718
5.650000	6.335758	-0.6857586	-0.5407354
5.820000	6.475176	-0.6551762	-0.5166205
6.620000	6.394775	0.2252245	0.1775943
5.860000	6.216175	-0.3561754	-0.2808520
6.099999	6.467246	-0.3672466	-0.2895818
6.500000	6.463087	0.3691292E-01	0.2910662E-01

6.480000	6.468183	0.1181698E-01	0.9317940E-02
6.520000	6.317667	0.2023325	0.1595435
6.070000	6.372327	-0.3023272	-0.2383915
6.049999	6.481307	-0.4313078	-0.3400955
6.270000	6.445546	-0.1755466	-0.1384223
6.049999	6.327826	-0.2778263	-0.2190720
5.719999	6.335758	-0.6157589	-0.4855391
7.509999	6.481307	1.028692	0.8111458
6.750000	6.445546	0.3044538	0.2400683
7.099999	6.270913	0.8290863	0.6537522
5.809999	6.003121	-0.1931219	-0.1522808
6.629999	6.253039	0.3769598	0.2972409
6.389999	6.283586	0.1064138	0.8390959E-01
6.469999	6.229603	0.2403965	0.1895578
5.559999	5.713383	-0.1533833	-0.1209460
6.099999	6.143804	-0.4380417E-01	-0.3454053E-01
6.639999	6.304709	0.3352900	0.2643833
6.349999	6.270191	0.7980824E-01	0.6293049E-01
6.790000	5.793820	0.9961796	0.7855089
6.400000	5.748468	0.6515312	0.5137463
5.809999	5.680187	0.1298122	0.1023597
6.379999	5.756392	0.6236076	0.4917279
7.599999	5.400577	2.199423	1.734292
4.440000	4.782805	-0.3428059	-0.2703098
2.240000	4.149226	-1.909226	-1.505466
3.160000	2.827332	0.3326674	0.2623153
6.480000	6.055430	0.4245691	0.3347818
5.700000	5.703501	-0.3500938E-02	-0.2760565E-02
3.230000	5.294816	-2.064816	-1.628152
2.550000	4.829988	-2.279989	-1.797820
7.110000	6.469578	0.6404219	0.5049863
5.950000	6.469578	-0.5195780	-0.4096984
7.129999	6.469578	0.6604214	0.5207564
7.200000	6.469578	0.7304220	0.5759534
6.360000	6.469578	-0.1095781	-0.8640471E-01
6.540000	6.469578	0.7042217E-01	0.5552939E-01
5.440000	6.297028	-0.8570280	-0.6757849
6.410000	6.255799	0.1542006	0.1215904
6.730000	6.288687	0.4413128	0.3479846
6.129999	6.173958	-0.4395866E-01	-0.3466235E-01
6.309999	6.069370	0.2406292	0.1897413
5.740000	6.255799	-0.5157995	-0.4067190
5.540000	6.304756	-0.7647562	-0.6030266
6.750000	6.250532	0.4994678	0.3938410
3.130000	5.852849	-2.722849	-2.147025
6.580000	6.162016	0.4179840	0.3295893
6.900000	6.285694	0.6143055	0.4843930
5.709999	6.257086	-0.5470867	-0.4313896
6.419999	6.397839	0.2216053E-01	0.1747405E-01
3.310000	5.981867	-2.671867	-2.106824
4.139999	6.232156	-2.092156	-1.649710
5.419999	6.138083	-0.7180834	-0.5662242
5.500000	6.001534	-0.5015345	-0.3954707
5.799999	5.852165	-0.5216599E-01	-0.4113400E-01
5.669999	5.728003	-0.5800343E-01	-0.4573695E-01
5.549999	5.506139	0.4386044E-01	0.3458489E-01
4.520000	5.267131	-0.7471313	-0.5891291

```
 5.309999        6.064188      -0.7541885      -0.5946939
 5.639999        5.926043      -0.2860432      -0.2255512
 5.400000        5.816261      -0.4162617      -0.3282313
 5.030000        5.617781      -0.5877810      -0.4634779
 4.580000        5.397246      -0.8172464      -0.6444163
 6.120000        5.971783       0.1482172       0.1168724
 6.120000        5.999149       0.1208506       0.9529325E-01

COEF # BEST VALUE CORRELATION STD. ERROR        T
   0     4.872201      0.1532939      0.4965340       9.812422
   1    0.1456611      0.3159698E-01 0.2254287      0.6461514
   2    0.3264541      0.6287679E-02 0.1005615       3.246313
   3   -0.1526891      0.1344724E-02 0.4650537E-01 -3.283257
   4   -0.1517558E-02 0.2435994E-03 0.1979359E-01-0.7666917E-01
   5   -0.1929272E-01 0.2324250E-04 0.6114035E-02 -3.155480
   6    0.7932583E-02 0.6081740E-05 0.3127522E-02  2.536379
   7    0.2191484E-02 0.1163888E-05 0.1368176E-02  1.601756
   8   -0.5236040E-03 0.1997498E-06 0.5667998E-03-0.9237900
   9    0.2638865E-03 0.5952408E-08 0.9784370E-04  2.697021


      ANALYSIS OF VARIANCE

SOURCE OF VARIATION SUM OF SQUARES DOF MEAN SQUARE
TOTAL                902.6241      290
REGRESSION           450.6854        9  50.07616
RESIDUAL             451.9385      281  1.608322

R SQUARED = 0.4993058     R = 0.7066157
THE STANDARD ERROR OF Y ABOUT THE REGRESSION PLANE IS   1.268196

THE F RATIO TESTING THE NULL HYPOTHESIS THAT ALL THE
COEFFICENTS ARE ZERO, I.E. B1=B2=...=BK=0, IS   31.13565
BASED ON THE DEGREES OF FREEDOM    9/ 281



NOW A STEP-WISE DOWN REGRESSION WILL TAKE PLACE
THE VARIABLE WITH THE LOWEST T WILL BE DELETE
THIS WILL CONTINUE UNTIL THERE ARE JUST TWO VARIABLES LEFT


COEF # BEST VALUE CORRELATION STD. ERROR        T
   0     4.895369      0.9651806E-01 0.3933001      12.44691
   1    0.1345059      0.1843446E-01 0.1718838     0.7825398
   2    0.3226420      0.4750544E-02 0.8725522E-01  3.697682
   3   -0.1522233      0.1321769E-02 0.4602540E-01 -3.307375
   5   -0.1915219E-01 0.2115357E-04 0.5822528E-02 -3.289325
   6    0.7939885E-02 0.6076099E-05 0.3120557E-02  2.544381
   7    0.2147755E-02 0.9616221E-06 0.1241429E-02  1.730067
   8   -0.5560268E-03 0.8855436E-07 0.3767252E-03 -1.475948
   9    0.2624116E-03 0.5722304E-08 0.9576465E-04  2.740172
```

ANALYSIS OF VARIANCE

SOURCE OF VARIATION	SUM OF SQUARES	DOF	MEAN SQUARE
TOTAL	902.6241	290	
REGRESSION	450.6760	8	56.33450
RESIDUAL	451.9481	282	1.602653

R SQUARED = 0.4992953 R = 0.7066083
THE STANDARD ERROR OF Y ABOUT THE REGRESSION PLANE IS 1.265959

THE F RATIO TESTING THE NULL HYPOTHESIS THAT ALL THE
COEFFICENTS ARE ZERO, I.E. B1=B2=...=BK=0, IS 35.15078
BASED ON THE DEGREES OF FREEDOM 8/ 282

COEF #	BEST VALUE	CORRELATION	STD. ERROR	T
0	4.987683	0.8783478E-01	0.3749345	13.30281
2	0.3255821	0.4741736E-02	0.8711457E-01	3.737401
3	-0.1187190	0.1779785E-03	0.1687741E-01	-7.034195
5	-0.1946494E-01	0.2105390E-04	0.5804815E-02	-3.353240
6	0.6000717E-02	0.2244512E-05	0.1895322E-02	3.166067
7	0.1933137E-02	0.9146887E-06	0.1209926E-02	1.597732
8	-0.4888172E-03	0.8395169E-07	0.3665530E-03	-1.333551
9	0.2668135E-03	0.5702560E-08	0.9553379E-04	2.792871

ANALYSIS OF VARIANCE

SOURCE OF VARIATION	SUM OF SQUARES	DOF	MEAN SQUARE
TOTAL	902.6241	290	
REGRESSION	449.6945	7	64.24207
RESIDUAL	452.9295	283	1.600458

R SQUARED = 0.4982080 R = 0.7058385
THE STANDARD ERROR OF Y ABOUT THE REGRESSION PLANE IS 1.265092

THE F RATIO TESTING THE NULL HYPOTHESIS THAT ALL THE
COEFFICENTS ARE ZERO, I.E. B1=B2=...=BK=0, IS 40.13981
BASED ON THE DEGREES OF FREEDOM 7/ 283

COEF #	BEST VALUE	CORRELATION	STD. ERROR	T
0	4.809273	0.7665141E-01	0.3507329	13.71207
2	0.3850728	0.3498266E-02	0.7492778E-01	5.139253
3	-0.1221848	0.1737582E-03	0.1669895E-01	-7.316917
5	-0.2425978E-01	0.1297624E-04	0.4563425E-02	-5.316135
6	0.7190097E-02	0.1747487E-05	0.1674648E-02	4.293498
7	0.4305980E-03	0.1214795E-06	0.4415379E-03	0.9752233
9	0.3456187E-03	0.3520603E-08	0.7516661E-04	4.598035

ANALYSIS OF VARIANCE

SOURCE OF VARIATION	SUM OF SQUARES	DOF	MEAN SQUARE
TOTAL	902.6241	290	
REGRESSION	446.8484	6	74.47472
RESIDUAL	455.7758	284	1.604844

```
R SQUARED = 0.4950548      R = 0.7036013
THE STANDARD ERROR OF Y ABOUT THE REGRESSION PLANE IS   1.266824

THE F RATIO TESTING THE NULL HYPOTHESIS THAT ALL THE
COEFFICENTS ARE ZERO, I.E. B1=B2=...=BK=0, IS   46.40620
BASED ON THE DEGREES OF FREEDOM    6/ 284


COEF #  BEST VALUE      CORRELATION     STD. ERROR       T
   0     4.806970      0.7664793E-01  0.3506948       13.70699
   2    0.3756840      0.3440512E-02  0.7430031E-01    5.056291
   3   -0.1188613      0.1665213E-03  0.1634610E-01   -7.271542
   5   -0.2323101E-01  0.1228282E-04  0.4439439E-02   -5.232871
   6    0.7416429E-02  0.1713925E-05  0.1658345E-02    4.472186
   9    0.3276729E-03  0.3309602E-08  0.7287305E-04    4.496490


      ANALYSIS OF VARIANCE

SOURCE OF VARIATION  SUM OF SQUARES  DOF  MEAN SQUARE
TOTAL                  902.6241      290
REGRESSION             445.3221        5   89.06441
RESIDUAL               457.3019      285   1.604568

R SQUARED = 0.4933639      R = 0.7023986
THE STANDARD ERROR OF Y ABOUT THE REGRESSION PLANE IS   1.266716

THE F RATIO TESTING THE NULL HYPOTHESIS THAT ALL THE
COEFFICENTS ARE ZERO, I.E. B1=B2=...=BK=0, IS   55.50678
BASED ON THE DEGREES OF FREEDOM    5/ 285


COEF #  BEST VALUE      CORRELATION     STD. ERROR       T
   0     4.423452      0.7206470E-01  0.3511621       12.59661
   2    0.4161844      0.3389400E-02  0.7615663E-01    5.464848
   3   -0.4793454E-01  0.9765912E-05  0.4087923E-02   -11.72589
   5   -0.2572381E-01  0.1208918E-04  0.4548255E-02   -5.655754
   9    0.3682456E-03  0.3258307E-08  0.7466934E-04    4.931684


      ANALYSIS OF VARIANCE

SOURCE OF VARIATION  SUM OF SQUARES  DOF  MEAN SQUARE
TOTAL                  902.6241      290
REGRESSION             413.2301        4   103.3075
RESIDUAL               489.3940      286   1.711168

R SQUARED = 0.4578097      R = 0.6766163
THE STANDARD ERROR OF Y ABOUT THE REGRESSION PLANE IS   1.308116

THE F RATIO TESTING THE NULL HYPOTHESIS THAT ALL THE
COEFFICENTS ARE ZERO, I.E. B1=B2=...=BK=0, IS   60.37251
BASED ON THE DEGREES OF FREEDOM    4/ 286
```

```
COEF #  BEST VALUE      CORRELATION      STD. ERROR          T
   0     5.742243      0.3027507E-01  0.2366758        24.26206
   2    0.7725544E-01  0.6292402E-03  0.3412083E-01    2.264172
   3   -0.5168957E-01  0.9427112E-05  0.4176386E-02  -12.37663
   5   -0.3784753E-02  0.5239919E-06  0.9846312E-03  -3.843828


      ANALYSIS OF VARIANCE

SOURCE OF VARIATION  SUM OF SQUARES  DOF  MEAN SQUARE
TOTAL                  902.6241      290
REGRESSION             371.6119        3   123.8706
RESIDUAL               531.0122      287   1.850217

R SQUARED = 0.4117017      R = 0.6416398
THE STANDARD ERROR OF Y ABOUT THE REGRESSION PLANE IS   1.360227

THE F RATIO TESTING THE NULL HYPOTHESIS THAT ALL THE
COEFFICENTS ARE ZERO, I.E. B1=B2=...=BK=0, IS   66.94923
BASED ON THE DEGREES OF FREEDOM    3/ 287


COEF #  BEST VALUE      CORRELATION      STD. ERROR          T
   0     6.227016      0.5498795E-02  0.1015861        61.29792
   3   -0.5185799E-01  0.9424121E-05  0.4205532E-02  -12.33090
   5   -0.1692082E-02  0.6229162E-07  0.3419128E-03  -4.948870


      ANALYSIS OF VARIANCE

SOURCE OF VARIATION  SUM OF SQUARES  DOF  MEAN SQUARE
TOTAL                  902.6241      290
REGRESSION             362.1267        2   181.0634
RESIDUAL               540.4973      288   1.876727

R SQUARED = 0.4011933      R = 0.6333982
THE STANDARD ERROR OF Y ABOUT THE REGRESSION PLANE IS   1.369937

THE F RATIO TESTING THE NULL HYPOTHESIS THAT ALL THE
COEFFICENTS ARE ZERO, I.E. B1=B2=...=BK=0, IS   96.47827
BASED ON THE DEGREES OF FREEDOM    2/ 288

COEF #  BEST VALUE      CORRELATION      STD. ERROR          T
   0     5.983677      0.4210507E-02  0.9243528E-01   64.73369
   3   -0.5422976E-01  0.9301735E-05  0.4344628E-02  -12.48203


      ANALYSIS OF VARIANCE

SOURCE OF VARIATION  SUM OF SQUARES  DOF  MEAN SQUARE
TOTAL                  902.6241      290
REGRESSION             316.1632        1   316.1632
RESIDUAL               586.4608      289   2.029276

R SQUARED = 0.3502712      R = 0.5918372
THE STANDARD ERROR OF Y ABOUT THE REGRESSION PLANE IS   1.424527

THE F RATIO TESTING THE NULL HYPOTHESIS THAT ALL THE
COEFFICENTS ARE ZERO, I.E. B1=B2=...=BK=0, IS   155.8010
BASED ON THE DEGREES OF FREEDOM    1/ 289
```

APPENDIX D: REGRESSION ANALYSIS WITH TWO COEFFICIENTS OF THE ORIGINAL POLYNOMIAL DELETED

```
# OF OBSERVATIONS = 291
# OF VARIABLES    =   8
DATA FORMAT       = ( 8G13.5)


 THE MATRIX OF CORRECTED SUMS OF SQUARES AND CROSS PRODUCTS
            VAR  1          VAR  2          VAR  3          VAR  4          VAR  5
            VAR  6          VAR  7          VAR  8
 VAR  1   13506.07
 VAR  2   3847.509          107506.8
 VAR  3   440245.8          150691.2        0.1626475E 08
 VAR  4   37844.24          1022243.         1454390.       0.1031309E 08
 VAR  5   233512.9          1462337.         7753955.       0.1416536E 08 0.3122043E 08

 VAR  6   1109542.          3080069.        0.3667886E 08  0.2841263E 08 0.8400481E 08
          0.2795254E 09
 VAR  7   0.1375857E 08     4340306.        0.5622751E 09  0.4307228E 08 0.2202168E 09
          0.1042440E 10  0.2109822E 11
 VAR  8   -821.6802         -5830.070       -35335.82       -50474.70      -85460.37
          -243978.2         -1176479.        902.6241


 THE INVERSE OF THE ABOVE MATRIX
 THE GAUSSIAN MULTIPLIERS - CIJ
            VAR  1          VAR  2          VAR  3          VAR  4          VAR  5
            VAR  6          VAR  7          VAR  8
 VAR  1  0.4975777E-02
 VAR  2-0.5676357E-04  0.2090964E-03
 VAR  3-0.3193991E-03  0.5567560E-05  0.2189042E-04
 VAR  4  0.1842201E-04-0.1891941E-04-0.1532943E-05  0.2324013E-05
 VAR  5-0.2736755E-04  0.3853160E-06  0.2157947E-05-0.6661299E-06  0.9229395E-06

 VAR  6  0.9865832E-05-0.4671066E-06-0.8024814E-06  0.1977934E-06-0.2601391E-06
         0.8447924E-07
 VAR  7  0.4999476E-05-0.8207830E-07-0.3535946E-06  0.2442903E-07-0.3540064E-07
         0.1324641E-07  0.5859736E-08
 VAR  8-0.7188362E-03  0.2621137E-03  0.4297565E-04-0.1324868E-04-0.4268074E-05
         0.1079235E-05-0.5890841E-06  0.2207849E-02


 THE SAMPLE PARTIAL CORRELATION COEFFICENTS:RIJ
 RIJ = CIJ / ( CII * CJJ )**.5
 THESE REPRESENT CORRELATIONS   BETWEEN THE VARIABLES
 THE CLOSER TO +- 1, THE MORE DEPENDENCE
 THE CLOSER TO 0 THE MORE INDEPENDENCE

            VAR  1          VAR  2          VAR  3          VAR  4          VAR  5
            VAR  6          VAR  7          VAR  8
 VAR  1   1.000000
 VAR  2-0.5565010E-01   1.000000
 VAR  3-0.9677791       0.8229331E-01   1.000000
 VAR  4  0.1713118     -0.8582521      -0.2149214        1.000000
 VAR  5-0.4038488       0.2773685E-01  0.4800948     -0.4548341        1.000000

 VAR  6  0.4812029     -0.1111393      -0.5901099       0.4463931     -0.9316313
         1.000000
 VAR  7  0.9258808     -0.7415084E-01-0.9872782       0.2093379     -0.4813772
         0.5953661       1.000000
 VAR  8-0.2168776       0.3857729       0.1954837     -0.1849560     -0.9454981E-01
         0.7902349E-01-0.1637773         1.000000


 THE STANDARD ERRORS OF THE ABOVE RIJ :      SIJ
 SIJ = (   ( 1 - RIJ*RIJ ) / DOF RESIDUAL   )**.5
            VAR  1          VAR  2          VAR  3          VAR  4          VAR  5
            VAR  6          VAR  7          VAR  8
 VAR  1  0.0000000
 VAR  2  0.5935171E-01  0.0000000
 VAR  3  0.1496799E-01  0.5924221E-01  0.0000000
 VAR  4  0.5856506E-01  0.3050825E-01  0.5805471E-01  0.0000000
 VAR  5  0.5438075E-01  0.5942096E-01  0.5214511E-01  0.5293926E-01  0.0000000

 VAR  6  0.5210901E-01  0.5907557E-01  0.4799037E-01  0.5319254E-01  0.2160218E-01
         0.0000000
```

```
VAR   7 0.2245882E-01 0.5928018E-01 0.9451695E-02 0.5812675E-01 0.5210332E-01
        0.4776041E-01 0.0000000
VAR   8 0.5802900E-01 0.5484251E-01 0.5829698E-01 0.5841823E-01 0.5917753E-01
        0.5925793E-01 0.5864118E-01 0.0000000
```

1	ACTUAL	PREDICTED	RESIDUAL	ST. RESIDUAL
	2.300000	4.304292	-2.004292	-1.584306
	5.000000	6.222622	-1.222622	-0.9664294
	5.480000	6.478003	-0.9980030	-0.7888778
	5.799999	6.557627	-0.7576275	-0.5988716
	6.160000	6.507816	-0.3478165	-0.2749338
	4.809999	6.508468	-1.698468	-1.342565
	6.200000	6.569000	-0.3690004	-0.2916788
	6.200000	6.569000	-0.3690004	-0.2916788
	6.690000	6.501635	0.1883650	0.1488943
	5.879999	5.264520	0.6154795	0.4865096
	1.270000	3.581354	-2.311354	-1.827024
A	1.260000	4.529723	-3.269723	-2.584574
	6.000000	5.156713	0.8432865	0.6665812
	6.129999	5.388437	0.7415619	0.5861722
	6.480000	5.651977	0.8280230	0.6545160
	6.679999	5.299209	1.380791	1.091455
	7.919999	5.859524	2.060475	1.628716
	7.009999	6.112702	0.8972969	0.7092741
	8.109999	6.165216	1.944782	1.537265
	6.200000	6.258952	-0.5895233E-01	-0.4659925E-01
	6.169999	6.308202	-0.1382027	-0.1092432
	6.000000	6.242105	-0.2421055	-0.1913738
	4.620000	3.961347	0.6586533	0.5206366
	4.620000	3.961347	0.6586533	0.5206366
	4.809999	4.632504	0.1774960	0.1403028
	5.480000	4.967206	0.5127935	0.4053409
	5.480000	4.967206	0.5127935	0.4053409
	4.250000	4.341399	-0.9139919E-01	-0.7224709E-01
	4.250000	4.341399	-0.9139919E-01	-0.7224709E-01
	6.129999	5.072552	1.057447	0.8358660
B	6.129999	5.072552	1.057447	0.8358660
	5.820000	5.592973	0.2270269	0.1794549
	5.490000	5.795798	-0.3057985	-0.2417204
	5.490000	5.795798	-0.3057985	-0.2417204
	5.330000	5.466882	-0.1368818	-0.1081991
	6.660000	5.848972	0.8110275	0.6410818
	6.660000	5.981642	0.6783581	0.5362124
	5.000000	5.908144	-0.9081440	-0.7178483
	5.580000	5.768806	-0.1888065	-0.1492434
C	5.490000	5.823181	-0.3331814	-0.2633654
	5.469999	5.875707	-0.4057074	-0.3206940
	3.260000	3.805850	-0.5458503	-0.4314709
	3.300000	5.699334	-2.399334	-1.896569
	3.300000	5.699334	-2.399334	-1.896569
	4.459999	5.594620	-1.134621	-0.8968682
	4.459999	5.594620	-1.134621	-0.8968682
	3.910000	5.760390	-1.850390	-1.462653
	3.910000	5.760390	-1.850390	-1.462653
	3.840000	5.560365	-1.720365	-1.359874
	3.840000	5.560365	-1.720365	-1.359874
	5.179999	5.566005	-0.3860054	-0.3051205
	5.179999	5.566005	-0.3860054	-0.3051205
	3.350000	5.980424	-2.630424	-2.079236
D	3.350000	5.980424	-2.630424	-2.079236
	6.059999	5.779963	0.2800360	0.2213562
	6.059999	5.779963	0.2800360	0.2213562
	3.910000	6.145840	-2.235840	-1.767334
	3.910000	6.145840	-2.235840	-1.767334
	6.059999	5.959550	0.1004496	0.7940099E-01
	6.059999	5.959550	0.1004496	0.7940099E-01
	3.910000	6.258507	-2.348507	-1.856392
	3.910000	6.258507	-2.348507	-1.856392
	5.190000	6.097091	-0.9070911	-0.7170160
	5.190000	6.097091	-0.9070911	-0.7170160
	3.660000	5.767786	-2.107786	-1.666113
	3.660000	5.767786	-2.107786	-1.666113
	6.969999	5.604772	1.365228	1.079153
	6.969999	5.604772	1.365228	1.079153

	6.520000	6.215023	0.3049765	0.2410706
	6.520000	6.215023	0.3049765	0.2410706
	5.490000	6.048194	-0.5581942	-0.4412282
	5.490000	6.048194	-0.5581942	-0.4412282
	5.490000	6.048194	-0.5581942	-0.4412282
	6.209999	5.420282	0.7897167	0.6242366
	6.209999	5.420282	0.7897167	0.6242366
E	6.209999	5.420282	0.7897167	0.6242366
	7.429999	6.294801	1.135199	0.8973249
	7.429999	6.294801	1.135199	0.8973249
	7.429999	6.294801	1.135199	0.8973249
	7.429999	6.294801	1.135199	0.8973249
	7.429999	6.294801	1.135199	0.8973249
	6.580000	5.731640	0.8483601	0.6705916
	6.580000	5.731640	0.8483601	0.6705916
	7.429999	6.416924	1.013075	0.8007914
	7.429999	6.416924	1.013075	0.8007914
	7.429999	6.416924	1.013075	0.8007914
	7.429999	6.416924	1.013075	0.8007914
	6.040000	6.422196	-0.3821964	-0.3021097
	6.040000	6.422196	-0.3821964	-0.3021097
	6.040000	6.422196	-0.3821964	-0.3021097
	6.520000	6.325628	0.1943712	0.1536420
	6.520000	6.325628	0.1943712	0.1536420
	6.520000	6.325628	0.1943712	0.1536420
	4.879999	5.934684	-1.054685	-0.8336823
	4.879999	5.934684	-1.054685	-0.8336823
	5.799999	2.412790	3.387209	2.677441
	3.480000	5.118457	-1.638457	-1.295129
	6.959999	5.777370	1.182629	0.9348162
F	3.480000	5.494771	-2.014771	-1.592589
	3.480000	5.494771	-2.014771	-1.592589
	3.480000	5.494771	-2.014771	-1.592589
G	7.309999	5.030637	2.279363	1.801737
	6.580000	6.373537	0.2064629	0.1631999
	6.559999	6.243827	0.3161726	0.2499206
	7.200000	5.998086	1.201514	0.9500604
	6.780000	5.586158	1.193842	0.9436799
	3.760000	4.958005	-1.198005	-0.9469709
	4.639999	4.404423	0.2355766	0.1862130
	6.919999	6.109731	0.8102684	0.6404817
	4.540000	3.066562	1.473438	1.164689
H	5.959999	5.919582	0.4041672E-01	0.3194765E-01
	6.750000	5.943994	0.8060064	0.6371129
	5.139999	5.483812	-0.3438129	-0.2717692
	3.040000	4.975507	-1.935507	-1.529934
	6.910000	5.915832	0.9941683	0.7858466
	3.600000	4.996451	-1.396451	-1.103834
	1.630000	3.909931	-2.279931	-1.802186
	8.539999	5.515058	3.024941	2.391084
	4.370000	3.179690	1.190310	0.9408877
	5.089999	4.957758	0.1322412	0.1045309
	5.759999	5.355804	0.4041948	0.3194984
I	5.450000	5.424920	0.2507973E-01	0.1982443E-01
	4.969999	5.340424	-0.3704243	-0.2928042
	2.920000	3.086395	-0.1663957	-0.1315285
	4.679999	4.952169	-0.2721701	-0.2151386
J	6.440000	5.629003	0.8109970	0.6410577
	8.779999	5.779058	3.000941	2.372113
	7.049999	6.339512	0.7104874	0.5616091
	7.400000	6.342347	1.057652	0.8360281
	7.049999	6.162768	0.8872309	0.7013172
	8.759998	6.268029	2.491969	1.969793
	7.610000	6.183640	1.426359	1.127475
	7.690000	5.962890	1.727110	1.365205
	7.469999	5.625905	1.844094	1.457676
	6.040000	4.450604	1.589396	1.256348
	6.250000	6.537173	-0.2871733	-0.2269979
	5.879999	6.504018	-0.6240187	-0.4932595
	8.129999	6.434383	1.695616	1.340310
	8.129999	6.410065	1.719934	1.359533
	8.500000	6.291588	2.208412	1.745653
	10.25000	6.108124	4.141876	3.273972
	7.870000	6.066779	1.803221	1.425367
	7.000000	5.892526	1.107474	0.8754101

K				
	6.879999	5.834808	1.045191	0.8261777
	3.810000	5.085202	-1.275202	-1.007992
	3.810000	4.584808	-0.7748084	-0.6124523
	4.500000	4.584808	-0.8480835E-01	-0.6703731E-01
	4.500000	3.577902	0.9220977	0.7288779
	4.440000	2.902813	1.537186	1.215078
	2.620000	2.339700	0.2802997	0.2215647
	5.940000	2.333649	3.606350	2.850662
	6.500000	5.498426	1.001574	0.7917001
	8.000000	4.557915	3.442085	2.720818
	3.500000	3.693379	-0.1933794	-0.1528580
	1.750000	4.596592	-2.846592	-2.250107
	3.000000	3.241274	-0.2412739	-0.1907165
	1.875000	2.093370	-0.2183700	-0.1726120
	3.500000	3.026183	0.4738169	0.3745315
	4.000000	3.026183	0.9738169	0.7697597
	1.500000	2.370481	-0.8704815	-0.6880777
	0.8750000	1.472952	-0.5979524	-0.4726553
	2.250000	0.9111086	1.338891	1.058335
	0.7500000	0.4908113	0.2591887	0.2048773
	0.0000000	0.6249524	-0.6249524	-0.4939976
	0.0000000	0.4501428	-0.4501428	-0.3558183
	5.849999	6.306839	-0.4568396	-0.3611118
	7.250000	5.548052	1.701948	1.345316
	8.500000	5.173577	3.326423	2.629392
	2.050000	4.069414	-2.019414	-1.596259
	3.970000	4.346027	-0.3760276	-0.2972334
	2.840000	5.282257	-2.442257	-1.930498
	3.290000	5.655828	-2.365828	-1.870084
	6.709999	5.373402	1.336597	1.056522
	6.150000	5.981842	0.1681576	0.1329212
	7.860000	6.302876	1.557124	1.230839
	7.200000	6.323264	0.8767357	0.6930213
	4.000000	2.270479	1.729521	1.367111
	6.650000	4.752628	1.897371	1.499789
	5.549999	5.764395	-0.2143955	-0.1694703
	5.750000	6.233960	-0.4839602	-0.3825494
	4.070000	2.786915	1.283085	1.014222
	4.910000	5.615028	-0.7050285	-0.5572944
	5.370000	5.223456	0.1465435	0.1158362
	5.410000	4.337351	1.072649	0.8478822
	4.169999	2.909764	1.260235	0.9961606
	5.500000	4.766063	0.7339373	0.5801454
	5.320000	5.383271	-0.6327152E-01	-0.5001338E-01
	5.379999	5.615028	-0.2350292	-0.1857803
	0.0000000	1.731690	-1.731690	-1.368825
	1.330000	4.513359	-3.183359	-2.516307
	6.120000	5.791569	0.3284311	0.2596105
	4.770000	6.414479	-1.644480	-1.299890
	2.560000	2.862070	-0.3020697	-0.2387729
	0.0000000	2.127031	-2.127031	-1.681326
	0.0000000	1.271621	-1.271621	-1.005161
	0.0000000	0.9473299	-0.9473299	-0.7488230
	5.250000	5.684149	-0.4341488	-0.3431757
	4.650000	5.822532	-1.172532	-0.9268355
	5.160000	5.990149	-0.8301497	-0.6561972
	7.459999	5.157099	2.302900	1.820342
	5.040000	6.300698	-1.260698	-0.9965271
	7.860000	6.441965	1.418035	1.120894
	8.119999	6.544386	1.575613	1.245453
	6.530000	6.533924	-0.3924370E-02	-0.3102043E-02
	6.900000	6.539952	0.3600473	0.2846017
	6.990000	6.549567	0.4404325	0.3481427
	5.820000	6.543996	-0.7239962	-0.5722874
	6.270000	6.477884	-0.2078848	-0.1643239
	6.400000	6.356975	0.4302502E-01	0.3400940E-01
	7.500000	6.534182	0.9658184	0.7634373
	6.580000	6.563098	0.1690197E-01	0.1336027E-01
	5.750000	6.408152	-0.6581516	-0.5202402
	6.440000	6.246051	0.1939487	0.1533080
	5.020000	6.542423	-1.522424	-1.203410
	5.540000	6.563098	-1.023098	-0.8087144
	6.139999	6.504490	-0.3644905	-0.2881139
	6.900000	6.392256	0.5077438	0.4013493
	6.669999	6.428136	0.2418633	0.1911823

6.549999	6.563098	-0.1309872E-01	-0.1035397E-01
7.250000	6.496949	0.7530508	0.5952537
6.919999	6.402647	0.5173521	0.4089442
5.650000	6.365749	-0.7157497	-0.5657690
5.820000	6.535571	-0.7155714	-0.5656281
6.620000	6.465433	0.1545668	0.1221783
5.860000	6.297429	-0.4374294	-0.3457689
6.099999	6.513018	-0.4130182	-0.3264729
6.500000	6.524581	-0.2458096E-01	-0.1943018E-01
6.480000	6.528156	-0.4815674E-01	-0.3806581E-01
6.520000	6.393059	0.1269407	0.1003411
6.070000	6.406540	-0.3365402	-0.2660204
6.049999	6.528833	-0.4788342	-0.3784975
6.270000	6.509317	-0.2393179	-0.1891704
6.049999	6.402949	-0.3529501	-0.2789917
5.719999	6.365749	-0.6457500	-0.5104373
7.509999	6.528833	0.9811659	0.7755687
6.750000	6.509317	0.2406826	0.1902491
7.099999	6.348620	0.7513790	0.5939323
5.809999	5.947769	-0.1377697	-0.1089009
6.629999	6.209372	0.4206276	0.3324877
6.389999	6.246623	0.1433764	0.1133327
6.469999	6.216037	0.2539625	0.2007463
5.559999	5.657181	-0.9718132E-01	-0.7681760E-01
6.099999	6.092915	0.7084846E-02	0.5600262E-02
6.639999	6.272431	0.3675680	0.2905465
6.349999	6.255570	0.9442902E-01	0.7464200E-01
6.790000	5.734200	1.055799	0.8345634
6.400000	5.689133	0.7108669	0.5619092
5.809999	5.638890	0.1711092	0.1352544
6.379999	5.726476	0.6535234	0.5165817
7.599999	5.346547	2.253452	1.781256
4.440000	4.748641	-0.3086414	-0.2439676
2.240000	4.158751	-1.918751	-1.516689
3.160000	2.916095	0.2439051	0.1927963
6.480000	5.998654	0.4813452	0.3804823
5.700000	5.646690	0.5330944E-01	0.4213879E-01
3.230000	5.253700	-2.023701	-1.599647
2.550000	4.815727	-2.265728	-1.790959
7.110000	6.527246	0.5827541	0.4606417
5.950000	6.527246	-0.5772457	-0.4562876
7.129999	6.527246	0.6027536	0.4764504
7.200000	6.527246	0.6727543	0.5317829
6.360000	6.527246	-0.1672459	-0.1322006
6.540000	6.527246	0.1275444E-01	0.1008183E-01
5.440000	6.265694	-0.8256941	-0.6526752
6.410000	6.212502	0.1974974	0.1561130
6.730000	6.259886	0.4701138	0.3716044
6.129999	6.168585	-0.3858566E-01	-0.3050029E-01
6.309999	6.016543	0.2934561	0.2319642
5.740000	6.212502	-0.4725027	-0.3734928
5.540000	6.279718	-0.7397184	-0.5847152
6.750000	6.240209	0.5097914	0.4029678
3.130000	5.796247	-2.666247	-2.107552
6.580000	6.110955	0.4690447	0.3707593
6.900000	6.249181	0.6508188	0.5144439
5.709999	6.238689	-0.5286903	-0.4179067
6.419999	6.392898	0.2710152E-01	0.2142256E-01
3.310000	5.926182	-2.616182	-2.067978
4.139999	6.187001	-2.047002	-1.618066
5.419999	6.085236	-0.6652365	-0.5258405
5.500000	5.943583	-0.4435835	-0.3506334
5.799999	5.793288	0.6711006E-02	0.5304758E-02
5.669999	5.670807	-0.8077621E-03	-0.6385008E-03
5.549999	5.455698	0.9430122E-01	0.7454100E-01
4.520000	5.227554	-0.7075548	-0.5592912
5.309999	6.007665	-0.6976652	-0.5514740
5.639999	5.866920	-0.2269211	-0.1793712
5.400000	5.757479	-0.3574791	-0.2825717
5.030000	5.563276	-0.5332766	-0.4215319
4.580000	5.351203	-0.7712030	-0.6096025
6.120000	5.913620	0.2063799	0.1631343
6.120000	5.940900	0.1791000	0.1415707

COEF # BEST VALUE CORRELATION STD. ERROR T

0	4.987683	0.8783478E-01	0.3749345	13.30281
1	0.3255821	0.4741736E-02	0.8711457E-01	3.737401
2	-0.1187190	0.1779785E-03	0.1687741E-01	-7.034195
3	-0.1946494E-01	0.2105390E-04	0.5804815E-02	-3.353240
4	0.6000717E-02	0.2244512E-05	0.1895322E-02	3.166067
5	0.1933137E-02	0.9146887E-06	0.1209926E-02	1.597732
6	-0.4888172E-03	0.8295169E-07	0.3665530E-03	-1.333551
7	0.2668135E-03	0.5702560E-08	0.9553379E-04	2.792871

ANALYSIS OF VARIANCE

SOURCE OF VARIATION	SUM OF SQUARES	DOF	MEAN SQUARE
TOTAL	902.6241	290	
REGRESSION	449.6945	7	64.24207
RESIDUAL	452.9295	283	1.600458

R SQUARED = 0.4982080 R = 0.7058385
THE STANDARD ERROR OF Y ABOUT THE REGRESSION PLANE IS 1.265092

THE F RATIO TESTING THE NULL HYPOTHESIS THAT ALL THE
COEFFICENTS ARE ZERO, I.E. B1=B2=...=BK=0, IS 40.13981
BASED ON THE DEGREES OF FREEDOM 7/ 283

NOW A STEP-WISE DOWN REGRESSION WILL TAKE PLACE
THE VARIABLE WITH THE LOWEST T WILL BE DELETE
THIS WILL CONTINUE UNTIL THERE ARE JUST TWO VARIABLES LEFT

COEF #	BEST VALUE	CORRELATION STD. ERROR	T
0	4.809273	0.7665141E-01 0.3507329	13.71207
1	0.3850728	0.3498266E-02 0.7492778E-01	5.139253
2	-0.1221848	0.1737582E-03 0.1669895E-01	-7.316917
3	-0.2425978E-01	0.1297624E-04 0.4563425E-02	-5.316135
4	0.7190097E-02	0.1747487E-05 0.1674648E-02	4.293498
5	0.4305980E-03	0.1214795E-06 0.4415379E-03	0.9752233
7	0.3456187E-03	0.3520603E-08 0.7516661E-04	4.598035

ANALYSIS OF VARIANCE

SOURCE OF VARIATION	SUM OF SQUARES	DOF	MEAN SQUARE
TOTAL	902.6241	290	
REGRESSION	446.8484	6	74.47472
RESIDUAL	455.7758	284	1.604844

R SQUARED = 0.4950548 R = 0.7036013
THE STANDARD ERROR OF Y ABOUT THE REGRESSION PLANE IS 1.266824

THE F RATIO TESTING THE NULL HYPOTHESIS THAT ALL THE
COEFFICENTS ARE ZERO, I.E. B1=B2=...=BK=0, IS 46.40620
BASED ON THE DEGREES OF FREEDOM 6/ 284

COEF #	BEST VALUE	CORRELATION STD. ERROR	T
0	4.806970	0.7664793E-01 0.3506948	13.70699
1	0.3756840	0.3440512E-02 0.7430031E-01	5.056291
2	-0.1188613	0.1665213E-03 0.1634610E-01	-7.271542
3	-0.2323101E-01	0.1228282E-04 0.4439439E-02	-5.232871
4	0.7416429E-02	0.1713925E-05 0.1658345E-02	4.472186
7	0.3276729E-03	0.3309602E-08 0.7287305E-04	4.496490

ANALYSIS OF VARIANCE

SOURCE OF VARIATION	SUM OF SQUARES	DOF	MEAN SQUARE
TOTAL	902.6241	290	
REGRESSION	445.3221	5	89.06441
RESIDUAL	457.3019	285	1.604568

R SQUARED = 0.4933639 R = 0.7023986

```
THE STANDARD ERROR OF Y ABOUT THE REGRESSION PLANE IS    1.266716

THE F RATIO TESTING THE NULL HYPOTHESIS THAT ALL THE
COEFFICENTS ARE ZERO, I.E. B1=B2=...=BK=0, IS    55.50678
BASED ON THE DEGREES OF FREEDOM     5/ 285


COEF #  BEST VALUE      CORRELATION      STD. ERROR        T
   0     4.423452      0.7206470E-01  0.3511621        12.59661
   1     0.4161844     0.3389400E-02  0.7615663E-01     5.464848
   2  -0.4793454E-01   0.9765912E-05  0.4087923E-02   -11.72589
   3  -0.2572381E-01   0.1208918E-04  0.4548255E-02    -5.655754
   7   0.3682456E-03   0.3258307E-08  0.7466934E-04     4.931684


      ANALYSIS OF VARIANCE

SOURCE OF VARIATION  SUM OF SQUARES  DOF  MEAN SQUARE
TOTAL                  902.6241      290
REGRESSION             413.2301        4   103.3075
RESIDUAL               489.3940      286   1.711168

R SQUARED = 0.4578097      R = 0.6766163
THE STANDARD ERROR OF Y ABOUT THE REGRESSION PLANE IS    1.308116

THE F RATIO TESTING THE NULL HYPOTHESIS THAT ALL THE
COEFFICENTS ARE ZERO, I.E. B1=B2=...=BK=0, IS    60.37251
BASED ON THE DEGREES OF FREEDOM     4/ 286


COEF #  BEST VALUE      CORRELATION      STD. ERROR        T
   0     5.742243      0.3027507E-01  0.2366758        24.26206
   1   0.7725544E-01   0.6292402E-03  0.3412083E-01     2.264172
   2  -0.5168957E-01   0.9427112E-05  0.4176386E-02   -12.37663
   3  -0.3784753E-02   0.5239919E-06  0.9846312E-03    -3.843828


      ANALYSIS OF VARIANCE

SOURCE OF VARIATION  SUM OF SQUARES  DOF  MEAN SQUARE
TOTAL                  902.6241      290
REGRESSION             371.6119        3   123.8706
RESIDUAL               531.0122      287   1.850217

R SQUARED = 0.4117017      R = 0.6416398
THE STANDARD ERROR OF Y ABOUT THE REGRESSION PLANE IS    1.360227

THE F RATIO TESTING THE NULL HYPOTHESIS THAT ALL THE
COEFFICENTS ARE ZERO, I.E. B1=B2=...=BK=0, IS    66.94923
BASED ON THE DEGREES OF FREEDOM     3/ 287


COEF #  BEST VALUE      CORRELATION      STD. ERROR        T
   0     6.227016      0.5498795E-02  0.1015861        61.29792
   2  -0.5185799E-01   0.9424121E-05  0.4205532E-02   -12.33090
   3  -0.1692082E-02   0.6229162E-07  0.3419128E-03    -4.948870


      ANALYSIS OF VARIANCE

SOURCE OF VARIATION  SUM OF SQUARES  DOF  MEAN SQUARE
TOTAL                  902.6241      290
REGRESSION             362.1267        2   181.0634
RESIDUAL               540.4973      288   1.876727

R SQUARED = 0.4011933      R = 0.6333982
THE STANDARD ERROR OF Y ABOUT THE REGRESSION PLANE IS    1.369937

THE F RATIO TESTING THE NULL HYPOTHESIS THAT ALL THE
COEFFICENTS ARE ZERO, I.E. B1=B2=...=BK=0, IS    96.47827
BASED ON THE DEGREES OF FREEDOM     2/ 288


COEF #  BEST VALUE      CORRELATION      STD. ERROR        T
   0     5.983677      0.4210507E-02  0.9243528E-01    64.73369
```

```
   2  -0.5422976E-01 0.9301735E-05 0.4344628E-02 -12.48203

       ANALYSIS OF VARIANCE

SOURCE OF VARIATION SUM OF SQUARES DOF MEAN SQUARE
TOTAL                 902.6241      290
REGRESSION            316.1632        1  316.1632
RESIDUAL              586.4608      289  2.029276

R SQUARED = 0.3502712      R = 0.5918372
THE STANDARD ERROR OF Y ABOUT THE REGRESSION PLANE IS   1.424527

THE F RATIO TESTING THE NULL HYPOTHESIS THAT ALL THE
COEFFICENTS ARE ZERO, I.E. B1=B2=...=BK=0, IS   155.8010
BASED ON THE DEGREES OF FREEDOM    1/ 289
```